THE ROLE OF THE CXCL12/CXCR4 SIGNALING AXIS IN ADIPOCYTE BIOLOGY

A Dissertation
Presented to the Faculty of the Graduate School
of Cornell University
in Partial Fulfillment of the Requirements for the Degree of
Doctor of Philosophy

by
Benjamin Michael Steiner
May 2022

THE ROLE OF THE CXCL12/CXCR4 SIGNALING AXIS IN ADIPOCYTE BIOLOGY

Benjamin Michael Steiner, Ph. D.

Cornell University 2022

General Abstract:

Mammalian adipose tissue can broadly be divided into two types of fat: brown adipose tissue (BAT) and white adipose tissue (WAT). While BAT is responsible for non-shivering thermogenesis via lipid metabolism, WAT stored fatty acids for long term energy use. However, BAT is primarily present in children and is all but lost by adulthood. Opposingly, WAT has the capacity to expand throughout life and contributes to negative health consequences. In BAT, sympathetic innervation drives adaptive thermogenesis, though molecular mechanisms contributing to BAT innervation are poorly understood. We have found that the administration of CXCL12 to mice causes an upregulation in BAT activity through sympathetic neuronal growth. Specifically, CXCL12 produced by smooth muscle cells is indirectly responsible for increased BAT presence and decreased BAT lipid accumulation, heightening thermogenic defense to cold stimuli. Here, CXCL12 is shown to retain CXCR4/CD301+ cells (M2 macrophages) within BAT, which directly influences sympathetic innervation of BAT, allowing for environmental stimulation for lipid-burning non-shivering thermogenesis.

While CXCL12 influences BAT activation, the CXCL12/CXCR4 pathway plays a different role in WAT. Though body fat distribution is dictated by sex, molecular signaling governing adiposity remains elusive. Here, we identify that CXCL12/CXCR4 signaling is regulating adiposity in a sex-dependent manner. Deletion of CXCR4 in females, but not males, leads to a lipodystrophic phenotype and leads to an upregulation of estrogen receptor alpha, thus promoting estradiol sensitivity and blocking adipogenesis. Removal of estrogen restores WAT expansion in adipose lineage-specific CXCR4-deficient mice, highlighting the antiadipogenic role of estrogen in women. Overall, these studies suggest that the CXCL12/CXCR4 signaling axis is influencing maintenance and expansion of BAT and WAT. Targeting this pathway could pose a new therapy to combat metabolic dysregulation.

BIOGRAPHICAL SKETCH

OMB No. 0925-0001 and 0925-0002 (Rev. 10/2021 Approved Through 09/30/2024)

BIOGRAPHICAL SKETCH

Provide the following information for the Senior/key personnel and other significant contributors.
Follow this format for each person. **DO NOT EXCEED FIVE PAGES.**

NAME:Steiner, Benjamin

eRA COMMONS USER NAME (credential, e.g., agency login): N/A

POSITION TITLE: Graduate Researcher

EDUCATION/TRAINING

INSTITUTION AND LOCATION	DEGREE *(if applicable)*	Start Date MM/YYYY	Completion Date MM/YYYY	FIELD OF STUDY
Victor Valley College	Transfer	08/2008	08/2014	Math and Science
California State Polytechnic Uni., Pomona	Bachelor of Science	08/2014	06/2016	Food and Nutrition: Dietetics
California State Polytechnic Uni., Pomona	Master of Science	08/2016	06/2018	Agriculture: Food and Science
Cornell University	PhD	08/2018	05/2022	Molecular Nutrition

A. Personal Statement

I first became interested in health and nutrition after graduating from high school. As exercise became an important part of my life, I decided to pursue a degree in dietetics to both further my personal knowledge and to join the workforce in a field that I was passionate about. Starting at my community college, I was fortunate enough to find my first mentor, Thomas Kennedy, who gave me a chance to teach chemistry laboratory courses, a position I would maintain throughout my undergraduate education. After transferring to my four-year university, I met new mentors who would guide me academic process and aid in developing my passion for teaching. At the close of my undergraduate degree, I was accepted into the master's program at the same institution and was provided an opportunity by one of my most major influences, Dr. Martin Sancho-Madriz, to teach courses within the department. This opportunity opened my eyes to the world of education and changed my career trajectory. Knowing that I now wanted to enter the world of academia, I began applying for doctoral programs and was accepted to Cornell University. As I close this final chapter as a student, I have come to realize that I will be a lifelong learner as the pursuit of knowledge is never ending.

B. Positions, Scientific Appointments and Honors

Positions and Scientific Appointments

2019-2022: Cornell University Teaching Assistant (TA)
2018-2022: Cornell University Graduate Researcher
2016-2018: California State Polytechnic University, Pomona Graduate Researcher
2016-2018: California State Polytechnic University, Pomona Teaching Associate
2016-2018: California State Polytechnic University, Pomona Dean's Advisory Council Student Representative
2015-2016: California State Polytechnic University, Pomona Student Assistant
2013-2016: Victor Valley College Chemistry Teaching Assistant (TA)

Honors

2018-2022: Phi Tau Sigma Honor Society
2018-2019: Graduate Presidential Fellowship
2017-2018: MENTORES Scholarship
2015-2022: Phi Upsilon Omicron Honor Society
2015-2022: Gamma Sigma Delta Honor Society
2014-2018: Dean's List
2014-2018: President's List

C. Contributions to Science

Publications

Steiner, B.M., Shukla, V., McClements, D.J., Li, Y.O., Sancho-Madriz, M. and Davidov-Pardo, G. (2019), Encapsulation of Lutein in Nanoemulsions Stabilized by Resveratrol and Maillard Conjugates. Journal of Food Science, 84: 2421-2431. doi:10.1111/1750-3841.14751

Steiner, B.M., McClements, D.J. and Davidov-Pardo, G. (2018), Encapsulation Systems for Lutein: A Review. Trends in Food Science and Technology, 82: 71-81. doi:10.1016/2018.10.003

Steiner, B.M. (2018), Encapsulation of Lutein in Multilayered Nanoemulsions Stabilized by Resveratrol And Maillard Conjugates. California State Polytechnic University, Pomona.

Conference Presentations

2020: Cornell Stem Cell Retreat – Lightening Talk - A CXCL12:CXCR4 Signaling Axis Controls White Adipogenesis via Estrogen Receptor Transcriptional Activation
2019: Cornell Precision Nutrition Symposium – Poster Presentation – A CXCL12:CXCR4 Signaling Axis Controls White Adipogenesis via Estrogen Receptor Transcriptional Activation
2018: CSU Annual Biotechnology Symposium - Ternary Complexes Through Maillard Conjugation of Sodium Caseinate, Dextran, and Resveratrol to be Used as Emulsifiers

2017: Agricultural Research Institute – Poster Presentation - Encapsulation of Lutein in Multilayered Nanoemulsions Stabilized by Polyphenolic Extracts and Maillard Conjugates

D. Scholastic Performance

YEAR	COURSE TITLE	GRADE
	Victor Valley College	
2008	Elementary Algebra	C
2009	Intermediate Algebra	B
2010	College Algebra	B
2011	Weight Training	A
2011	Intro to American Government	B
2011	History of the US to 1876	A
2011	Introductory Psychology	A
2012	General Biology	A
2012	Introduction to Sociology	A
2012	English Composition	A
2012	Introduction to Logic	A
2012	Introduction to Music	A
2012	History of US From 1876	A
2012	Introductory Chemistry	A
2013	Interpersonal Communication	A
2013	Introduction to Chemistry II: Organic Chemistry	A
2013	General Microbiology	A
2013	General Chemistry	A
2013	Human Anatomy	B
2013	Survey Art History	A
2014	Introduction to Statistics	B
2014	General Chemistry	B
2014	Human Physiology	B
2014	Introduction to Chemistry III: Biochemistry	A
	California State Polytechnic University, Pomona	
2014	Ethical Issues – Food, Ag & Apperal Industry	A
2014	Introduction to the Profession	A
2014	Introduction to Foods	A
2014	Introduction to Foods Lab	A
2014	Nutrition	A
2015	Agriculture and the Modern World	A
2015	Introduction to Research Methods	A
2015	Advanced Nutrient Metabolism I	A-
2015	Introduction to Food Science and Technology	A

YEAR	COURSE TITLE	GRADE
2015	Trigonometry	C-
2015	Accounting for Agribuisness	A
2015	Freshman English II	A-
2015	Advanced Nutrient Metabolism II	A-
2015	Food Safety and Current Issues	B+
2015	Genetics & Human Issues	A
2015	Nutrition through the Life Cycle	A
2015	Nutrition Education	A
2015	Nutrition Education Lab	A
2015	Institutional Food Service I	A
2015	Institutional Food Service I Lab	A
2015	Advanced Nutrient Metabolism III	A
2016	Community Nutrition	A
2016	Community Nutrition Lab	A
2016	Institutional Food Service II	A
2016	Institutional Food Service II Lab	A
2016	Medical Nutrition Therapy I	A-
2016	Medical Nutrition Therapy I Lab	A
2016	Experimental Food Science	B+
2016	Experimental Food Science Lab	A
2016	History of California	B+
2016	Culture and Meal Patterns	A-
2016	Culture and Meal Patterns Lab	A
2016	Nutrition Counseling	A
2016	Nutrition Counseling Lab	A
2016	Food Service Administration	A
2016	Medical Nutrition Therapy II	A-
2016	Medical Nutrition Therapy II Lab	A-
2016	Introduction to Grad Research AG Science	A
2016	Special Study U.D. Students	A
2016	Food Chemistry I	A
2016	Food Chemistry I Lab	A
2017	Special Topics for Grad Students	A
2017	Sensory Evaluation of Foods	A-
2017	Sensory Evaluation of Foods Lab	A
2017	Special Study U.D. Students	A
2017	Food Chemistry II	A-
2017	Food Chemistry II Lab	A
2017	Research Proposal	A
2017	Presentation of Research Proposal	A

YEAR	COURSE TITLE	GRADE
2017	Food Laws and Regulations	A
2017	Food Analysis	A
2017	Food Analysis Lab	A
2017	Research Design	A
2017	Directed Study	A
2017	Thesis Research	A
2017	Food Product Development	A-
2017	Food Product Development Lab	B
2018	Quantitative Analysis	B
2018	Quantitative Analysis Lab	B
2018	Directed Study	A
2018	Thesis Research	A
2018	Special Topics UD Students	A
2018	Master's Degree Thesis	A
2018	Stretching	A
	Cornell University	
2018	Genomics	B
2018	Graduate-Level Research	NG
2018	Seminar	SX
2019	Stem Cells and Regeneration	B
2019	Graduate-Level Research	NG
2019	Seminar	SX
2019	Graduate-Level Research	NG
2019	Human Genomics	B+
2019	Graduate-Level Research	NG
2019	Seminar	SX
2020	Graduate-Level Research	NG
2020	Graduate-Level Research	NG
2020	Seminar	SX
2020	Seminars in Stem Cell Research	SX
2020	Graduate-Level Research	NG
2020	Grant Writing	SX
2021	Graduate-Level Research	NG
2021	Doctoral Dissertation Research	NG
2021	Mouse and Stem Cell Pathology	B+
2022	Doctoral Dissertation Research	NG

Cornell seminar courses are graded satisfactory (SX) or unsatisfactory (UX). Cornell research enrollment is not graded (NG).

This dissertation is dedicated to my love, my life, my wife, Jennifer Yoo Steiner.

ACKNOWLEDGMENTS

This dissertation would not be possible without the training from my principal investigator, Dr. Daniel C. Berry, and my lab mate, Abby Benvie. With any graduate-level research, undergraduate students play a role in daily tasks. Olivia Stamatatos, Derek Lee, and Travis Steiner all aided me in both day-to-day operations as well as research driven tasks. They were not only dedicated but driven in the lab. Heather Roman aided in initial training as my skillset grew in the lab. Scott Butler, the telemetry surgery core facility manager, performed all ovariectomies for my experiments and this research would be incomplete without his aid. My committee was always willing to bend an ear whether it be about research or personal matters. Thank you Dr. Natasza Kurpios, Dr. Elizabeth Johnson, and Dr. Tashara Leek for supporting me throughout this journey.

Finally, research cannot continue without appropriate funding. I was fortunate enough to secure a fellowship through the Cornell Graduate School as a Dean's Scholar for my first year allowing me to spend more time in the lab learning crucial skills. Additionally, my project was partially funded by the NIH through a NIDDK K01 award (DK101153). Thank you to everyone who has supported me along the path to achieving this goal.

TABLE OF CONTENTS

Table of Contents

LIST OF FIGURES

PREFACE

From chemistry to biology and everything in between, a variety of subjects have piqued my interest since the beginning of my educational journey, but the core fundamental of my education has always been nutrition centered. My fascination for science began with learning that the cell was the smallest thing in the body. While classmates simply turned the page from that concept, I wanted to know what made up cells. I wanted to know how they worked, especially with the digestion and absorption of nutrients. As I began to discover metabolism, I began to wonder how scientists discovered these pathways. My curiosity only grew as I gained more knowledge, which lead to graduate degrees. The research presented in this dissertation was fueled by curiosity and stayed true to my core interest of nutrition.

This dissertation is comprised of four chapters, each with its own story but all building on each other. The first chapter will cover background information relevant to what the reader will be exposed to throughout the remainder of the dissertation. The information in the first chapter will provide the reader with rationale regarding the direction of the research. The second chapter will expose the reader to the first scientific endeavor covering the integral protein CXCR4, it's ligand CXCL12, and innervation in brown adipose tissue. This chapter will introduce the reader to the role of sympathetic innervation within the brown adipose tissue as well as the response of these nerves in the presence and absence of CXCL12/CXCR4 signaling. The third chapter will cover the role of CXCR4 and CXCL12 on white adipose tissue as well as differences of this role due to sex steroid influence. The findings of this study suggest that the CXCL12/CXCR4 signaling pathway is regulating estrogen receptor transcriptional activity by downregulating estrogen activity. These findings and future directions will be discussed in the fourth chapter.

CHAPTER 1

INTRODUCTION AND STATEMENT OF PURPOSE

1.1.1. The Effects of Obesity:

Obesity is defined by an excess amount of body fat and is characterized by chronic low-grade inflammation. Phenotypically, obesity is generally simple to identify as excess body weight is not easily concealable. Once thought of as a sign of wealth and beauty, excess body weight has become commonplace as the industrial revolution brought food from the farm to the marketplace. In the modern age, one needs not hunt nor gather, but rather shop in grocery stores or from their smart phones. As technology advanced, humans became less mobile and increased their consumption of sustenance due to availability. This shift in energy balance gave rise to new negative ideas about obesity as those faced with low socioeconomical standings consumed affordable foods full of calories but limited in nutrients. These calorically rich highly processed foods contribute to satiation but not satiety, leading to frequent high-calorie consumption resulting in weight gain. Suddenly, obesity was no longer associated with wealth and beauty, but rather over-indulgence and cheap inexpensive foods. However, the impacts of obesity reach far beyond a mere cosmetic nuisance. It is associated with an increase in risk factors for ailments such as heart disease, high blood pressure, type 2 diabetes and insulin resistance, and certain types of cancer. While each of these diseases alone limit quality and longevity of life, having obesity as a comorbidity greatly increases the risk of death due to inflammation and high levels of insulin. Indeed, obesity is a common and serious disease growing in the United States. While factors such as genetics, race, and socioeconomical status can contribute, obesity can affect anyone. Over the past several decades, obesity rates have grown to unfathomable numbers. Obesity rates in the US was at 42.4% as of 2017, a rise from 30.5% in 2000 according to the CDC. One out of every five

children are classified as obese as well. Conjoined to the health implications associated with obesity, the financial aspects regarding medical treatment are astounding. In 2008 alone, the US spent $147 billion due to obesity-related health care. As inactivity and overconsumption of food becomes more prevalent, the rise in weight continues to increase. In order to therapeutically combat the obesity epidemic, we have been faced with, it is critical to develop our understanding of the body's physiological responses to overnutrition.

1.1.2. Adipose Tissue in Obesity:

White adipose tissue (WAT) is a highly dynamic organ capable of expansion and contraction dependent on nutrient availability (1). Due to its plasticity and role as the storage center of potential energy, WAT plays a myriad of roles in regulation of physiological and metabolic responses such as in appetite, thermogenesis, lipid metabolism, sexual reproduction, and glucose homeostasis. In a positive energy balance state, WAT stores excess lipids within the fat cells known as adipocytes. The role of the adipocyte as a reservoir for triglycerides was a crucial evolutionary step for the survival of animals when faced with famines. However, the ability to collect and distribute energy-packed lipids has negatively skewed since the industrial revolution due to more readily available food supplies and a more sedentary lifestyle. The lack of exercise coupled with an increased intake has resulted in a surplus of stored energy, leading to excess body fat and, thus, obesity. In the obese state, overaccumulation of lipids within the adipocytes, making up the fat pads, is seen as the hallmark of WAT expansion. These swollen adipocytes contribute to cellular stress and inflammation which can have systemic impacts resulting in metabolic syndrome (2). As these adipocytes grow in volume, the fat pads themselves enlarge, resulting in a measurable and observable phenotype. Due to the cellular enlargement, adipocytes begin to produce proinflammatory cytokines signaling macrophage infiltration resulting in apoptosis and

lipotoxicity. However, other tissues within the body will remove the lipids from circulation in an effort prevent hypertriglyceridemia, resulting in ectopic fat distribution, as seen in individuals suffering from nonalcoholic fatty liver disease (3). In addition to ectopic fat distribution, fat accumulation develops in the viscera surrounding the organs, which contributes to metabolic dysfunction and an imbalance in sex steroids (1, 4).

WAT can be divided into two main regions known as subcutaneous (SAT) and intra-abdominal visceral (VAT) adipose tissue. While both SAT and VAT share energy storing features, they differ in metabolic outcomes. It is widely accepted that expansion of VAT is associated with increased metabolic risk while SAT is associated with protective effects on energy balance (5, 6). Furthermore, these generalized anatomical locations expand in different ways. While VAT expands through a process known as hypertrophy, or the swelling of the adipocyte, SAT expands through hyperplasia which is the enlargement through an increase in adipocytes. Hypertrophy of WAT results not only in adipokine dysregulation, but also a decrease in vascularization resulting in hypoxia (7). The change in vascularity could represent a decrease in nutrient availability, oxygen diffusion, adipose progenitor numbers, and metabolite uptake. Interestingly, obesity plays a role in anatomical lipid storage preference as fat pad expansion shifts from SAT to VAT with morbidly increased weight. This shift in anatomical fat pad expansion not only places more strain on internal organs but causes metabolic dysregulation in a variety of ways such as impaired glucose uptake, insulin resistance, and inflammation. Indeed, the anatomical placement and type of WAT expansion plays a pivotal part in determining metabolic health.

Once thought of as simply the storage center for energy demands, adipose tissue has recently become known as an endocrine organ that regulates metabolism through communication with the entire body through adipokine secretion. Adipokines, WAT's cell signaling proteins, are

known to regulate various physiological responses such as insulin sensitivity, appetite, cardiovascular homeostasis, reproduction, and inflammation (8-10). The first adipokine discovered was leptin in 1994, and it clearly demonstrated the endocrine capabilities of WAT due to its ability to decrease food intake and increase energy consumption by communicating with the hypothalamus (11). Since the discovery of leptin, many other adipokines with different roles in energy regulation have been discovered. Adiponectin, for example, was found to be primarily expressed in SAT and increases fatty acid oxidation while reducing glucose synthesis in the liver (12). However, not all adipokines have a positive influence on WAT. Resistin has been reported to induce pro-inflammatory cytokines such as interleukin 6 (IL-6), MCP-1, and tumor necrosis factor-alpha (TNF-α) (13, 14). These proinflammatory cytokines emanating from VAT, IL-6 and TNFα, have been linked to the activation and recruitment of macrophages (15). These deleterious macrophages promote adipocyte cell death, insulin resistance, hypertriglyceridemia, and chronic low-grade inflammatory responses within SAT and VAT. Visfatin, also produced in VAT, additionally plays a role in macrophage infiltration as it promotes macrophage survival through decreasing apoptosis and is considered to play a major role in atherosclerosis and hepatic inflammation (16, 17). Furthermore, the VAT adipokine retinol-binding protein 4 (RBP4) becomes elevated in response to caloric excess, promoting insulin resistance by multiple mechanisms (18). While these adipokines typically maintain a homeostatic balance, they become dysregulated in response to obesity as cellular expansion, extracellular matrix remodeling, and immune cell infiltration cause altered secretion of leptin and adiponectin as well as upregulation of resistin and visfatin (19-21). Indeed, location of the fat pad determines which adipokines are expressed and, in obesity, contribute to metabolic and systemic risk of developing comorbidities.

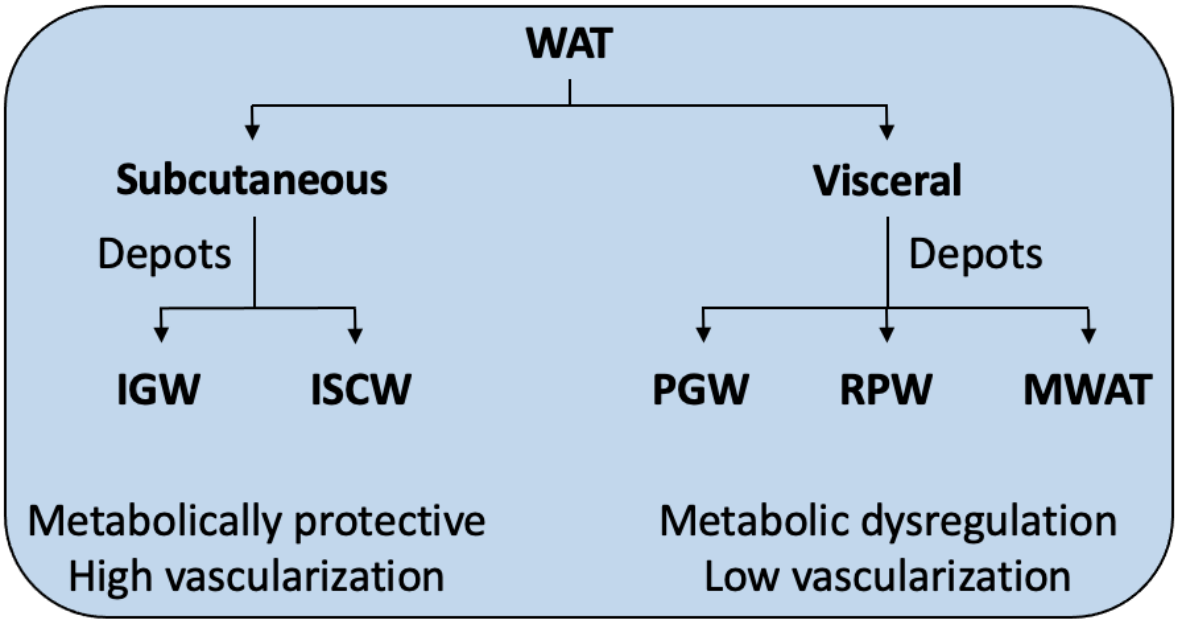

Figure 1: Adipose Tissue Hierarchy. WAT can be demarcated into two main anatomical locations, subcutaneous and visceral. These two locations are further separated into distinct compartments termed depots. While subcutaneous fat lies below the dermis of the skin, visceral fat surrounds internal organs within the body cavity. The anatomical placement of fat pads also has significant metabolic implications. While subcutaneous fat has been shown to be metabolically protective, visceral fat contributes to metabolic dysregulation.

1.2.1. Adipose Tissues at a Glance:

When discussing adipose tissue, the first thing that comes to mind is that fat pads are the storage center for lipids, and rightfully so. The need for long-term energy storage is not specific to any one species. Fat storing tissue can be found in both invertebrates and vertebrates which gives the capacity for energy storage in a fasted state (22, 23). This fat storing tissue is called WAT due to its coloring and can be found throughout the body. Functionally, WAT is responsible for lipid uptake in the fed state and lipid release, or lipolysis, in the fasted state. However, removing the stored lipids from the adipocyte in an energy-deprived state relies on several factors such as hormone signaling and anatomical placement of the fat pad itself. As previously stated, the main two regions of WAT locations are SAT and VAT. While VAT is considered unhealthy, it is the

first region to release fatty acids into circulation for energy supplementation (24). It has been proposed that VAT has variations in insulin receptor functions and higher adrenoreceptor numbers which is mechanistically responsible for the increased lipolysis ability of VAT. These variations in VAT receptors could be evolutionarily due to the energy demands of internal organs as well as proximity to major veins and arteries for circulation purposes. While both SAT and VAT are crucial for energy homeostasis, they are not the only adipose tissue.

1.2.2. Thermogenic Adipose Tissue:

In the addition to WAT, two additional types of adipose tissue can be found in mammals, known as beige (brite) and brown adipose tissue (BAT). Both these tissues contain specialized adipocytes that participate in thermoregulation by burning lipids for heat. While BAT and beige store energy as WAT, they are much quicker to utilize lipids for heat production when they are activated by environmental stimuli. BAT and beige adipose tissue differ from their WAT counterparts by color, location, and function. They take on a darker appearance due to an increased level of mitochondria present in the cells. The mitochondrial function in BAT and beige adipocytes play a unique role with respect to the electron transport chain. As the hydrogen ion concentration in the intermembrane space follows the typical mitochondrial gradient role, the hydrogen ions are allowed to pass back through the membrane using not only the ATP synthase, but the integral uncoupling protein 1 (UCP1). While ATP synthase is responsible for providing cellular energy, the passing of hydrogen ions through UCP1 induces non-shivering thermogenesis. With rapid breakdown of fatty acids to provide fuel for the excess mitochondria, BAT and beige fat contain multiple, small lipid droplets within each cell (multilocular), in contrast to WAT adipocytes with a single large lipid droplet (unilocular) and are considered metabolically healthy. However, BAT

and beige adipose tissue are distinct from one another as they develop, reside, and function in different anatomical locations.

1.2.3. Beige Adipose Tissue:

Beige adipose tissue has recently been of interest due to its influence on metabolic health through its elevated lipid-burning ability. Beige fat in humans seems to be produced and embedded within WAT throughout the lifecycle, though the embryonic origin and cellular hierarchy remains unclear (25). Originally identified to emerge transdifferentiationally from pre-existing mature adipocytes, beige adipocytes have been suggested to arise from white adipocytes in response to stimuli such as β3-adrenergic agonists and cold exposure (26-29). Beige adipocytes have an increased number of UCP1-expressing mitochondria and regulate non-shivering thermogenesis, though this thermogenic capability is reversible. As cold exposure or β3-adrenergic agonists induce beiging of white adipocytes, the removal of stimuli results in a loss of UCP1 expression and reversion to the white phenotype of storing lipids for long term energy availability in a unicellular lipid droplet (30). However, re-exposure to the cold revamps UCP1 and they again take on a thermogenic and metabolically protective role.

Though most abundant in SAT, beige adipocytes can additionally be found in VAT but at much lower numbers (26, 27, 31). For example, a study conducted by Wang and colleagues demonstrated that only a minute amount of beige fat was identified in VAT when mice were exposed to either 1-3 days in the cold or 7 days of β3-adrenergic agonists administration (19). However, exposure to cold has other effects on adipose tissue to optimize heat production. Cold exposure stimulates sympathetic nerve branching within WAT while inducing growth of blood vessels to aid in oxygenation and heat exchange (32-34). Increased vascularization is due not only to cold exposure, but also to enhanced Vegf-a signaling produced by adipose tissue itself. This

increased Vegf-a production further enhances the recruitment of beiging adipocytes while reducing apoptosis in the tissue (35). These findings help to highlight the importance of anatomical placement of WAT as well as the beneficial effects of beige adipocytes. Regardless of adipocyte type, adipose depots are discontinuously dispersed throughout the body, resulting in adipose tissue heterogeneity.

1.2.4. Brown Adipose Tissue:

In contrast to beige adipocytes, BAT is derived from distinct progenitors expressing Myf5 and Pax7 (36, 37). After organogenesis from these progenitors during embryonic development, BAT is primarily and most robustly found in newborns within the interscapular and neck region to protect against the cold and is all but lost by puberty (25). But how is BAT activated to protect against cold exposure? While beige adipocytes are activated due to external stimuli, BAT expresses high levels of UCP1 under basal conditions and is therefore constantly burning lipids making it highly metabolic. Through use of the β-adrenergic receptor, the sympathetic nervous system (SNS) functions as the principal stimulator of BAT thermogenesis. The importance of innervation within BAT has been demonstrated through surgical severance of unilateral postganglionic nerves on a single lobe. In response to cold, the innervated lobe acted as usual with an increase in UCP1 concentration, blood flow, and glucose uptake while the denervated lobe had a severe reduction in thermogenic potential (38, 39). The loss of innervation is detrimental to BAT as it can no longer function to regulate temperature. While it is well known that BAT is the major contributor to non-shivering thermogenesis, recent studies have suggested that BAT might also play a major role in lipid and carbohydrate metabolism due to its energy-burning potential.

In rodent studies, BAT was identified to protect against HFD-induced obesity while loss of BAT mass and/or UCP1 activity resulted in an increased susceptibility to rapid weight gain (40,

41). When exposed to cold, the increase in BAT activity for thermogenic purposes reduces circulating triglyceride-rich lipoproteins in mice by removing the lipids for energy consumption while increasing HDL levels, resulting in healthier lipid panels (42). In order to remove lipids from these lipid-rich lipoproteins, BAT increases expression of lipoprotein lipase and Vegf-a, resulting in degradation of triglycerides and increased lipoprotein permeability (43, 44). It has also been suggested that increasing BAT in humans through cold exposure results in a reduced triglyceride content and increased metabolism (45). Furthermore, BAT mitochondria utilize pyruvate for combustion, thereby potentially regulating carbohydrate metabolism (46). Due to these factors, the interest in utilizing BAT to combat obesity has grown immensely in the past several decades.

1.3.1 Adipogenesis:

Adipose stem cells reside along the vasculature and are capable of both self-renewal and differentiation into mature adipocytes when given the proper adipogenic cues. The resulting adipocytes have the capability to remove lipids from circulation, thus creating an energy storage system for future usage. While WAT organogenesis occurs during embryogenesis throughout early postnatal life, adipogenesis takes place throughout the lifecycle. Adipocytes have a limited lifespan and their turnover rate is approximately 10% each year (47). Creating new adipocytes, termed adipogenesis, requires transcription factor upregulation involving a myriad of genes (48). The first step in creating an adipocyte from an adipose progenitor cell (APC) is through insulin's hormonal signaling which increases intracellular levels of cyclic adenosine monophosphate (cAMP). cAMP then activates cAMP response element binding protein (CREB) through phosphorylation which initiates adipogenic genes CCAAT/enhancer binding protein β (C/EBPβ) and cAMP response element binding modulator (CREM) (49). C/EBPβ expression peaks by 24 hours and upregulate expression of both nuclear hormone receptors peroxisome proliferator activated receptor γ

(PPARγ) and C/EBPα (50). By the second day of differentiation, C/EBPα becomes phosphorylated and allows the cell to undergo the final stage of differentiation by accumulating lipids (51). However, PPARγ and C/EBPα continue to play a role in adipocyte function as PPARγ regulates genes involved in fatty acid uptake while C/EBPα plays a role in insulin dependent glucose uptake (52). However, there are other factors regulating adipogenesis such as FOXO1/A2 and Tgf-β (53). Regardless of additional factors, adipogenesis relies on PPARγ as no other factor has been identified that can promote adipogenesis in PPARγ's absence (54). In order to replicate physiological adipogenesis in vitro, a differentiation cocktail including insulin, 3-isobutyl-1-methylxanthine (IBMX), and the glucocorticoid agonist dexamethasone is used to induce adipocyte formation from APCs (55). Insulin, used to induce both proliferation and differentiation of APCs, mimics insulin-like growth factor-1 which activates mitogen-activated protein kinase (MAPK) pathways (56, 57). IBMX is known to inhibit phosphodiesterases which increases intracellular cAMP and protein kinase A (PKA), which is required for transcriptional activation of peroxisome proliferator activated receptor gamma (PPARγ) and adipogenesis (58). Dexamethasone stimulates osteogenic and adipogenic differentiation, though higher concentrations result in a shift to sole adipogenesis (59, 60). Both IBMX and dexamethasone stimulate the upregulation of C/EBPβ and C/EBPδ (61). After this adipogenic induction cocktail has been administered, in vitro adipocytes can be observed within 7 days.

1.3.2. Identifying the Adipose Progenitor Cell:

By volume, adipocytes make up about 70-90% of adipose tissue; however, they only represent 30-50% of the total cellular content (62). Other cell types such as vascular cells, immune cells, fibroblast, and APCs comprise the majority of the tissue. Adipocyte number and volume appear to be tightly balanced and may depend upon various dietary stimuli and nutrient availability

(excess or deficiency). Adipose tissue expansion via hyperplasia requires an active progenitor pool capable of meeting energy storage demands. While certain fields have studied stem/progenitor cells extensively, adipose tissue progenitors remain elusive. However, recent research has made a strong push to uncover the cellular hierarchy within WAT while new technologies have allowed new questions to be answered. Lineage tracing has allowed researchers to identify and label cells based on the cell surface marker expression associated with their tissue of interest. In the field of adipose tissue, APCs have been identified through their expression of adipogenic markers such as CD24, ZFP423, DPP4, PDGFRα, PPARγ, and adiponectin to name a few. However, each marker comes with its own caveat. For example, CD24 positivity is found only within early APCs and loses expression during differentiation into adipocytes (63, 64). ZFP423 expression is not exclusive to APCs as it is seen in a variety of tissues including neuronal, glial, B-cell, skeletal muscle, and olfactory progenitors (65-68). Platelet derived growth factor receptor-α (PDGFRα) cells have been suggested as both pro- and antiadipogenic while also marking cells outside of the APC lineage such as muscle, skin, fibroblasts, and other mesenchymal cell lineages (63, 69-71). Furthermore, PDGFRα has been suggested to have highest expression during development compared to adulthood. The question becomes which marker to use. Is one better than another? The answer might not be clear as other researchers have shown that APCs arise from multiple lineages while being evenly distributed throughout WAT (72). A mosaic of lineages could provide an explanation as to why visceral adipocytes have a greater triglyceride storage capacity than

subcutaneous adipocytes as well as why SAT expands via hyperplasia.

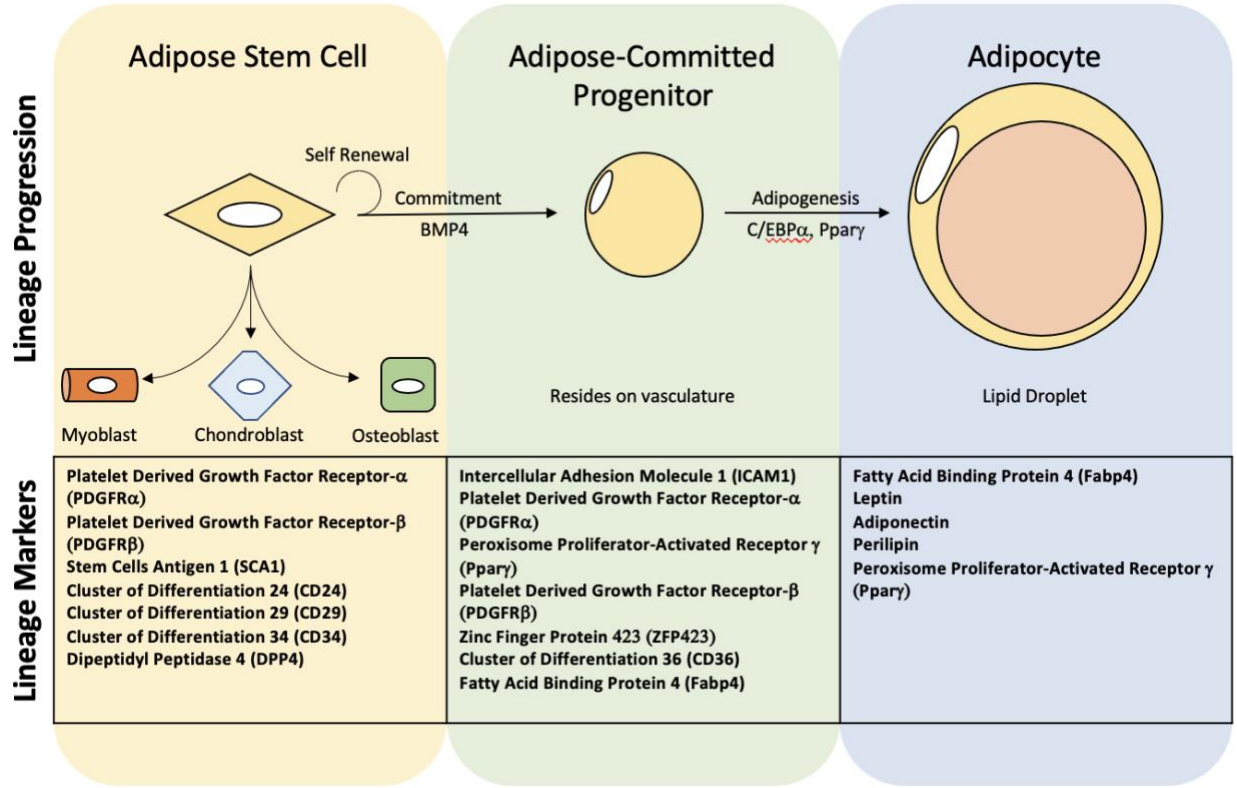

Figure 2: Lineage progression from stem cell to mature adipocyte. Adipocytes begin as ASCs before moving to lineage commitment and ultimately mature adipocytes. Throughout the progression from ASC to mature adipocyte, cellular markers have been identified correlating with each step within the lineage. Moreover, markers for one step are not necessarily expressed from ASC to adipocyte. That is, many markers are exclusive to specific points of lineage progression, allowing for identification of ASCs, progenitors, or adipocytes.

1.3.3. Identifying the APC Niche:

As previously stated, adipocytes make up the majority of adipose tissue volume, though they represent only about half of the cellular content (62). The other half of adipose tissue content includes immune cells, fibroblasts, APCs, nerve processes, and vascular cells (73). Adipose tissue is also located in close proximity to large blood vessels such as the aorta and mesenteric vessels. Not only does the vasculature provide adipose tissue with circulating lipids and nutrients for long-term energy storage, but it also provides transportation for liberated triglycerides in energy-

deprivation states. Indeed, the vasculature plays an important role in energy homeostasis. However, obesity is detrimental to the vasculature as it is strongly associated with the development of hypertension. Blood pressure is regulated by the renin-angiotensin-aldosterone system (RAAS) as angiotensin 1-7 has vasodilatory properties (74). This bioactive compound is secreted by adipocytes, primarily from VAT, and has been shown to be overexpressed in obesity, resulting in elevated blood pressure (75). CVD risk is not only attributed to hypertension as obese individuals also carry a higher risk of developing coronary artery calcification, carotid artery intimal media thickening, and left ventricular hypertrophy (76). Furthermore, as adipocytes swell due to overnutrition, they become too distant from the vasculature for nutrient exchange, thus causing inflammation (77). Though adipose tissue mass expands in obesity, cardiac output nor blood flow are increased, resulting in hypoxia (78-80). But how can the body avoid hypoxia and promote vascular growth? The answer lies in vascular smooth muscle cells (VSMC).

VSMCs are essential for vascular development as they play major roles in proliferation and contraction. These specialized cells are not terminally differentiated, therefore retaining plasticity and have the ability to make phenotypic changes in response to environmental stimuli (81). For example, it has been suggested that obesity regulates these specialized cells as a decrease in leptin and increase in adiponectin causes impairment of VSMC migration (82). Interestingly, VSMCs and APCs share several similarities. For example, both VSMCs and APCs have been identified taking up residence in the tunica adventitia (83, 84). Additionally, they share cell surface markers αSMA, PDGFRα, and PDGFRβ and express CD24 (85-88). These findings point to a vascular residency not only for VSMCs, but also for APCs.

Every progenitor lives in a specialized microenvironment termed the niche. This niche provides the progenitor with nutrients and cues for retention and/or differentiation. APCs are no

different as they ultimately form mature adipocytes once they leave their niche. However, the APC niche is not yet confirmed due to a lack of interest until recently. To identify any niche, a host of genetic tools such as fate mapping and lineage tracing is needed. These tools can be used for a variety of investigatory experiments from fluorescence-activated cell sorting (FACs) for isolating progenitors to single-cell RNA sequencing for gene expression of progenitor populations. In order to conduct such in vitro experimentation on adipocytes, the stromovascular fraction (SVF) must be isolated from the fat pad. The SVF is a heterogeneous mixture of fibroblasts, endothelial cells, hematopoietic cells, and neural cells and has been suggested to contain APCs, making it an ideal candidate for APC identification (64, 84, 89). Utilizing genetic markers and FACs, CD24+ cells within the SVF have been transplanted from healthy mice to lipodystrophic mouse models resulting in adipose-like tissues, indicating that the CD24 cellular population contains adipocyte progenitor cells (64). It was also noted that APCs expression of CD24 expression dissipated once the cell moved into a committed preadipocyte, indicating that APCs reside on and migrate from the vasculature. Further suggesting a vascular niche, the vascular smooth muscle and pericyte cell marker platelet derived growth factor-β (PDGFRβ) has been associated with APCs. PDGFRβ perivascular precursors expressing PPARγ and ZFP423, PPARγ's upstream regulator, reside adjacent to blood vessels and are highly adipogenic, which indicates that APCs might live along the capillaries (84). Additionally, the excision of PDGFRβ led to a reduction of adult adipose tissues by ~50% (90). This is further supported by lineage tracing studies showing that αSMA, a marker for vascular smooth muscle cells, is being expressed in these adipocyte progenitors (91, 92). These findings suggest that APCs reside along the vasculature within the depot.

Recently, the superficial fascia has been suggested as an APC niche as progenitor markers such as CD24 and CD29 have been identified in cells residing in the capillaries in the connective

tissue, giving rise to subcutaneous adipose tissue (93). Supporting the idea that the APC niche lies within adipocyte-surrounding connective tissue, a study in 2019 identified the reticular interstitium, the connective tissue surrounding fat pads, as a potential location of APCs in juvenile mice. In this study, DPP4+ cells were used as a progenitor marker while ICAM1+ cells identified committed preadipocytes. Location of DPP4+ cells indicated that the progenitors are residing in the mesh connective tissue surrounding the fat pads. Once removed from this niche, the DPP4+ cells produced adipocytes in vitro as well as through transplant in animal models (94). While these DPP4+ cells reside in a collagen-rich matrix similar to vasculature, they express no pericyte markers, and are thus excluded from a perivascular lineage. Though these findings suggest a connective tissue niche for APCs, it is important to note that it has been long accepted that APCs reside in the vasculature (95). However, the identification of this new connective tissue niche could be the result of developmental versus adult APCs as these studies were conducted using mice one week of age or younger. These findings highlight the need for a better understanding of this dynamic tissue.

1.3.4. The Role of PPARγ:

Identified in 1990, peroxisome proliferator activated receptors are ligand-activated transcription factors of nuclear hormone receptors and are divided into three types; PPARα, PPARβ/δ, and PPARγ (96). While PPARα and β/δ are expressed in various places such as the liver, heart, muscle, and bone, PPARγ is primarily expressed in adipocytes. In humans, PPARγ is minimally expressed in tissues such as the kidney, liver, and intestines while having high expression in adipose tissues. However, in mice, PPAR has an adipose tissue restricted pattern of expression, making it a tool for adding and deleting genes within the adipocyte lineage (97).

PPARγ was identified to be the driver of adipogenesis in 1995 due to its interaction with thiazolidinediones (TZDs) and insulin sensitization (98). PPARγ plays a major role in adipose cellular differentiation, modulation of metabolism, and inflammation in immune cells. This is accomplished through the control of expression on genes associated with lipid uptake into adipocytes as well as lipid metabolism (99). Lipid uptake is the final process of adipogenesis and is reliant on gene expression of CD36 and lipoprotein lipase. While PPARγ regulates these genes during differentiation, it also plays a role in mature adipocyte function through regulating fatty acid uptake, as previously mentioned (52). Understanding that PPARγ would be expressed specifically within the adipocyte lineage gave rise to new ideas regarding how to trace adipogenesis as reporters could be incorporated exclusively into adipocytes. More recent studies identified that PPARγ expression begins in utero at embryonic day 10.5 in mice through both genetic deletion and doxycycline suppression studies (92). In humans, PPAR expression takes place between week 15 and 16 of gestation while precursors of fat pads are found in the fetus at week 14, though not recognized as distinct adipose tissue until week 28 (100, 101). Though APCs are present, commitment and differentiation into mature adipocytes is not possible without PPARγ. The requirement of PPARγ on adipogenesis was further highlighted as loss-of-function studies diminished vascular sprouting in adipose tissue while loss-of-function rescue showed a full recovery of the phenotype (90). Developmental fate mapping tools have also been used to identify that not only adipocytes, but APCs express PPARγ (84). These studies have shown that PPARγ is both sufficient and necessary for adipogenesis. Due to the role of PPARγ on adipogenesis, genetic mouse models have been constructed utilizing PPARγ in order to investigate fate mapping and lineage tracing of APCs.

1.3.5. White Adipose Tissue Organogenesis:

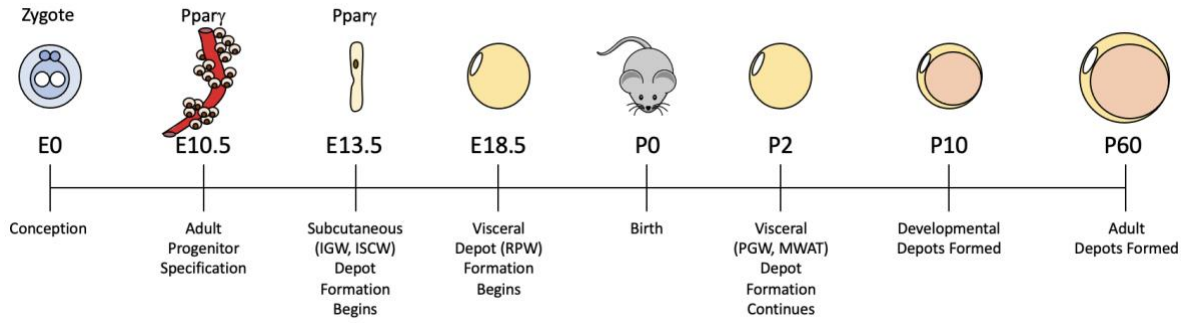

Figure 3: Development and Progression of Adipose Tissue. APC differentiation, marked by expression of PPARγ, takes place in two stages. The adult APCs are responsible for maintenance and expansion of WAT throughout the lifecycle and begin specification on embryonic day 10.5 (E10.5), though are not active until sexual maturity. The developmental APC population, responsible for constructing the fat pads, begins depot formations on E13.5 and continues through postnatal day 10 (P10). By P60, adult APCs completely take over adipogenic functions within WAT.

Murine embryogenesis begins with the emergence of the zygote on embryonic day 0 (E0) (102, 103). As cells divide the zygote becomes a blastocyst (E3.5) before going through the pre-gastrula (E5.5), gastrulation (E6.5), and organogenesis (E8.0) stages (104, 105). During gastrulation, there is an emergence of three specific germ layers that will provide the foundation for all tissues and organs during organogenesis. The emergence of these layers, known as the endoderm, mesoderm, and ectoderm, mark the beginning of lineage segregation(106, 107). Each of these three germ layers give rise to their own tissues (108). For example, the ectoderm is responsible for tissues such as the nervous system and epidermis while the endoderm is responsible for certain internal organs such as the stomach and liver. The mesoderm, however, is responsible for connective tissue throughout the body including muscle, bone, blood, cartilage, and adipose tissue (22).

Adipose tissue was associated with the mesoderm in the late 1800s due to histological identification of a connective tissue lineage. Since this initial observation, research methodologies

have advanced and paved the way for stem and progenitor identification (109). Through these studies, the mesenchyme, the embryonic connective tissue, was said to contain the stem compartment responsible for producing the various connective tissue known as mesenchymal stem cells (22). Thought to be multipotent, the idea of the mesenchymal stem cell maintaining the entirety of the mesoderm was pushed to the wayside as the mesoderm itself was later identified to consist of three compartments, the lateral plate, somite, and intermediate mesoderm, all which house numerous progenitors with their own independent trajectories (110). The lateral plate houses posterior lateral plate mesoderm (PLPM) progenitors which gives rise to the splanchnic PLPM progenitor responsible for mesenteric VAT as well as the somatic PLPM progenitor responsible for limb-associated SAT (111). The somite contains somitic progenitors which gives rise to the dorsomedial and central dermomyotomal progenitors resulting in BAT and visceral retroperitoneal VAT as well as the ventrolateral dermomyotomal progenitor yielding perigonadal VAT (111-113). Through multiple studies, these progenitors have been identified to be responsible for WAT organogenesis. Indeed, adipose tissue is initially derived from the mesoderm during embryogenesis.

WAT organogenesis begins as early as E13.5 in mice and the developmental depots are completely formed by postnatal day 10. However, studies have shown that developmental adipose progenitors are not the same as adult progenitors. Two populations of APCs have been identified and serve two different functions: developmental progenitors which are responsible for adipose organogenesis, and adult progenitors which maintain and expand the tissue throughout the lifecycle (92). While both populations are specified during embryogenesis, they are expressed at different timepoints and reside in different locations. Adult progenitor specification along with PPARγ expression begins at E10.5 while developmental progenitor specification begins around

E13.5. By postnatal day 30 the developmental progenitor pool is replaced by the adult compartment allowing for tissue maintenance and expansion. However, the accumulation of lipids into specific depots is dependent on sex steroids after sexual maturity.

1.4.1. Sex Steroid Signaling in Metabolism:

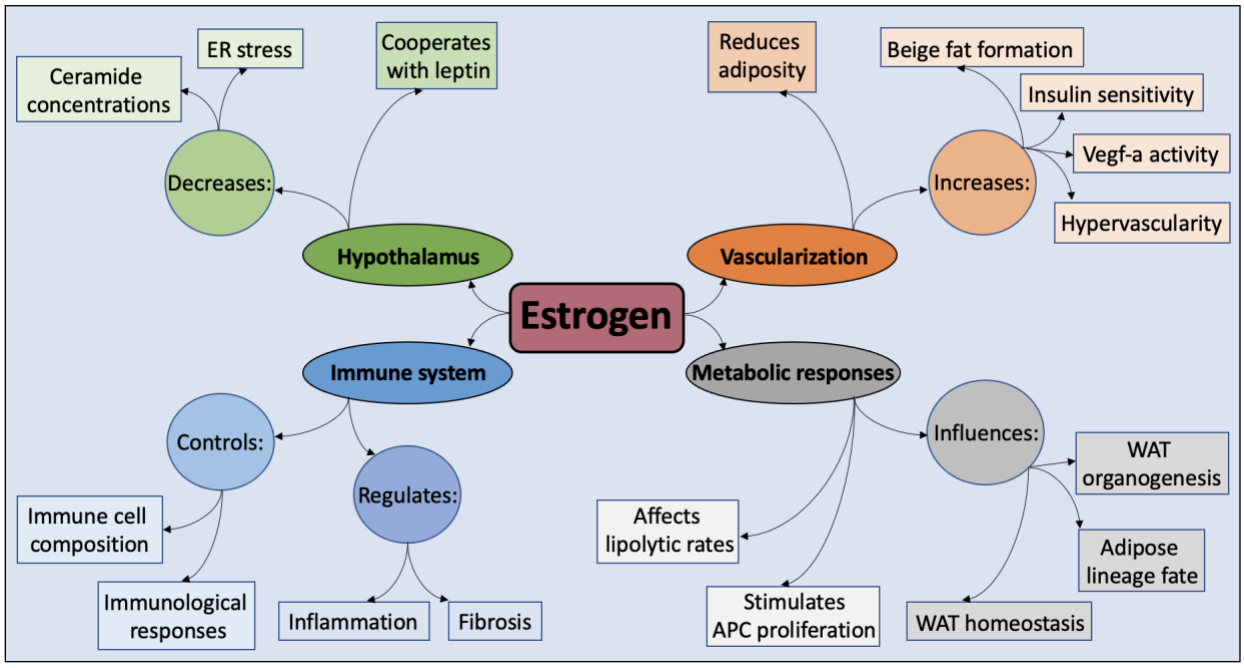

Figure 4: Influence of Estrogen on Whole Body Energy Regulation. Estrogen plays a large role in metabolic balance due to hormonal signaling to the hypothalamus, vasculature, immune system, and adipose tissue. Each tissue type affected by estrogen influences energy regulation in various ways but work synergistically to maintain adipose tissue homeostasis. A decreased level of estrogen has the potential to disrupt many physiological processes, especially within WAT.

Sex steroids are known to have an influential role on both location and maintenance of adipose tissues and their influence can be observed as early as puberty. Sexual maturity gives way to the rise of sex steroids, which then appear to control both adipocyte size and number, thus regulating total WAT size. Influencing WAT homeostasis, sex steroid action is mediated by nuclear hormone receptors such as estrogen receptor α (Esr1) and β (Esr2) which are ultimately responsible for the cellular proliferation and differentiation of specific fat pads. Sex steroid influence on WAT can be anatomically and macroscopically observed as males develop more

visceral fat at the waistline, promoting metabolic and cardiovascular disease, while females tend to develop subcutaneous fat around the hips and thighs, favoring metabolic protection. It is not entirely understood why women accumulate more adiposity than males but may be due to reproduction status and lactation. Furthermore, the placement of subcutaneous adipose tissue in females is thought to be due to 17-β estradiol (E2), as studies have demonstrated that estrogens decrease lipolysis in SAT while promoting lipolysis in VAT (114, 115). These findings could explain how E2 maintains the typical female fat distribution.

1.4.2. Estrogen's Influence on WAT:

As previously mentioned, SAT is healthier due to a reduced risk of diseases such as cardiovascular disease and insulin resistance. As females tend to reap the benefits of SAT, the shift to menopause causes a rapid increase in visceral adiposity (116). Menopause causes a decrease of serum E2 levels by 85-90% due to stunted production in the ovaries (117), though E2 replacement therapies are often utilized to reduce side effects and are less likely to develop intra-abdominal adiposity (118). Ovariectomies highlight the role of E2 on controlling adiposity through an increase in adiposity while E2 replacement therapies decrease fat mass. In addition, the deficiency in the aromatase enzyme, responsible for converting androgens to E2, show the same pattern of obesity (119, 120). Interestingly, Esr1 knockout mice are obese, regardless of sex (121). In addition, examination of fat distribution in women suffering from polycystic ovarian syndrome, resulting in overproduction of ovarian androgens, showed an expansion of VAT combined with a decrease in SAT (122). These changes are suggested to be the result of increased plasma androgen levels which act to block lipolysis and promote adipogenesis in VAT (123-125) E2 has also been suggested to influence APC proliferation, adipose lineage fate, and beige fat formation while Esr1 has been shown to promote thermogenic adipocytes within WAT (126, 127). Furthermore,

embryonic deletion of Esr1 within adipose tissue of both male and female mice showed inflammation and fibrotic markers were increased by sexual maturity (6 weeks of age) while body weight remained constant in both controls and mutants. Interestingly, adipocyte size was increased in Esr1-deleted mice from both sexes when compared to controls, though body weights were matched indicating estrogen aids in regulating hypertrophy (128). While Esr1 deletion showed the metabolically unhealthy hypertrophic phenotype, Esr2 compensated by playing a protective role against inflammation and fibrosis in females, possibly through enhanced E2 signaling. These findings highlight the importance of sex steroid influence on WAT homeostasis. However, sex steroids influence metabolism through other avenues as well.

E2 has been shown to play a role in energy metabolism through communication with the brain, both directly and indirectly. Indirect approaches for communication revolve around adipokines as E2 has been shown to work synergistically with adipokines to regulate metabolic responses. For example, E2 has been shown to cooperate with leptin, an adipokine that regulates food intake within the hypothalamus (129). E2 has been suggested to sensitize leptin signaling in the hypothalamus. Withdrawal of E2 through ovariectomies causes leptin resistance though E2 replacement therapy reverses this phenotype (130). Direct influence can be seen as Esr1 is highly expressed in the hypothalamus, and genetic loss of function models result in obese mice exhibiting hypometabolism (121, 131). Furthermore, E2 reduces both endoplasmic reticulum stress within the ventromedial nucleus leading to increased insulin and leptin sensitivity as well as decreases ceramide content within the mediobasal hypothalamus. This results in ameliorated lipotoxicity, ultimately yielding metabolic improvement, weight loss, and increased BAT thermogenesis (132). While it has been established that E2 plays a major role in energy metabolism through WAT and

BAT, regulation of Esr1 activity within APCs remains unclear. Understanding these pathways would allow for a greater understanding of Esr1 influence on AT biology.

Esr1 has also been suggested to influence vascularization. Esr1 activation appears to regulate vascular endothelial growth factor-A (Vegf-a), a major controller of angiogenesis expression (133). Adipose tissue overexpression of Vegf-a stimulates hypervascularity, reduces adiposity, and improves insulin sensitivity. Additionally, Vegf-a stimulates the appearance of thermogenic beige fat cells in SAT. Interestingly, blocking Esr1 activity showed a decrease in Vegf-a gene expression, resulting in adipocyte hypertrophy, inflammation, and insulin resistance (134). SAT also appears to express more angiotensinogen, regulating blood flow and pressure. E2 signaling has been shown to regulate angiotensinogen in the liver, and it would be of interest if a similar mechanism existed in WAT (38). Thus, it could be speculated that the loss of estrogen increases the risk for metabolically dysfunctional WAT and type 2 diabetes due to changes in angiogenic potential.

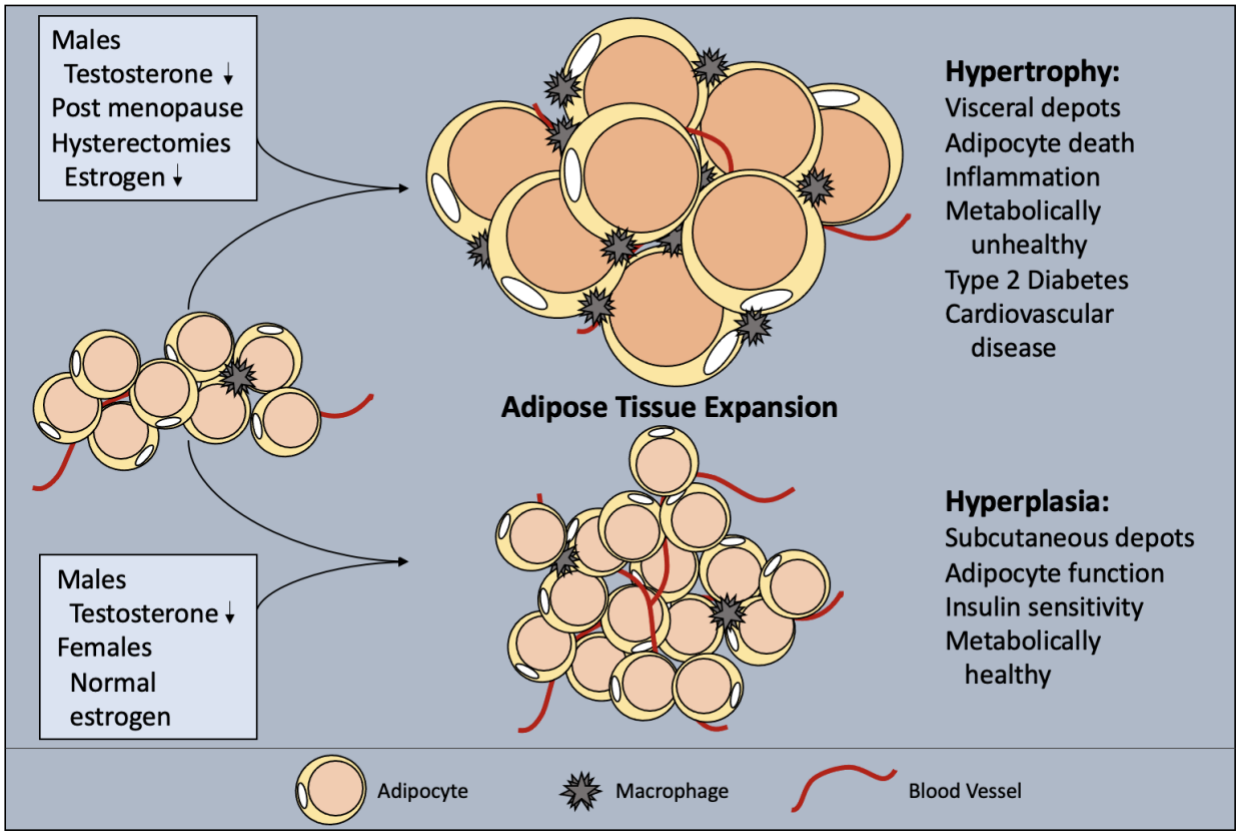

Figure 5: Sex Steroid Influence on Adipocyte Expansion. Adipose tissue can expand through either hypertrophy, the swelling of individual adipocytes, or hyperplasia, the increase of adipocyte numbers. Estrogen levels play a role in determining the type of expansion and location which shifts as estrogen decreases due to pharmacological drugs, medical procedures, and/or age. While normal estrogen levels result in hyperplastic subcutaneous adipose tissue growth, reduced estrogen leads to metabolically unhealthy hypertrophic visceral adipose tissue expansion.

1.4.3. Testosterone's Influence on WAT:

The amount of visceral fat accumulation in men is twice as high as it is in women, though women suffering from polycystic ovarian syndrome and menopause tend to narrow the margins (135). This is believed to be a result of plasma androgen levels, specifically testosterone (136, 137) which results in lipolysis inhibition and lipogenesis stimulation in the visceral compartments (138). As testosterone increases (or E2 decreases) in females, visceral adiposity increases. However, males show a different reaction to testosterone. Low plasma concentrations of testosterone in males increases visceral adiposity, though this can be combatted through testosterone treatment

therapy (139, 140). This indicates that regardless of sex, a decrease in the primary sex steroid results in an increase in visceral adiposity. In vitro studies using human adipose stem cells showed addition of testosterone during cell differentiation reduced PPARγ and C/EBPα expression, indicating androgen inhibition of preadipocyte differentiation (141). Supporting the notion that testosterone decreases VAT, a marker for androgen metabolism in males, 3α-diol-G, has a positive association with visceral adiposity accumulation and increases with weight gain (142, 143). As males gain weight, testosterone levels decrease due to the increase of 3α-diol-G, which results in an even greater increase of VAT. However, it remains unclear how sex steroids affect APCs in order to generate WAT depots.

1.5.1. G Protein-Coupled Receptors:

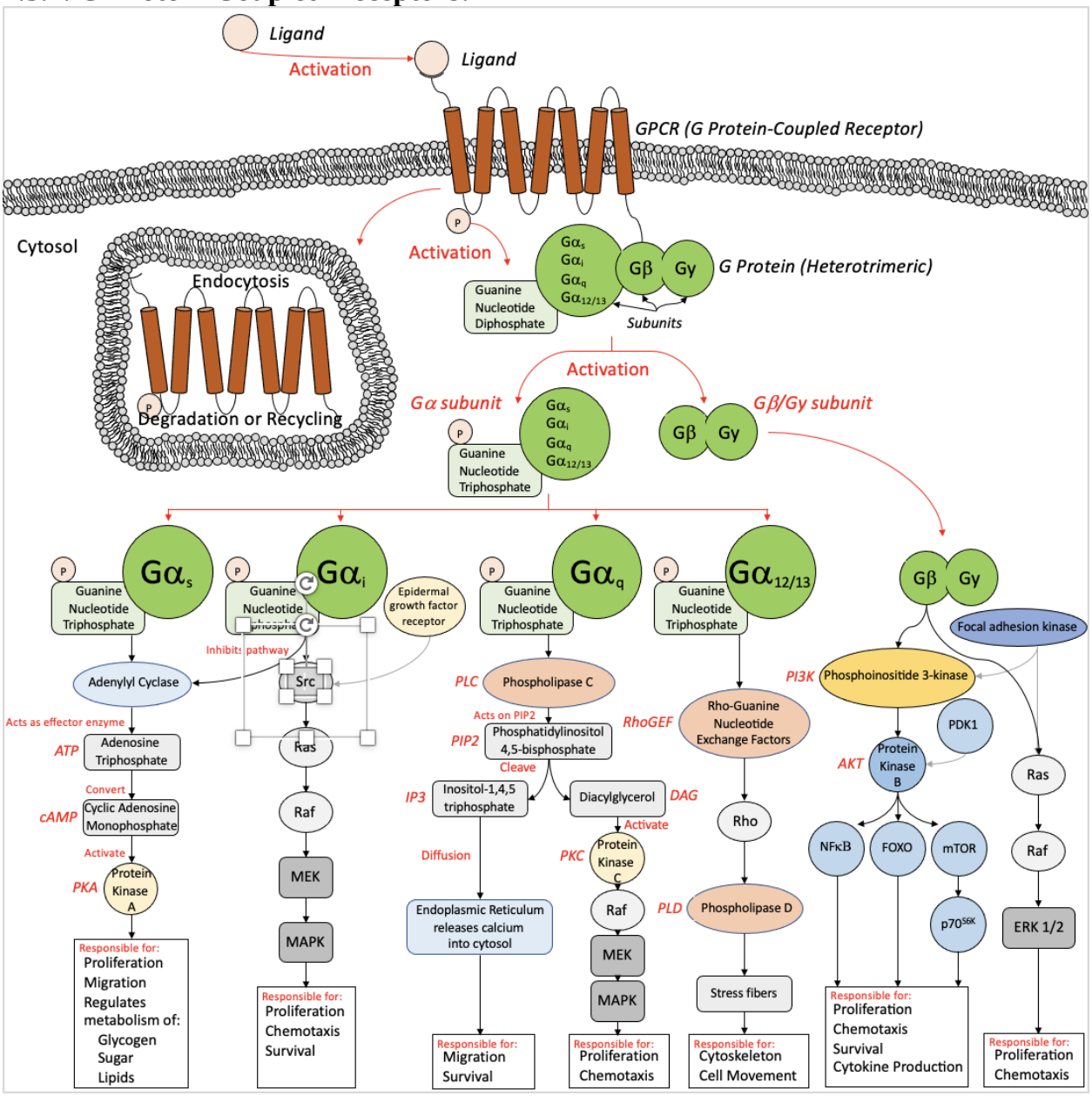

Figure 6: Model of Signaling Pathways for GPCRs. GPCR activation through ligand binding results in GDP exchange for GTP leading to Gα and Gβ/γ subunit dissociation. Though the Gβ/γ subunit consistently follows the same pathway, Gα subunits have multiple mechanisms dependent on which Gα is present. Regardless of Gα subunit present, the common outcome from GPCR signaling is migration whether undirected or through directed through chemoattractants.

G protein-coupled receptors (GPCRs) are identified as seven-pass-transmembrane receptors and have been under investigation in the medical field as they make up more than 30% of current drug targets. GPCRs are classically known for their involvement of exchanging GDP for GTP once activated by phosphorylation, which is activated with their respective ligand thus causing a conformational change in helices 3 and 6 (144). The ligands differ depending on which GPCR is being targeted and include neurotransmitters, peptide hormones, lipids, environmental stimuli, and chemokines (145). Anchored intracellularly to the GPCR, heterotrimeric G proteins play a major role in cell signaling and are ultimately responsible for the GPCR's ability to influence transcription. The heterotrimeric G protein unit will remain intact and anchored to the GPCR until ligand activation of the GPCR takes place. Once activated by the ligand, the GCPR will release the heterotrimeric G protein which stimulates a series of signaling pathways set in motion beginning with the dissociation of the G protein α (Gα) subunit and βγ dimer causing various events to happen with the cell. However, most signaling specificity within the cell is caused by the Gα subunits, not the βγ dimer. Several Gα subunits have been identified including $G\alpha_s$ (s for stimulation, expressed in most cells), $G\alpha_I$ (I for inhibition, largest and most diverse), $G\alpha_q$ (ubiquitously expressed), and $G\alpha_{12/13}$ (expressed in most cells) (146). Each Gα subunit relays signaling from the GPCR through different routes with different cellular responses, as seen in Figure 6. Subunit $G\alpha_s$ causes a signaling cascade resulting in proliferation, migration, and metabolism regulation through adenyl cyclase stimulation (147, 148). Subunit $G\alpha_i$, once activated, follows a different pathway as it increases migration and metabolism downregulation by inhibiting adenyl cyclase activity. Instead, subunit $G\alpha_i$ activates proliferation, chemotaxis, and survival of the cell. Subunit $G\alpha_q$ stimulates yet another pathway but yields results similar to both $G\alpha_s$ and $G\alpha_I$ (147, 148). Once activated, $G\alpha_q$ is ultimately responsible for cellular migration, survival,

proliferation, and chemotaxis through phospholipase C (PLC) activation (148, 149). Though not yet well established, $G\alpha_{12/13}$ is reported to influence both cellular movement and cytoskeletal formation and is associated with Rho proteins (147, 148). Furthermore, the dissociation of the G protein from the GPCR yields the $\beta\gamma$ complex which plays roles in proliferation, chemotaxis, survival, and cytokine production (150-152). Many of the roles of the G-proteins overlap which is thought to be due to their ability to affect the same signaling pathways such as adenylyl cyclase and MAPK. Once the $G\alpha$ and $\beta\gamma$ complexes have dislodged, the GPCR is then either degraded or recycled through endocytosis using β-arrestin and is no longer available for use (153).

1.5.2. C-X-C Chemokine Receptor 4:

First identified as the orphan receptor leukocyte-derived seven transmembrane receptor, C-X-C chemokine receptor type 4 (CXCR4) (fusin or cluster of differentiation 184) belongs to a family of integral proteins that bind with cytokines (154, 155). This family, known as C-X-C chemokine receptors belongs to the larger cohort, GPCRs. CXCR4 has been of great interest due to its role in hematopoietic stem cell chemotaxis (HSC), HIV-1 entry into T-cells, and various types of cancer such as leukemia, breast, lung, prostate, and colorectal cancers (156). Though there are 4 classes of $G\alpha$ proteins associated with GPCRs, CXCR4 seems mainly coupled to the $G\alpha_i$ subunit, triggering MAPK and PI3K activation leading to chemotaxis (157-159). Furthermore, the $\beta\gamma$ dimer triggers intracellular calcium mobilization resulting in proliferation and enhanced cellular chemotaxis (151, 160). It is important to note the difference between cellular migration and chemotaxis as migration is undirected while chemotaxis is cellular migration toward a chemoattractant; in the case of CXCR4, the chemoattractant is CXCL12. The role of CXCR4 in chemotaxis has been identified to be of great importance as CXCL12/CXCR4 signaling is involved in the colonization of bone marrow HSCs. Furthermore, a lack of CXCR4 in HSCs results in an

expansion of differentiated progenitors and a reduction in HSCs (161, 162). This suggests that the production of CXCL12 within the bone marrow is maintaining the HSC pools through CXCR4's chemoattraction in the environment. The removal of CXCL12 causes HSCs to vacate their niche and enter the peripheral blood stream. Alternatively, CXCL12 signaling from another location causes HSCs to migrate toward the chemoattractant. Due to these factors, many drugs have been developed to specifically target CXCR4 for various purposes such as HIV treatment and stem cell therapy. However, the drug that has been most widely used and approved by the Food and Drug Administration in 2008 is plerixafor, or AMD3100, which is a specific antagonist of CXCR4. AMD3100 was initially used to inhibit HIV virus entry into T-cells but was abandoned due to the lack of effect on M-tropic CCR5 HIV strains and the absence of oral bioavailability (163). AMD3100 and its effectiveness would find use with hematopoietic stem cell mobilization though as researchers identified that single-dose administration increased blood circulation of CD34+ hematopoietic progenitor cells which could be used in both lymphoma and multiple myeloma (164, 165). The effects of AMD3100 on cellular chemotaxis appear to be cell-type specific though as administration in rats with spinal cord injury showed a decrease in both migration and proliferation in neural stem cells after injury and treatment with AMD3100 (166).

1.5.3. C-X-C Chemokine Ligand 12:

C-X-C chemokine ligand 12 (CXCL12, also known as stromal cell-derived factor-1 [SDF-1]) was initially identified as pre-B-cell growth-stimulating factor in 1994 and was shown to stimulate the proliferation of bone marrow-derived B-cell progenitors (167). Identified in 1996 as the sole ligand for CXCR4, CXCL12 has been implicated in reducing the viral load for HIV-1 infections due to the inhibition of infection in cells expressing CD4 (168, 169). Belonging to the cytokine family, CXCL12 has been linked to several cancers such as melanoma and pancreatic

cancer (170, 171) due to its chemoattractant nature signaling fibroblasts to infiltrate tissues. Expressed in an array of tissues including stem, immune, and endothelial cells, CXCL12's interaction with CXCR4 affects growth and angiogenesis through homing of progenitors to the ligand-producing tissue (172). However, these interactions retaining progenitor cells to the lineage, known as the CXCL12/CXCR4 signaling axis, can be blunted through the use of AMD3100 (173, 174). This indicates that AMD3100 assumes the role of CXCL12 and is able to cause chemotaxis of CXCR4-expressing cells to the injection site. As previously discussed, hematopoietic stem cell chemotaxis is influenced by AMD3100 after intravenous injections, causing these stem cells to migrate to the vasculature. Once in circulation, the hematopoietic stem cells could then be phlebotomized, isolated from other blood cells, and used for therapy in cancer patients. As these findings came to light and the CXCL12/CXCR4 signaling axis was found to be responsible for hematopoietic stem cell chemotaxis and proliferation, other fields in human biology began to postulate if this axis could have the same impact on different tissue types.

1.5.4. CXCL12/CXCR4 Signaling in Adipocyte Biology:

CXCR4 has proven essential within the adult bone marrow and maintains the hematopoietic stem cell pool (175) and has been studied relentlessly in the hematopoietic lineage. However, it is in its infancy with respect to adipose tissue. Due to the recent interest that it might have the same effects in APC retention and homing, CXCR4 in adipocyte biology has begun to bear fruit.

The first step in identifying the role of CXCR4 in WAT was to delete it within the adipocyte and observe any phenotypic outcomes. Using fatty acid-binding protein 4 (Fabp4) Cre-recombinase as a driver, CXCR4 was deleted within the adipose tissue of male and female mice exposed to either a chow or high-fat diet for 24 weeks. Under a normal chow diet, the deletion of

CXCR4 had no impact on body weight nor overall health, though there was an increase in neutrophils and lymphocytes found in the peripheral blood. In a HFD setting, the deletion of CXCR4 resulted in a significant increase in white adiposity with a hypertrophic phenotype. Interestingly, brown adipose tissue in the same genetic mice were cold intolerant as they showed no increase from basal UCP1 activity when the mice were exposed to the cold, indicating that that environmental stimulus did not upregulate UCP1 expression levels. These findings suggest that CXCR4 is critical in both white adipocyte maintenance and brown adipocyte thermogenic regulation (176). Complimenting this study, pharmacological inhibition utilizing AMD3100 have shown that CXCR4 is responsible for APC chemotaxis. Administration of AMD3100 both in vivo and in vitro on the stromal vascular fraction from adipose tissue demonstrated that CXCR4 mediates the chemotaxis of the adipose progenitor cells located within the white adipose tissue (177). Furthermore, injecting wildtype mice with AMD3100 for 8 weeks while mice were on a high-fat diet yielded ectopic lipid deposition. Excess nutrients caused the adipocyte progenitors to migrate from the fat pad to skeletal muscles, indicating that CXCR4 is important in the retention of adipose progenitor cells to the adipose tissue (178). These studies highlight the role of CXCR4 on APC proliferation and retention as deletion results in stunted hyperplasia with increased hypertrophy within adipose tissue. However, CXCR4, as well as any GPCR, require activation to begin it's signaling cascade. Therefore, would the deletion of CXCR4's ligand CXCL12 yield the same results?

Over the past several years as interest in adipose tissue biology has increased, the CXCL12/CXCR4 signaling pathway has gained traction as a possible mechanism for hyperplastic tissue expansion. It has been suggested that adipocytes themselves secrete CXCL12 (179), thereby retaining CXCR4-expressing APCs to AT and reducing ectopic lipid deposition. However,

CXCL12 produced by adipocytes in the obese state has also been shown to recruit macrophages to AT resulting in inflammation as well as contribute to systemic insulin resistance (180), which is a hallmark of metabolically unhealthy, hypertrophic AT expansion. Additionally, it has been suggested by Shin and colleagues that CXCL12 expression in adipocytes is upregulated in the obese state, thus increasing insulin desensitization and degreasing glucose uptake while inhibition of CXCL12 causes a total recovery in mice (179). This could suggest that while CXCL12 is maintaining the APC pool, the overexpression of CXCL12 in obese populations spills over into the vasculature, causing macrophage infiltration. Interestingly, human studies conducted by Wolf and colleagues have suggested that CXCL12 expression is downregulated in the obese state and with bariatric surgery, CXCL12 climbs as weight drops (181). Though these studies seemingly contradict one another, there are differences that could explain the varying levels of CXCL12 in the obese state. For example, the research conducted by Shin used mice while Wolf used human subjects. Furthermore, Shin used epidydimal WAT for RNA analysis while Wolf used serum. However, it could be hypothesized that while highly expressed in AT and recruiting macrophages, CXCL12 does not enter blood circulation in the obese state. Regardless, it appears that the CXCL12/CXCR4 signaling axis is playing a major role in AT homeostasis and expansion.

1.6.1. Sex Steroid Roles on the CXCR4/CXCL12 Signaling Axis:

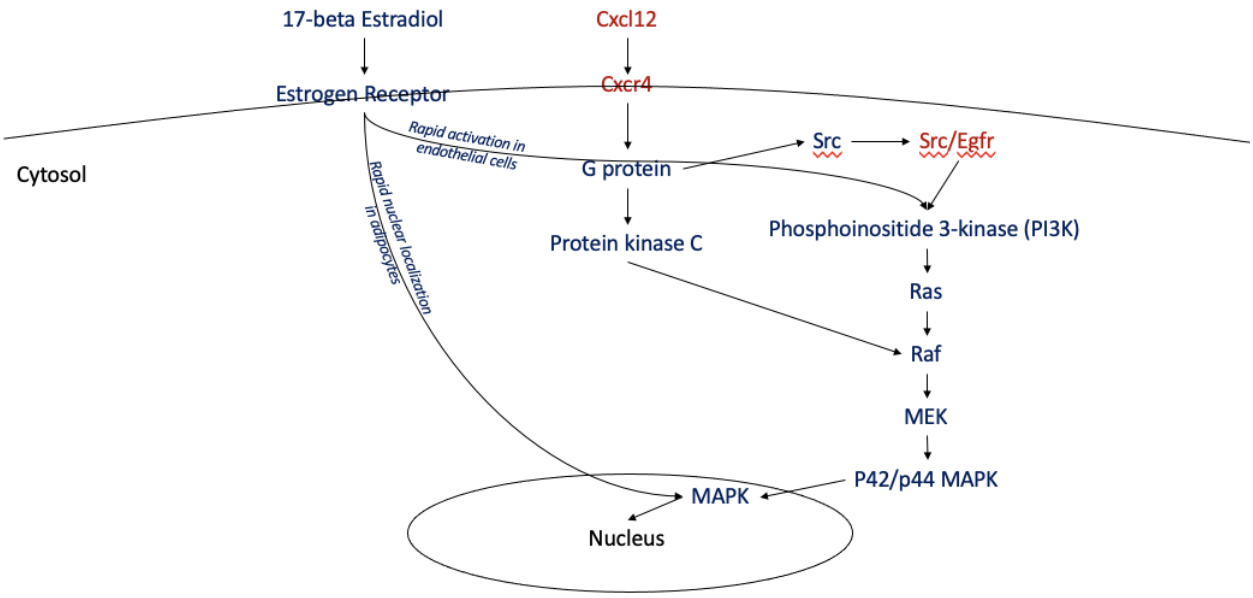

Figure 7: Model of E2 Influence on the CXCL12/CXCR4 Signaling Pathway. Estrogen receptor (ER) activation through the binding of 17β estradiol results in cellular signaling through the MAPK pathway. Within endothelial cells, ER is shown to cooperate with the CXCL12/CXCR4 signaling pathway through phosphoinositide 3-kinase activation and ultimately MAPK activation, indicating crosstalk between both receptors to influence nuclear transcription within the cell.

The expression of Esr1 has recently been shown to be driven by both E2 and the CXCL12/CXCR4 signaling axis. In white adipocytes, the $G\alpha_i$ protein/Src/PI3K pathway both up- and downstream of Ras have been shown to intervene in E2 signaling to P42/P44 MAPK, indicating a crosstalk between GPCRs and E2 (182). Interestingly, Esr1 in breast cancer also activates the CXCL12/CXCR4 pathway which completes an autocrine loop as both systems seemingly work synergistically (183). These findings were further explored as in vivo inhibition of Esr1 through tamoxifen injections blunted CXCR4 expression suggesting the necessity of E2

for proper tissue development (184). As previously mentioned, WAT development and homeostasis relies on APCs leaving the vasculature and taking up residence in the fat pads as mature adipocytes. With the CXCL12/CXCR4 signaling axis responsible for cellular chemotaxis and E2 expression increased in pubescent females, it could be postulated that this autocrine loop is responsible for the hyperplastic WAT growth in SAT. Accompanying hyperplasia is angiogenesis and. as mentioned prior, E2 has been proposed to regulate Vegf-a. This suggests E2 is regulating vascular growth in adipose tissue, and thus APCs as they reside on a vascular niche. In accordance, inhibition of E2's receptor, Esr1, shows a decrease of Vegf-a resulting in hypoxia, adipocyte hypertrophy, inflammation, and insulin resistance (133). Solidifying the role on WAT growth and angiogenesis, Esr1 has been shown to play a regulatory role in APC identity and potency as deletion of Esr1 causes these progenitors to enter smooth muscle fates (126). As Esr1 is the only estrogen receptor expressed in pre-adipocytes, all estrogenic effects on adipogenesis are thought to be mediated through this receptor (185). Therefore, a loss of E2 via menopause results in a shift from healthier subcutaneous to visceral adiposity while increasing risk factors of metabolic dysfunction due to decreased angiogenesis through the decrease of Vegf-a. Furthermore, the loss of E2 promotes hypertrophy due to the estrogenic promotion of proliferation of pre-adipocytes. However, the role of the CXCL12/CXCR4 axis on Esr1 within adipose tissue has yet to be explored as the bulk of estrogen research has been focused on various types of cancers.

Interestingly, testosterone plays a role in the CXCL12/CXCR4 signaling axis similar to estrogen. Recent studies have shown that a loss of testosterone results in a decrease in CXCR4 expression, resulting in lower numbers of migrated and differentiated cells (186, 187). These findings could explain why as males increase fat mass it is localized to hypertrophic visceral fat

pads. However, as with estrogen, current knowledge is lacking as androgen effects on the CXCL12/CXCR4 signaling axis within the adipose lineage has yet to be fully explored.

1.7.1. Genetic Tools for Exploiting APCs:

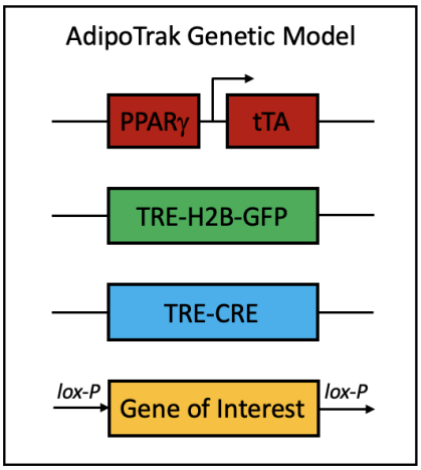

Figure 8: Schematic of the Genetic Tool, AdipoTrak.

As previously mentioned, there are a variety of cellular markers that can be utilized for tracing the lineage of adipocytes, though all come with their own limitations. Due to its exclusivity to the adipose lineage, PPARγ is a unique tool for adding and deleting genes in both APCs and mature adipocytes (97). By utilizing a tetracycline transactivation (tTA) control element allowing for tracing and deletion capabilities within adipocytes, researchers have created a genetic mouse model incorporating PPARγ to identify when both the developmental and adult APCs undergo organogenesis. This system, labeled AdipoTrak, consists of tTA under the control of PPARγ. AdipoTrak can be further utilized by incorporating a tTA-responsive Cre allele for genetic deletion (84), indicating that once PPARγ is expressed, tTA is activated and drives the tTA-responsive element (TRE) Cre, excising floxed sites within the adipose lineage unless the system is under suppression. AdipoTrak has the ability to be suppressed with doxycycline food/water added to the diet, allowing for a variety of uses as genes can be excised spatiotemporally. For example, a deletion can take place before, during, or after WAT organogenesis takes place. Furthermore, labeling of the adipocyte lineage is possible through florescent identification of adipocytes expressing PPARγ. Green fluorescence protein (GFP) is fused to histone H2B, thereby labeling of the adipocyte lineage through the tTA response element (TRE-H2B-GFP) (188). TRE-H2B-GFP

is incorporated into proliferating cells and will only be expressed in the lineage specified by the driver; in the case of AdipoTrak, the driver being PPARγ. Additionally, as mature non-mitotic adipocytes express PPARγ, TRE-H2B-GFP is activated. By adding lox-p sites in genes of interest, this system can be used to delete a myriad of genes expressed in the adipocyte lineage while marking APCs and adipocytes. While the AdipoTrak model labels both APC and adipocytes, there are caveats to be addressed. This system labels the lineage without exclusivity to APC nor adipocyte, therefore the deletion of genes within a specific adipose population is not possible. Furthermore, lineage tracing capacities are limited due to the lack of ability to identify when and where the Cre driver occurred. This specific caveat can be somewhat corrected for through doxycycline suppression studies at various timepoints. Unfortunately, doxycycline suppression for extended periods has the potential to confound research as exposure at any concentration increases glycolytic metabolism while reducing oxygen consumption due to effects on the mitochondria (189). While these effects are minimal, they can skew results dependent on the nature of the research. To combat these caveats, additional genetic systems have been utilized within adipose tissue. The tamoxifen inducible Cre^{ERT2} system provides temporal precision as administration of tamoxifen transiently activates Cre, thus inducing deletion of a specific gene at a specific timepoint (190). Coupling this Cre^{ERT2} tool with αSMA yields αSMA-Cre^{ERT2} which allows for deletion within cells expressing αSMA, such as APCs (191-193). Utilizing this system, fate mapping of adipocytes is possible. Taken together, these tools can be used for a variety of technologies from flow cytometry to fluorescent microscopy. The ability to mark adipocytes and delete genes specific to the adipose lineage allows new questions to be asked regarding the functionality and necessity of proteins and signaling pathways. These studies and technologies have moved adipose tissue biology further toward understanding this complex organ.

1.8.1. Statement of Purpose:

The purpose of this dissertation is to explore the role of the CXCL12/CXCR4 signaling axis on WAT and BAT function. Previous reports have shown that CXCL12/CXCR4 signaling regulates both WAT and BAT biology. However, the use of gene expression and genetic necessity tools for critical evaluation of this signaling pathway remain elusive. Sympathetic innervation of BAT is necessary for thermogenesis, but there is a lack of understanding on molecular factors responsible for the growth of these nerves. The first part of this dissertation, Chapter 2, focuses on CXCL12's influence on BAT sympathetic innervation. The hypothesis driving this first study is that CXCL12 regulates BAT function through increasing sympathetic innervation. Additionally, the CXCL12/CXCR4 pathway has been recently explored in WAT. While this pathway has been identified as necessary for WAT expansion and homeostasis, the role of CXCL12/CXCR4 signaling on sex steroids is lacking. The regulation of depot-specific WAT expansion and homeostasis by E2 has been established. However, CXCl12/CXCR4 signaling in WAT is still unclear. Furthermore, the relationship between CXCL12/CXCR4 and E2 signaling in WAT is lacking. The second study of this dissertation is aimed at examining the roles of CXCL12/CXCR4 on the maintenance and expansion of WAT through regulation of estrogen receptors in a sex-dependent manner. The hypothesis driving this research is that the CXCL12/CXCR4 signaling axis controls adipocyte differentiation and lipid accumulation by downregulating Esr1 transcriptional activity.

CHAPTER 2

CXCL12 SECRETED FROM SMOOTH MUSCLE CELLS INCREASES MACROPHAGE ACCRUAL AND SYMPATHETIC INNERVATION IN BROWN ADIPOSE TISSUE

Benjamin M. Steiner[1]*, Derek Lee[1]*, Abigail M. Benvie[1]*, Josie Ford[1], Yuwei Jiang[2], and Daniel C. Berry[1, 3]

[1]Division of Nutritional Sciences, Cornell University, Ithaca, NY 14853

[2]Department of Physiology and Biophysics, University of Illinois at Chicago, Chicago IL 60612 USA

[3]Lead contact: dcb37@cornell.edu

*These authors contributed equally

Pending journal submission as of dissertation completion

2.1. Abstract

Sympathetic innervation of brown adipose tissue (BAT) controls adaptative thermogenesis. However, the cellular and molecular underpinnings contributing to brown fat innervation remain poorly defined. Here we show that smooth muscle cell expression of Cxcl12 regulates brown adipocyte lipid accumulation. However, Cxcl12 does not directly regulate brown adipocyte thermogenic function *per se*. Instead, the genetic loss of Cxcl12 reduces BAT sympathetic innervation, thereby increasing lipid accumulation and dampening thermogenic responses to cold temperatures. Moreover, ablation of Cxcl12 induces high-fat diet-induced insulin resistance and BAT "whitening". Mechanistically, the loss of Cxcl12 reduces the abundance and accrual of BAT Cxcr4/Cd301+ macrophages that are required for sympathetic neuron maintenance. Finally, we

find that systemic administration of Cxcl12 is sufficient to boost BAT resident Cd301+ macrophages to restore sympathetic neuronal growth in models of reduced BAT sympathetic presence. Our data reveal a smooth muscle cell chemokine-dependent mechanism linking immunological infiltration and sympathetic innervation with BAT thermogenesis.

2.2. Introduction

Brown adipose tissue (BAT), a tissue specialized in non-shivering thermogenesis, has provided a significant evolutionary advantage for mammals to survive cold temperature exposure (34). This is because brown adipocytes contain specialized mitochondria that futilely burn glucose and free fatty acids to generate heat rather than the chemical energy, ATP (194). Specifically, the unique expression of the mitochondria protein, uncoupling protein 1 (UCP1), provides brown adipocytes the ability to collapse the proton gradient, disconnecting the electron transport chain and preventing ATP synthesis. Because of UCP1's function in creating heat, mice lacking this protein develop obesity under environmental conditions of thermoneutrality (195). Also, this thermogenic ability of brown adipocytes has generated plenty of clinical research attention as a potential mechanism to counteract obesogenic induced white adipose tissue (WAT) expansion and metabolic dysregulation (196-198). However, BAT prevalence in humans diminishes with adult maturation and aging (199, 200). While the reasons for this decline are unclear, the identification of cellular and molecular mechanisms controlling brown adipocyte thermogenic potential and perdurance are crucial for harness thermogenic fat to combat excess body fat.

To achieve thermogenesis, BAT is densely innervated with sympathetic neurons that release the neurotransmitter, noradrenaline, to stimulate fat cell lipolysis and energy uncoupling (201, 202). Thus the amount of BAT innervation is correlated with thermogenic capacity and macronutrient burning potential (203). Recently, adipocyte-expressing genes such as Prdm16,

CLSTN3b, and S100B have been linked to the amount of innervation of BAT and WAT (204, 205). In agreement, the discovery of "batokines" have also driven this notion that intrinsic secreted factors from brown adipocytes foster changes in angiogenesis, lipid trafficking, neurite growth, and immunometabolism (206). Specifically, adipocyte regulatory genes have been shown to cooperate with immunological cells to control sympathetic axons, regulating the amount of innervation (207, 208). For example, adipocyte-specific ablation of IL-17 receptor C (IL-17RC) reduces the expression of transforming growth factor beta (Tgfb1) to impair sympathetic innervation by regulating a T cell subpopulation, γδT cells (209). Correspondingly, alternatively activated (M2) macrophages have been shown to stimulate thermogenic fat cell biogenesis by inducing tyrosine hydroxylase expression and catecholamine production (210-212). However, this notion that M2 macrophages can generate catecholamines has recently been argued against (213, 214). Nevertheless, the molecular spectrum controlling sympathetic innervation of thermogenic tissue and the regulatory cell-types remain to be fully determined and elucidated.

Chemokine signaling has been shown to influence stem cell behavior, systemic metabolism, and lipid accumulation (215). Specifically, CXC ligand (CXCL) 12 (CXCL12) and its receptor, CXC motif receptor (CXCR) 4 (CXCR4), have been suggested to regulate adiposity, WAT inflammation, ectopic lipid accumulation, and insulin sensitivity (176, 178, 180, 216, 217). Additionally, it has been posited that CXCR4 within white and brown adipocytes promotes lipid accumulation in response to high-fat diet (HFD) feeding (176, 216). These observations appear to be in contradiction to other reports demonstrating that the sole ligand for CXCR4, CXCL12, acts as an insulin sensitization molecule (217). Critically, specific expression profiling and genetic and function tests examining CXCL12 activity within WAT and BAT are lacking clarity and, consequently, its role in adipose tissue biology and thermogenesis remains unrealized.

Here, we investigated the functional role of BAT-resident smooth muscle cells to regulate brown adipocyte thermogenesis. We find that smooth muscle actin (SMA) positive cells secrete CXCL12 to support basal sympathetic tone to suppress lipid accumulation. In supporting, we observe that mice lacking CXCL12 from SMA cells are delayed in thermogenic and metabolic flexibility in response to cold temperature exposure. However, CXCL12 does not appear to directly regulate brown adipocyte differentiation or thermogenesis. Moreover, we find that blocking CXCR4 activity by AMD3100 administration results in brown adipocyte lipid accumulation and decreased sympathetic innervation. However, brown adipocyte loss of CXCR4 does not appear to emulate the SMA-CXCL12 loss of function phenotype. Instead, we find that CXCL12 ablation regulates M2 macrophage presence to support sympathetic innervation and neurite growth. Collectively, these findings suggest a critical role for BAT-resident smooth muscle cells in supporting sympathetic function and tone to provide thermogenic plasticity in response to cold temperature fluctuations.

2.3. Results

CXCL12 is not expressed within mature white adipocytes

Several studies have reported varying effects of CXCL12 on adipose-derived stromal cell and adipocytes, potentially linking its function to metabolic regulation (176, 178, 180, 216, 217). However, CXCL12 expression, function, and genetic necessity tests within WAT or APCs are lacking. To begin to delineate CXCL12 WAT expression, we employed the CXCL12-dsRed knock-in mouse model. In this model, the fluorescent marker, dsRed, is expressed from the endogenous CXCL12 promoter, reporting on active CXCL12 expression (218). To provide adipose lineage tracking (stem-to-adipocyte), we combined the CXCL12-dsRed reporter mouse with the adipose lineage tracking mouse model, AdipoTrak (AT) (84). AT incorporates a

doxycycline suppressible tetracycline-controlled transactivator (tTA) knocked into the endogenous locus of peroxisome proliferator activated receptor gamma (PPARγ), creating a PPARγ-promoter driven tTA. To fluorescently visualize the adipose lineage, we have combined the PPARγ-tTA mouse model with the complementary tetracycline-responsive report system, TRE-H2B-GFP (188). Specifically, H2B-GFP will be incorporated into nucleosomes of proliferating PPARγ+ APCs which can subsequently be transferred to postmitotic adipocytes (Figure 9A). Importantly, AT-labeled cells are committed to the adipose lineage and can generate adipocytes; thus, serving as a tool to determine if CXCL12 is expressed within the adipose lineage. To broadly assess if CXCL12-dsRed expression overlaps with AT, we performed whole-mount immunofluorescence imaging of inguinal (iWAT) and perigonadal (gWAT) WAT from AT-CXCL12-dsRed mice. This cursory imaging revealed minimal overlap between the two reporters (GFP and RFP) and showed that CXCL12-dsRed expression appeared restricted to the vasculature and did not localize within adipocytes (Figure 9B). In agreement, directed qPCR analysis revealed that CXCL12 mRNA expression was enriched within the stromal vascular (SV) compartment compared to the floated adipocyte fraction isolated from iWAT and gWAT depots (Figure 9C). Similarly, we could not detect dsRed signal within isolated iWAT or gWAT floated adipocytes (Figure 9D). Gene expression analysis did not reveal changes in CXCL12 mRNA expression between depots. But flow cytometric analysis showed an overall increase in the number of CXCL12-dsRed+ cells in gWAT vs iWAT (Figure 9E, F). To confirm these findings, we performed immunostaining on iWAT cryosections to detect CXCL12-dsRed expression and adipocyte labeling. CXCL12-dsRed expression was undetectable in perilipin+ adipocytes (Figure 9G).

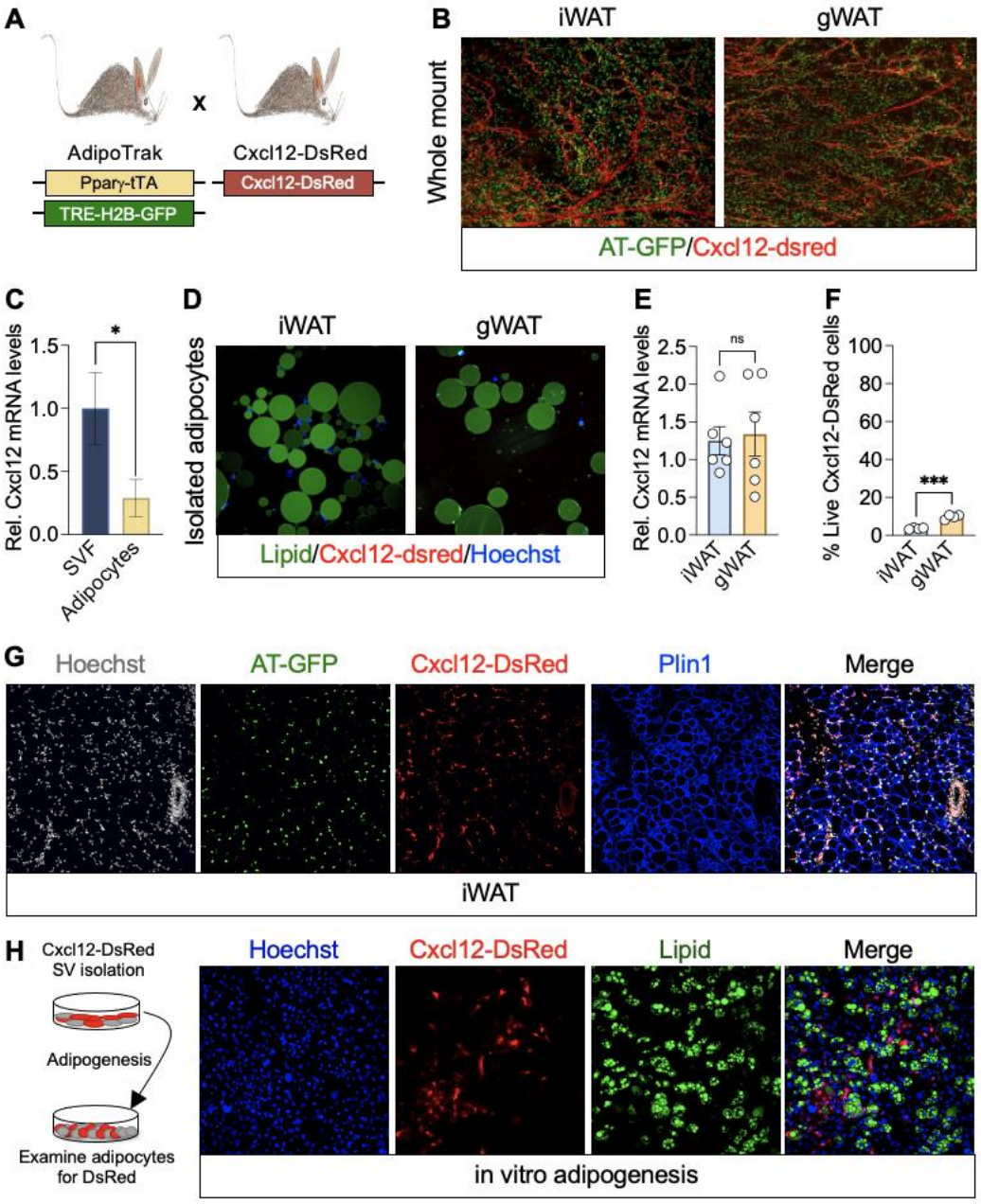

*Figure 9: CXCL12 is Not Expressed in Mature White Adipocytes. A) Genetic schema: AdipoTrak mice (AT; Pparg-tTA; TRE-H2B-GFP) were combined with the CXCL12-dsRed mouse model. B) Representative images of whole mount fluorescence microscopy of periscapular WAT (psWAT) from AT-GFP and CXCL12-dsRed mice. C) mRNA levels of CXCL12 within inguinal WAT (iWAT) stromal vascular fraction (SVF) or floated adipocytes. *P ≤ 0.033 by ordinary one-way ANOVA. Data are mean ± s.e.m. D) Representative images of floated adipocytes from iWAT depots from CXCL12-dsRed mice. Hoechst was used to visualize nuclei. E) mRNA levels of CXCL12 within iWAT and perigonadal WAT (gWAT) F) Flow cytometric analysis of live CXCL12-dsRed positive cells within the the SVF of iWAT and gWAT. ***P ≤ 0.001 by ordinary one-way ANOVA. Data are mean ± s.e.m. G) Representative images of GFP, dsRed, and perilipin (Plin1) immunostaining*

from iWAT depots from AT-Cxcl12-DsRed mice. H) Representative images of native DsRed fluorescence and lipid staining of in vitro derived adipocytes from iWAT SV cells from Cxcl12-DsRed mice.

To further assess if CXCL12-dsRed expression could be detected within in vitro derived adipocytes, we provided adipogenic media to SV cells isolated from iWAT depots from CXCL12-dsRed mice. However, CXCL12-dsRed expression was undetectable within lipid+ adipocytes but could be observed in non-lipid stromal cells within the dish (Figure 9H). Further supporting this notion, directed qPCR analysis showed that CXCL12 mRNA expression trended downwards throughout the adipogenic time course while PPARγ was upregulated (Supplemental Figure 1A). Previous reports have suggested that CXCL12 expression and circulating levels are elevated in response to high-fat diet (HFD) feeding (180). Indeed, we found that CXCL12 mRNA expression was elevated in iWAT and gWAT after 8-weeks of HFD (Supplemental Figure 1B) Yet, we were unable to detect dsRed signal within mature adipocytes (Supplemental Figure 1C). Collectively, under our gene expression and marking studies, it does not appear that CXCL12 is expressed in mature adipocytes.

To continue to assess if CXCL12 has a functional role in adipogenic potential, we performed in vitro adipogenic assays using recombinant CXCL12 protein. We isolated iWAT SV cells and treated them with recombinant Sdf-1α or Sdf-1β (50 ng/ml), the two most abundant CXCL12 isoforms (219), throughout adipogenesis. However, based upon lipid staining and mRNA expression of adipocyte markers, we found that neither ligand appeared to impact adipocyte maturation (Supplemental Figure 1D, E).

CXCL12 is minimally expressed within the APC lineage

Our whole-mount imaging and immunostaining studies suggests that CXCL12 is not expressed in mature adipocyte but may overlap with AT-GFP+ preadipocyte progenitors (90, 92,

220-225). To continue to probe if CXCL12 is expressed within the APC lineage, we used FACS based approaches to quantify AT-APC adipose lineage overlap with CXCL12-dsRed active expression, we found that ~17% (iWAT) and ~25% (gWAT) of AT-GFP labeled cells overlapped with CXCL12-dsRed signal (Figure 10A, B and Supplemental Figure 2A). We also used FACs analysis to evaluate the total dsRed expressing population and found that ~20% (iWAT) and ~15% (gWAT) of dsRed cells overlapped with AT-GFP signal (Figure 10C). Confirming our FACS analysis, isolated SV cells from AT-CXCL12-dsRed mice showed that the majority of AT labeled APCs were RFP negative 12 hrs. post-plating (Figure 10D). Our whole mount imaging suggested CXCL12 may be expressed within the vasculature, therefore, we FACs isolated CXCL12-dsRed cells and performed directed qPCR against vascular markers (Figure 10E). We found that both smooth muscle and endothelial cell markers were enriched in dsRed+ cells (Figure 10F). We also performed immunostaining of iWAT and gWAT sections for SMA and found co-localization between SMA and dsRed (Figure 10G). Of note, we also observed that some dsRed+ cells colocalized with Cd31 endothelial cells suggesting that CXCL12 may also be expressed within the vascular wall (Supplemental Figure 2B). Flow cytometric analysis revealed that CXCL12-SMA+ represented a small subset of the total iWAT and gWAT SMA+ cell population (Figure 10H).

Loss of CXCL12 within SMA+ cells does not alter WAT function

Our data suggested that CXCL12 is expressed within the vascular smooth muscle cell compartment. Interestingly, a subset of APCs has been shown to resemble smooth muscle cells (90, 92, 222); thus, we hypothesized that CXCL12 might a have a functional role in regulating WAT homeostasis from an APC source. To probe if smooth muscle cell-derived CXCL12 effects WAT biology, we established a mouse model to conditionally delete CXCL12 within the smooth muscle cell compartment using SMA-Cre^{ERT2} (226) (Supplemental Figure 2C). To delete CXCL12

within SMA+ cells, in vivo, we administered one dose of tamoxifen (TMX; 50 mg/Kg) for two consecutive days by intraperitoneal injection. Subsequently, mice were chased for six-weeks and phenotypically evaluated (Figure 10I). We found that both control and mutant mice gained body weight at a similar rate (Figure 10J). In agreement, WAT and non-adipose tissue weight were similar between control and mutant mice. Consistently, iWAT and gWAT adipocyte size, architecture, and gene expression all appeared similar between control and mutant mice (Figure 10K, L Supplemental Figure 2D-G). Surprisingly, mutant mice demonstrated elevated blood glucose levels and mild insulin resistance (Figure 10M, N). Supporting our in vivo observations, the adipogenic potential of SV cells isolated from control and mutant iWAT depots appeared similar as assessed by lipid staining and adipocyte marker expression (Supplemental Figure 2H-I).

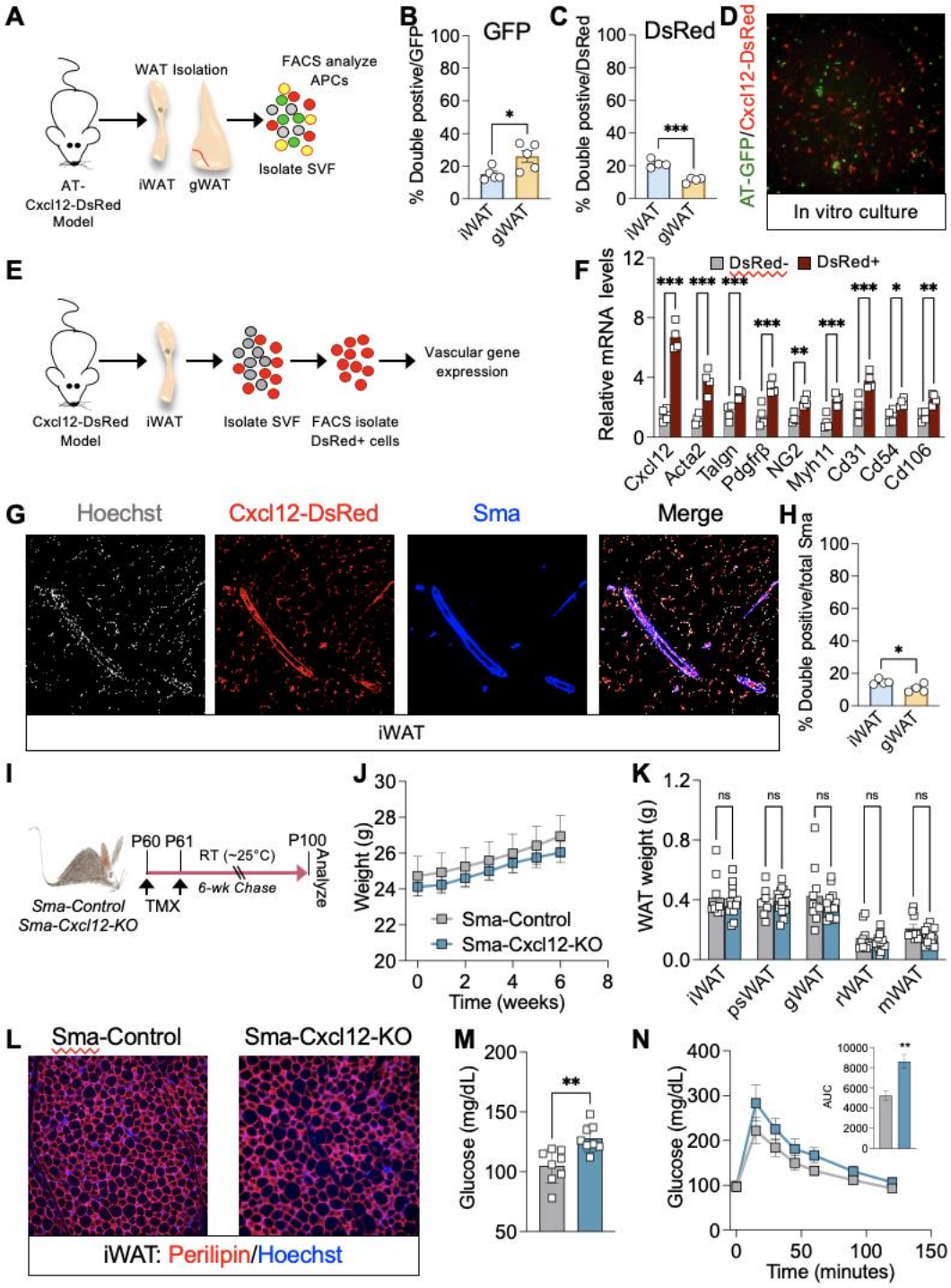

*Figure 10: CXCL12 is Minimally Expressed Within the White Adipocyte Lineage. A) Experimental schema: SV cells were isolated from iWAT and gWAT depots from AT-CXCL12-dsRed mice. Cells were FACS analyzed for colocalization between GFP and dsRed. B) Double positive (AT-GFP and CXCL12-dsRed) compared to the total AT-GFP population. *P ≤ 0.033 by ordinary one-way ANOVA. Data are mean ± s.e.m. C) Double positive (AT-GFP and CXCL12-dsRed) compared to the total CXCL12-dsRed population. ***P ≤ 0.001 by ordinary Students t-test. Data are mean ±*

*s.e.m. D) Representative images of GFP and dsRed colocalization within SV cells were isolated from mice described in (A). Cells were visualized 24 hrs. after plating. E) Experimental schema: SV cells were isolated from the iWAT depot from CXCL12-dsRed mice. Cells were FACS isolated based on dsRed and mRNA was isolated. *P ≤ 0.033; **P ≤ 0.002; ***P ≤ 0.001 by ordinary one-way ANOVA. Data are mean ± s.e.m. F) mRNA levels of denoted genes from cells isolated from mice described in (E). G) Representative images of dsRed and SMA immunostaining of iWAT depots from mice described in (E). Hoechst was used to visualize nuclei. H) SV cells isolated from CXCL12-dsRed mice were FACS analyzed for SMA. Data are presented out of total SMA-antibody positive cells. *P ≤ 0.05 by ordinary one-way ANOVA. Data are mean ± s.e.m. I) Experimental schema: SMA-Control (SMA-CreERT2; or CXCL12/fl) and SMA-CXCL12-KO (SMA-CreERT2; CXCL12$^{fl/fl}$) mice were administered tamoxifen (TMX) at P60 and chased for six-weeks at room temperature (RT). J) Body weight from mice described in (I). K) WAT weight from mice described in (I). L) Representative images of Plin1 immunostaining of iWAT sections from mice described in (I). M) Random fed blood glucose levels from mice described in (I). ; **P ≤ 0.002 by ordinary one-way ANOVA. Data are mean ± s.e.m. N) Glucose tolerance test mice described in (I). Inset: Area under the curve calculation. **P ≤ 0.002 by ordinary one-way ANOVA. Data are mean ± s.e.m.*

Loss of CXCL12 within SMA+ cells promote BAT lipid accumulation

While evaluating the SMA-CXCL12-KO mice, we noticed, upon visual inspection, that mutant BAT appeared paler compared to the reddish-brown hue of control BAT (Figure 11A). Moreover, mutant BAT was considerably smaller than control BAT (Figure 11B and Supplemental Figure 3A). Hematoxylin and eosin (H&E) staining of mutant BAT sections revealed an augmentation in lipid deposition compared to control BAT (Figure 11C and Supplemental Figure 3B). Additionally, triglyceride accumulation assessment demonstrated that SMA-CXCL12-KO BAT had more lipids than control BAT (Figure 11D). In agreement, lipid droplet surface area of CXCL12-KO brown adipocytes was also increased compared to controls (Figure 11E). We next analyzed the molecular phenotype of BAT from six-week chased SMA-Control and SMA-CXCL12-KO mice. Pan-adipocyte genes such as Fabp4, perilipin, and Pparg were equivalently expressed within control and mutant BAT (Figure 11F). In contrast, the levels of brown fat and thermogenic genes such as UCP1, Pgc1a, Cidea, and Cox8b were decreased in CXCL12-KO BAT (Figure 11G). In agreement, mutant BAT sections showed a reduction in UCP1 immunostaining

compared to control BAT sections (Figure 11H). Moreover, UCP1 immunoblotting demonstrated a reduction in UCP1 protein expression within mutant BAT compared to controls (Figure 11I and J). Next, we assessed if CXCL12 altered brown adipogenesis, we isolated BAT SV cells from non-TMX induced SMA-control and SMA-CXCL12-KO mice. In culture, SV cells were administered TMX (1 μM) for two consecutive days to induce genetic recombination and upon confluency cells were induced with brown adipogenic media for eight days. Control and CXCL12-KO BAT precursor cells differentiated with equivalent efficiency into lipid+ adipocytes and expressed similar levels of pan-adipocyte genes (Figure 11K, L). Consistently, both control and mutant brown adipocytes displayed a similar induction of UCP1 in response to CL316,243 treatment (Figure 11M).

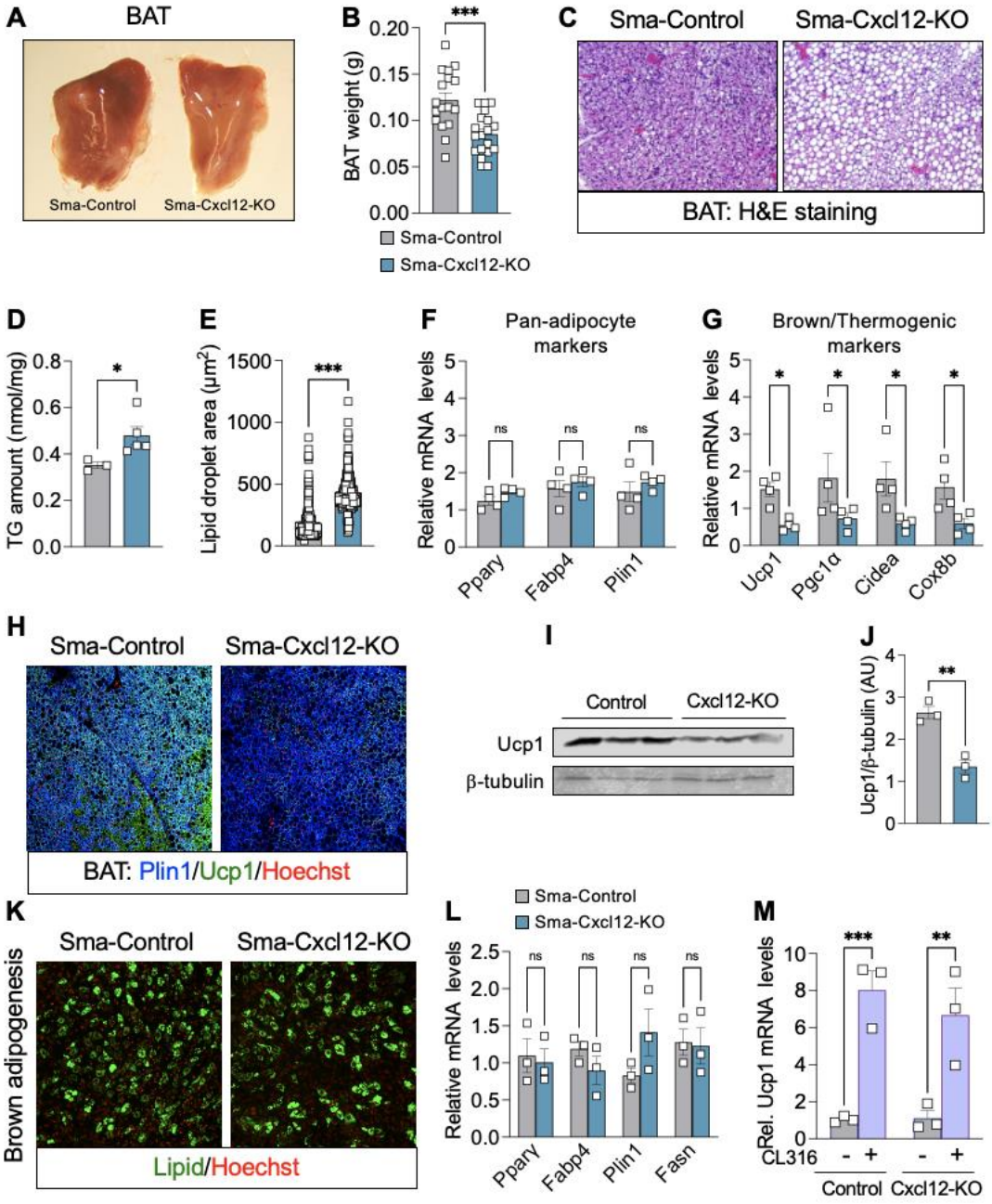

*Figure 11: CXCL12 Sourced from SMA Cells is Critical for Brown Adipocyte Lipid Homeostasis. A) Representative images of BAT from SMA-Control and SMA-CXCL12-KO mice six-weeks post TMX. B) BAT weight from mice described in (A). ***P ≤ 0.001 by ordinary Students t-test. Data are mean ± s.e.m. C) Representative images of hematoxylin and eosin (H&E) staining of BAT from mice described in (A). D) BAT triglyceride (TG) amount (nmol/mg) from mice described in (A). *P ≤ 0.033 by ordinary Students t-test. Data are mean ± s.e.m. E) Lipid droplet area quantification from BAT sections from mice described in (A). n = 5 mice/group (3 images/mouse were quantified). ***P ≤ 0.001 by ordinary Students t-test. Data are mean ± s.e.m. F) mRNA levels of pan-adipocyte markers within BAT from mice described in (A). G) mRNA levels of thermogenic markers within*

*BAT from mice described in (A). *P ≤ 0.033 by ordinary Students t-test. Data are mean ± s.e.m. H) Representative images of immunostaining of Plin1 and UCP1 from BAT sections from mice described in (A). I) Immunoblot of UCP1 and b-tubulin from BAT from mice described in (A). n = 3 individual mice/group. J) Densitometry quantification of UCP1/b-tubulin from the immunoblot in (I). **P ≤ 0.002 by ordinary one-way ANOVA. Data are mean ± s.e.m. K) Representative images of lipid staining of in vitro derived brown adipocytes from isolated BAT SV cells from mice described in (A). L) mRNA levels of denoted pan-adipocyte markers from in vitro derived adipocytes described in (K) M) UCP1 mRNA levels within in vitro derived brown adipocytes described in (K) treated with vehicle (PBS) or Cl316,243 (1 μM; for 12 hrs). **P ≤ 0.002; ***P ≤ 0.001 by ordinary one-way ANOVA. Data are mean ± s.e.m.*

CXCL12 is uniquely expressed within BAT resident SMA+ cells

As a next step, we assessed if CXCL12 expression could be detected within brown adipocytes using the AT-CXCL12-dsRed expression mouse model. But based upon whole-mount immunofluorescence, immunostaining of BAT sections, and in vitro adipogenesis, we were unable to detect dsRed signal within mature brown adipocytes (Supplemental Figure 3C-E). Because SMA+ cells do not generate brown adipocytes, we assessed if CXCL12 could influence brown adipogenesis by isolating brown adipocyte precursor cells from SMA-Control mice and treating them with 50 ng/ml of CXCL12 throughout adipogenesis. Comparably, vehicle and CXCL12 treated cells differentiated into lipid+ and functional brown adipocytes (Supplemental Figure 3F, G). Next, we assessed if BAT was uniquely enriched in CXCL12 cells compared to other organs. Indeed, we found that about ~15-20% of the SVF contained dsRed+ cell, having similar levels to bone marrow (Supplemental Figure 3H, I). In contrast, other tissues such as kidney, liver, and spleen all contained less dsRed+ cells than BAT. Next, we evaluated if BAT SMA+ cells were distinctively enriched with CXCL12. FACs analysis of BAT-derived CXCL12-dsRed cells showed that over 60% of cells were SMA positive (Supplemental Figure 3J, K). On the other hand, like iWAT, CXCL12-SMA+ cellular population represented a small subset of the total BAT SMA+ cellular pool (Supplemental Figure 3L). Collectively, these data suggested that CXCL12 is largely and may exclusively be expressed in BAT SMA+ cells compared to other organs.

Loss of CXCL12 within SMA+ cells block acute BAT thermogenic potential

The notion that deleting CXCL12 within SMA+ cells facilitate BAT reduction and brown adipocyte lipid accumulation made us question if brown adipocyte thermogenesis is impaired in SMA-CXCL12-KO mice. Towards this end, we performed a cold tolerance test on SMA-Control and SMA-CXCL12-KO mutant mice six-weeks post TMX-induced deletion (Figure 12A). We found that mutant mice were significantly more sensitive to cold temperatures within the first 24 hrs. compared to control littermates (Figure 12B). However, by 48 hrs. of cold exposure, body temperatures between control and mutant mice normalized and remained comparable throughout the cold challenge (Supplemental Figure 4A). Furthermore, we noted smaller mutant BAT depots at 24 hrs. but after seven days of cold exposure they appeared normalized to control levels (Figure 12C). Histological profiling identified the presence of enhanced lipid deposition within SMA-CXCL12-KO BAT at 0, 6, 12, and 24 hrs. post cold exposure. However, by 48 and 168 hrs. (7 days) of cold exposure, BAT histology looked similar between control and mutant mice (Figure 12D). Additionally, directed qPCR showed an initial reduction in UCP1 but was completely restored after seven-days of cold exposure (Figure 12E, F). Metabolic cage analysis showed comparable oxygen consumption between RT housed control and mutant mice (227). However, upon initial cold exposure mutant mice had a reduction in oxygen consumption (Figure 12G). Of note, a significant reduction in oxygen consumption remained after three days of cold exposure, while our histological and rectal temperature data a normalization between control and mutant mice. Because SMA+ cells can serve as beige adipocyte progenitors, we evaluated if beige fat formation was affected by CXCL12 deletion within the SMA lineage after seven days of cold exposure. Yet, beige fat appearance and thermogenic markers within iWAT depots appeared like controls (Supplemental Figure 4B-G).

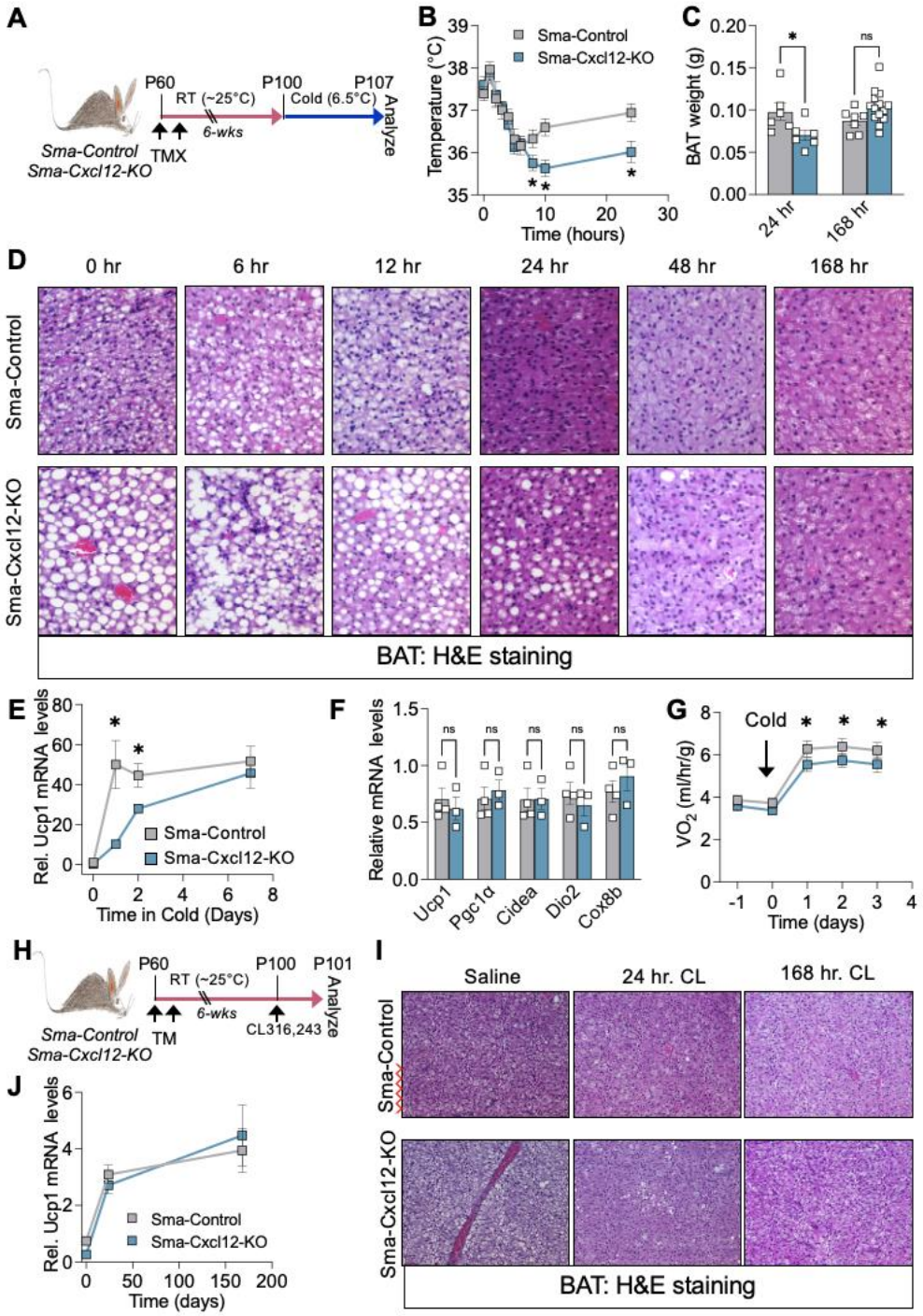

*Figure 12: CXCL12 Sourced from SMA Cells is Critical for Acute BAT Thermogenesis. A) Experimental schema: At P60, SMA-Control and SMA-CXCL12-KO mice were administered TMX. After a six-week chase, mice were exposed to cold temperature (6.5C) uptil seven days. B) Rectal temperatures of mice described in (A) were measured every hour for the first six hours then at 8, 10, and 24 hrs. *P ≤ 0.033 by ordinary Students t-test. Data are mean ± s.e.m. C) BAT weight from mice described in (A) after 24 hrs and 168 hrs (7 days) in the cold. *P ≤ 0.033 by ordinary*

*Students t-test. Data are mean ± s.e.m. D) Representative images of H&E staining of BAT from mice described in (A) after 0, 6, 12, 24, 48, and 168 hrs. of cold exposure. E) UCP1 mRNA levels within BAT from mice described in (A) maintained in the cold for 0, 24, 48, and 168 hrs. *P ≤ 0.033 by ordinary Students t-test. Data are mean ± s.e.m. F) mRNA levels of denoted brown adipocyte and thermogenic markers within BAT from mice described in (A). G) Mice described in (A) were placed in a metabolic cage and oxygen consumption (whole day) was measured at RT and cold exposure (3 days; 72 hrs). n= 4-5 mice/group. *P ≤ 0.033 by ordinary Students t-test. Data are mean ± s.e.m. H) Experimental schema: At P60, SMA-Control and SMA-CXCL12-KO mice were administered TMX. After a six-week chase, mice were administered CL316,243 (CL) daily for 24 and 168 hrs. I) Representative images of H&E staining of BAT sections from mice described in (H). J) UCP1 mRNA levels within BAT from mice described in (H) administered CL for 24 and 168 hrs.*

CXCL12 does not directly regulate brown adipocyte thermogenesis

Our cold temperature studies suggested that CXCL12 may regulate acute BAT thermogenesis. To test if CXCL12 directly impacts the thermogenic capacity of brown adipocytes, we acutely administered the β3-adrenergic receptor agonist, CL316,243 (CL) to SMA-Control and SMA-CXCL12-KO mice six-weeks post TMX-induction (Figure 12G) (31, 224, 228). As we observed above, histological staining of BAT from saline treated mutant mice showed increased BAT lipid deposition compared to control mice. In response to one injection (acute) of CL, mutant BAT appeared histologically comparable to control BAT (Figure 12H). In agreement, directed qPCR showed that brown and thermogenic genes were comparably induced (Figure 12I). Moreover, we treated a cohort of control and mutant mice chronically (seven days) with CL and evaluated brown adipose tissue recruitment and lipid accumulation. Both histological and gene expression analysis revealed no differences in brown fat appearance or function between control and mutant mice (Figure 12H, I). Based on these data it appears that CXCL12 may not directly regulate brown adipocyte thermogenesis.

Defective BAT function is often correlated with susceptibility to diet-induced obesity and metabolic dysfunction (198, 229). Therefore, we challenged SMA-Control and SMA-CXCL12-KO mice with high fat diet for eight-weeks (Supplemental Figure 4K). While on HFD no

significant differences in body weight or fat content were observed between control and mutant mice (Supplemental Figure 4L, M). Yet, we did note that glucose clearance was slightly impaired (Supplemental Figure 4N). WAT depots between control and mutants appeared similar in weight (Supplemental Figure 4O). However, SMA-CXCL12-KO BAT was significantly smaller than control BAT (Supplemental Figure 4P). In agreement, histological evaluation revealed more unilocular brown adipocytes could be observed in mutant BAT sections compared to controls (Supplemental Figure 4Q). Changes in BAT morphology were also associated with lower UCP1 and other thermogenic markers (Supplemental Figure 4R, S).

CXCR4 antagonism regulates BAT lipid accumulation

Two CXC-motif chemokine receptors (CXCR) have been shown to bind CXCL12 with high affinity: CXCR4 and CXCR7 (230). CXCL12 is the sole ligand for CXCR4, and CXCR4 has been implicated in brown adipocyte biology (216). Therefore, we first assessed if chemically inhibiting CXCR4 recapitulated the SMA-CXCL12-KO BAT phenotype by treating male mice for four-weeks with AMD3100 (5 mg/Kg; Plerixafor), a CXCR4 antagonist and FDA approved immunostimulant (Figure 13A) (231). We did not observe differences in body weight, body fat content, or glucose tolerance between vehicle and AMD3100 treated mice (Supplemental Figure 5A-C). Moreover, AMD3100 did not provoke distinguishable differences between WAT, BAT, or organ weight (Figure 13B and Supplemental 5D, E). Nonetheless, like the SMA-CXCL12-KO model, we did observe histological "whitening" of BAT specimens treated with AMD3100 (Figure 13C, D). BAT gene expression examination of AMD3100 treatment mice revealed a downregulation in thermogenic markers (Figure 13E). However, in vitro, AMD3100 did not appear to influence brown fat adipogenic potential (Figure 13F, G). On the hand, white adipocytes

appeared histologically similar between vehicle and AMD3100 treated mice (Supplemental Figure 5F).

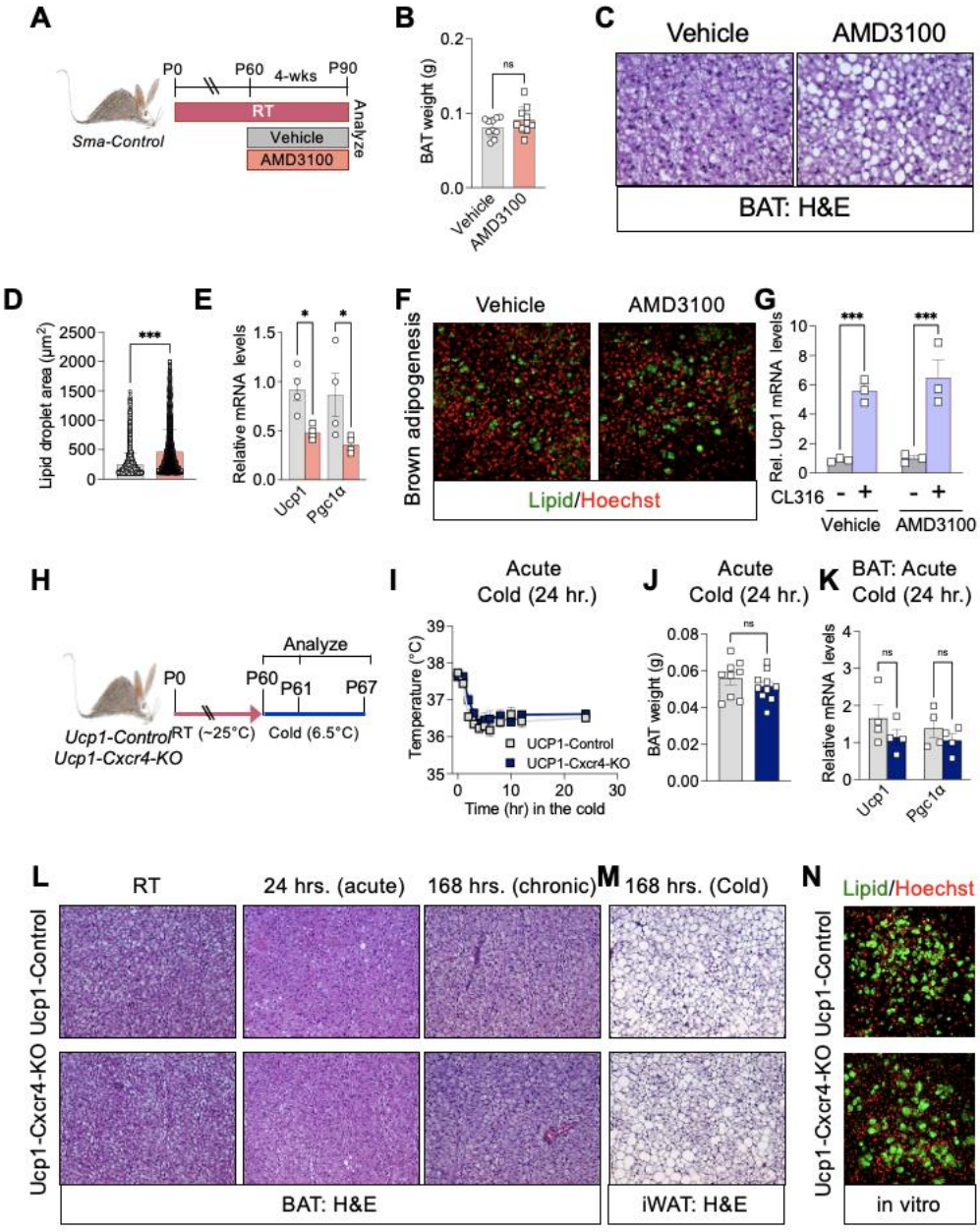

Figure 13: CXCR4 is Required for Brown Adipocyte Lipid Accumulation but Independent of CXCR4 Brown Adipocyte Expression. A) Experimental schema: At P60, Sma-Control were administered vehicle (PBS) or AMD3100 (5mg/Kg IP 4x/week for four weeks). n = 10 mice/group. B) BAT weight from mice described in (A). Rectal temperatures of mice described in (A) were measured every hour for the first six hours then at 8, 10, and 24 hrs. C) Representative images of H&E staining of BAT from mice described in (A) D) Lipid droplet area quantification from BAT

*sections from mice described in (A). n = 5 mice/group (3 images/mouse were quantified) ***P ≤ 0.001 by ordinary Students t-test. Data are mean ± s.e.m. E) UCP1 and Pgc1a mRNA levels within BAT from mice described in (A). *P ≤ 0.033 by ordinary Students t-test. Data are mean ± s.e.m. F) BAT SV cells were isolated from mice described in (A) and induced with brown adipocyte adipogenic media. Lipids were visualized for adipogenic potential. G) UCP1 mRNA levels within in vitro derived brown adipocytes described in (F) treated with vehicle (PBS) or Cl316,243 (1 µM; for 12 hrs). ***P ≤ 0.001 by ordinary Students t-test. Data are mean ± s.e.m. H) Experimental schema: UCP1-Control (UCP1-Cre) and UCP1-CXCR4-KO (UCP1-Cre; CXCR4$^{fl/fl}$) were maintained at RT until P60; subsequently, mice were cold exposure for 24 (acute) or 168 (chronic) hrs. n = 9-10 mice/group I) Rectal temperatures of mice described in (H) were measured every hour for the first six hours then at 8, 10, and 24 hrs. J) BAT weight from mice described in (H) after 24 hrs in the cold. K) UCP1 and Pgc1a mRNA levels within BAT from mice described in (H) after 24 hrs of cold exposure. L) Representative images of H&E staining of BAT sections from mice described in (H) after 24 and 168 hrs of cold exposure. M) Representative images of H&E staining of iWAT sections from mice described in (H) after 168 hrs of cold exposure. N) Representative images of lipid staining of in vitro derived brown adipocyte adipogenesis from BAT SV cells isolated UCP1-Control and UCP1-CXCR4-KO mice at P60.*

CXCR4 is not required for brown adipocyte lipid accumulation or thermogenesis

To directly evaluate if CXCR4 controls brown adipocyte lipid deposition, we generated UCP1-Cre; CXCR4$^{fl/fl}$ (UCP1-CXCR4-KO mice) and evaluated room temperature (RT) housed mice at P60 (Figure 13H). At P60, we found that mice maintained at RT harboring the brown adipocyte specific CXCR4 deletion did not have changes in body, WAT, or BAT weight (Supplemental Figure 5H-J). In contrast to the CXCR4 antagonist treated mice, UCP1-CXCR4-KO mice did not exhibit BAT morphological "whitening" (Figure 13L). To test the thermogenic capacity of CXCR4 deficient BAT, we cold temperature challenged UCP1-Control and UCP1-CXCR4-KO and evaluated them at 24 and 168 hrs. post cold exposure (Figure 13H). Phenotypic, histologic, and molecular profiling revealed that both control and mutant mice responded equivalently to acute and chronic cold temperature challenge (Figure 13I-L and Supplemental Figure 5K-M). In response to chronic cold (7 days), UCP1-CXCR4-KO did not display changes in WAT weight, beige adipocyte appearance, or thermogenic gene expression compared to UCP1-Control littermates (Figure 13M and Supplemental Figure 5M, N). We then took an in vitro

approach by isolating BAT SV cells from UCP1-Control and UCP1-CXCR4-KO mice and examined their differentiation potential. Control and mutant precursor cells differentiated equivalently into mature lipid droplet containing adipocytes (Figure 13N). Taken together, our BAT-specific CXCR4 studies do not appear to recapitulate the SMA-CXCL12-KO model, nor did we observe a functional role for CXCR4 in regulating BAT lipid levels as previously reported. Yet, our CXCR4 antagonist data do support the role of CXCL12/CXCR4 in regulating BAT lipid accumulation

CXCL12 regulates BAT sympathetic innervation

Our findings suggest that CXCL12 signaling controls BAT lipid deposition independent of brown adipocyte regulation. Because BAT is densely innervated and sympathetic neurons produce noradrenaline to stimulate lipolysis, we hypothesized that the loss of CXCL12 might foster brown adipocyte lipid accumulation by reducing BAT sympathetic innervation. To assess BAT sympathetic innervation, we performed tyrosine hydroxylase (TH) immunostaining on RT housed SMA-control and SMA-CXCL12-KO mutant mice six-weeks post TMX induction. Markedly, TH immunostaining was significantly reduced in Cxcl12 mutant mice compared to control BAT (Figure 14A). In support of this notion, immunoblotting confirmed less TH in mutant BAT than control BAT depots (Figure 14B, C). Quantification of TH neuron length from immunostained BAT sections revealed a reduction in sympathetic outgrowth in mutant BAT compared to controls (Figure 14D). Additionally, immunostaining against TUBB3, a neural-specific tubulin, showed less innervation in response to CXCL12 loss (Supplemental Figure 6A). We also evaluated if CXCL12 ablation affected iWAT innervation after cold exposure. However, iWAT TH presence appeared similar between control and mutants after seven-days of cold exposure (Supplemental Figure 6B). Based on H&E staining and molecular profiling in Figure 12, we hypothesized that

TH+ neurite growth might be restored in mutant mice after cold exposure. Indeed, after 24 hrs. of cold exposure, a reduction in TH immunostaining could still be observed in mutant mice (Figure 14E). But after seven days of cold exposure TH presence was indistinguishable between mutant and control BAT sections (Figure 14E). Overall, our data suggest that CXCL12 may regulate brown adipocyte lipid accumulation by supporting sympathetic neuron presence and growth.

We assessed if disrupting CXCR4 activity reduced BAT TH presence. We evaluated BAT sections from vehicle or AMD3100 treated mice for four weeks as described in Figure 13H for TH immunopositivity. We found that AMD3100 significantly reduced the amount of BAT TH presence throughout the tissue (Figure 14F). Moreover, TH+ sympathetic outgrowths were shorter in AMD3100 treated mice compared to vehicle (Figure 14G). Conversely, we did not observe changes in TH immunostaining between UCP1-Control and UCP1-CXCR4-KO BAT (Supplemental Figure 6C). Overall suggesting that CXCL12 can influence TH sympathetic neural presences in a CXCR4 dependent but independent of CXCR4-brown adipocyte function,

Rodents experience thermal stress at RT; accordingly, rearing or housing mice at 30ºC (thermoneutrality) alleviates cold-induced signals by deactivating adrenergic signaling allowing BAT to "whiten" (232-234). We hypothesized that CXCL12-induced brown adipocyte lipid accumulation and loss of sympathetic innervation resembled mice acclimated to thermoneutrality. Towards this end, RT reared SMA-Control and SMA-CXCL12-KO mice were housed at thermoneutrality (30ºC) starting at P30. Three weeks after TN (~P50), mice were administered TMX and chased for six-weeks (Figure 14G). Over the six-week period, control and mutant mice gained weight equivalently (Figure 14H). Additionally, WAT weight appeared indistinguishable between control and mutant mice (Figure 14I). But identifiable mutant BAT weighed less than control BAT (Figure 14J). H&E staining revealed more unilocular-like and lipid engorged brown

adipocytes in mutant BAT sections than in control specimens (Figure 14K). Directed qPCR analysis showed a reduction in thermogenic gene expression in mutant BAT compared to control samples; however, the pan-adipocyte marker, Plin1, remained unchanged (Supplemental Figure 6D). Moreover, TH immunostaining revealed a significant regression of sympathetic neurons within BAT of SMA-CXCL12-KO mice compared to TN controls (Figure 14M). In agreement with the notion of disrupted BAT, fed glucose levels were higher in mutant mice compared to controls (Figure 14N). These data support the notion that CXCL12 may regulate BAT sympathetic innervation to control brown adipocyte lipid levels.

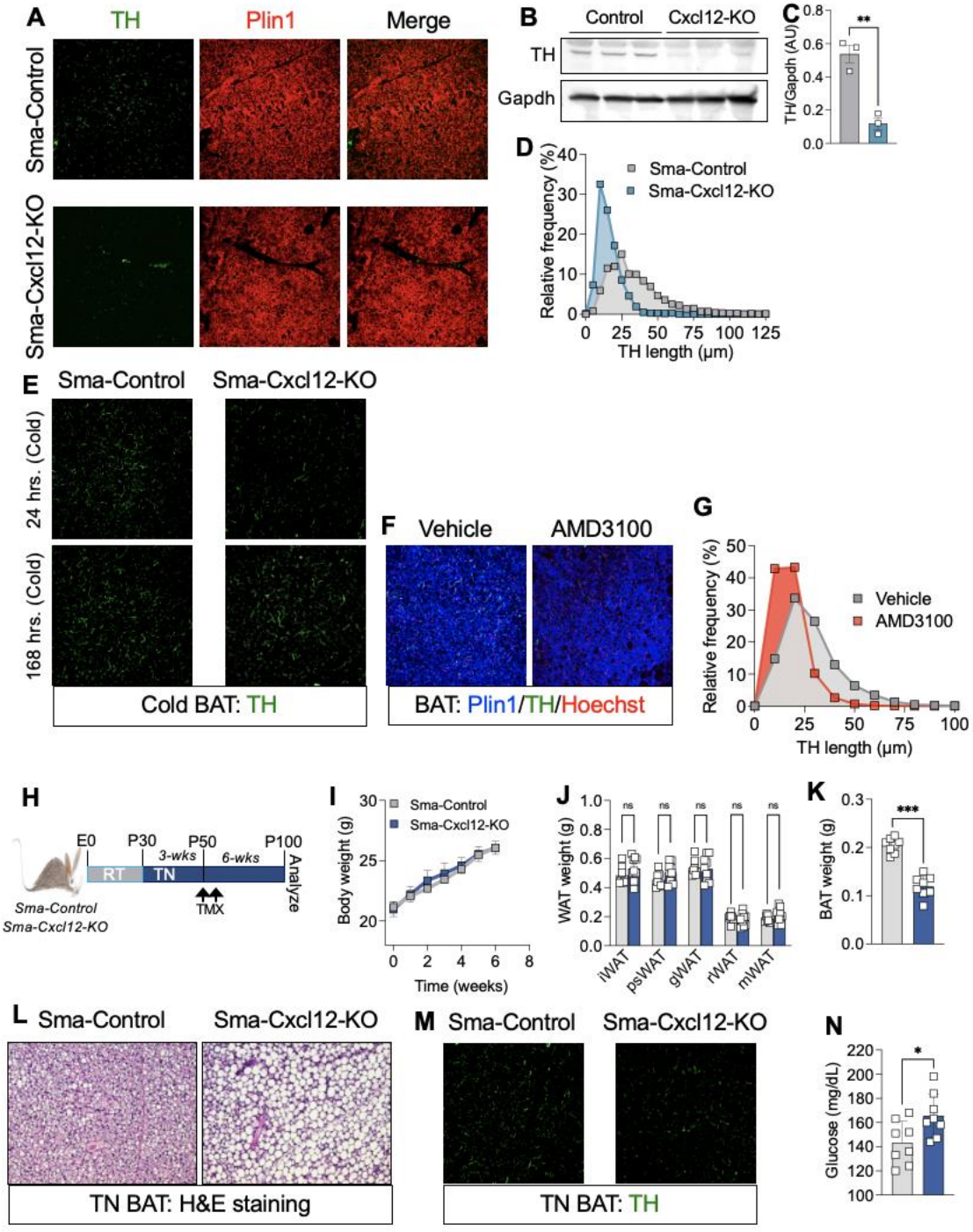

*Figure 14: CXCL12 is Required for BAT Sympathetic Innervation. A) Representative images of TH immunostaining of BAT sections from SMA-Control and Sma-Cxcl12-KO mice six-weeks post-TMX maintained at RT. B) Representative immunoblots of TH protein levels from BAT from mice described in (A). n = 3 mice/group. C) Quantification of the TH immunoblot described in (B). **P ≤ 0.002 by Students t-test. Data are mean ± s.e.m. D) Quantification of TH length from TH immunostaining images described in (A). E) Representative images of TH immunostaining of BAT sections from SMA-Control and Sma-Cxcl12-KO mice six-weeks post-TMX maintained at cold*

*temperatures for 24 and 168 hrs. F) Representative images of TH immunostaining of BAT sections from SMA-Control treated with vehicle or AMD3100 (5 mg/Kg 4x/week for four-weeks) maintained at RT. G) Quantification of TH length from TH immunostaining images described in (F). n = 5 mice/group (3 images/mouse were quantified) H) Experimental schema: SMA-Control and Sma-Cxcl12-KO mice were maintained at RT until P30. Subsequently, mice were housed at TN (30C) for three-weeks then administered TMX then chased for six-weeks then evaluated. n= 8 mice/group. I) Body weight after from mice described in (H). J) WAT weight after from mice described in (H). K) BAT weight from mice described in (H). ***P ≤ 0.001 by ordinary Students t-test. Data are mean ± s.e.m. L) Representative images of H&E staining of BAT from mice described in (H). M) Representative images of TH immunostaining from mice described in (H). N) Random blood glucose levels from mice described in (H). *P ≤ 0.033 by Students t-test. Data are mean ± s.e.m.*

CXCL12 maintains BAT M2 macrophage to support innervation

Our data suggest that CXCL12 regulates sympathetic extensions in BAT; yet, how does CXCL12 change sympathetic innervation? While examining SMA-CXCL12-KO BAT histological sections, we noticed a reduction in overall nuclei number compared to control sections (Figure 12D). This raised the possibility that the loss of CXCL12 might influence the surrounding niche cells to disrupt sympathetic innervation. In our model, CXCL12 is depleted in Sma+ smooth muscle cells thus, we evaluated changes in endothelial and smooth muscle cell markers within BAT (235). However, mRNA analysis revealed similar levels of gene expression between control and mutant BAT samples (Figure 15A). Since CXCL12/CXCR4 chemokine signaling can regulate immune cell mobilization and retention, we evaluated BAT macrophage and immunological markers from control and mutant mice. Gene expression of the generalized immunological marker, F4/80, was considerably lower in mutant BAT compared to control samples (Figure 15B). In agreement, flow cytometric analysis of CD68, a broad macrophage marker, revealed a reduction in the total number of BAT macrophages (Figure 15C). M2 macrophages are often associated with metabolic health and potential thermogenic function and can become disrupted in response to changes in temperature and diet. Therefore, we speculated that M2 macrophages may be altered in response to CXCL12 deletion. Consistent with this notion, directed qPCR analysis revealed a reduction in

anti-inflammatory markers (IL-10, IL-13) and lower M2 macrophage markers (Cd301 (Clec10a), CD163, and Arg1) (Figure 15D). However, we did not observe differences in pro-inflammatory markers such as tumor necrosis factor alpha (TNFα), interleukin-6 (IL-6) or IL-8 (Figure 15D). In alignment, flow cytometric analysis revealed a reduction in the frequency and abundance of Cd301+ macrophages in SMA-CXCL12-KO BAT compared to controls (Figure 15E and Supplemental Figure 7A, B). Yet, within iWAT depots the Cd301 cell frequency was equivalent between control and mutants (Supplemental Figure 7C). HFD signals also reduces M2 macrophage presence; therefore, we asked if M2 macrophage was exacerbated in SMA-CXCL12-KO mice fed a HFD. Indeed, by flow cytometric analysis, mice fed a HFD for eight weeks showed a significant reduction in the frequency and abundance of Cd301+ cells but this effect was heightened in the mutant mice in both BAT and iWAT depots (Figure 15E and Supplemental Figure 7C).

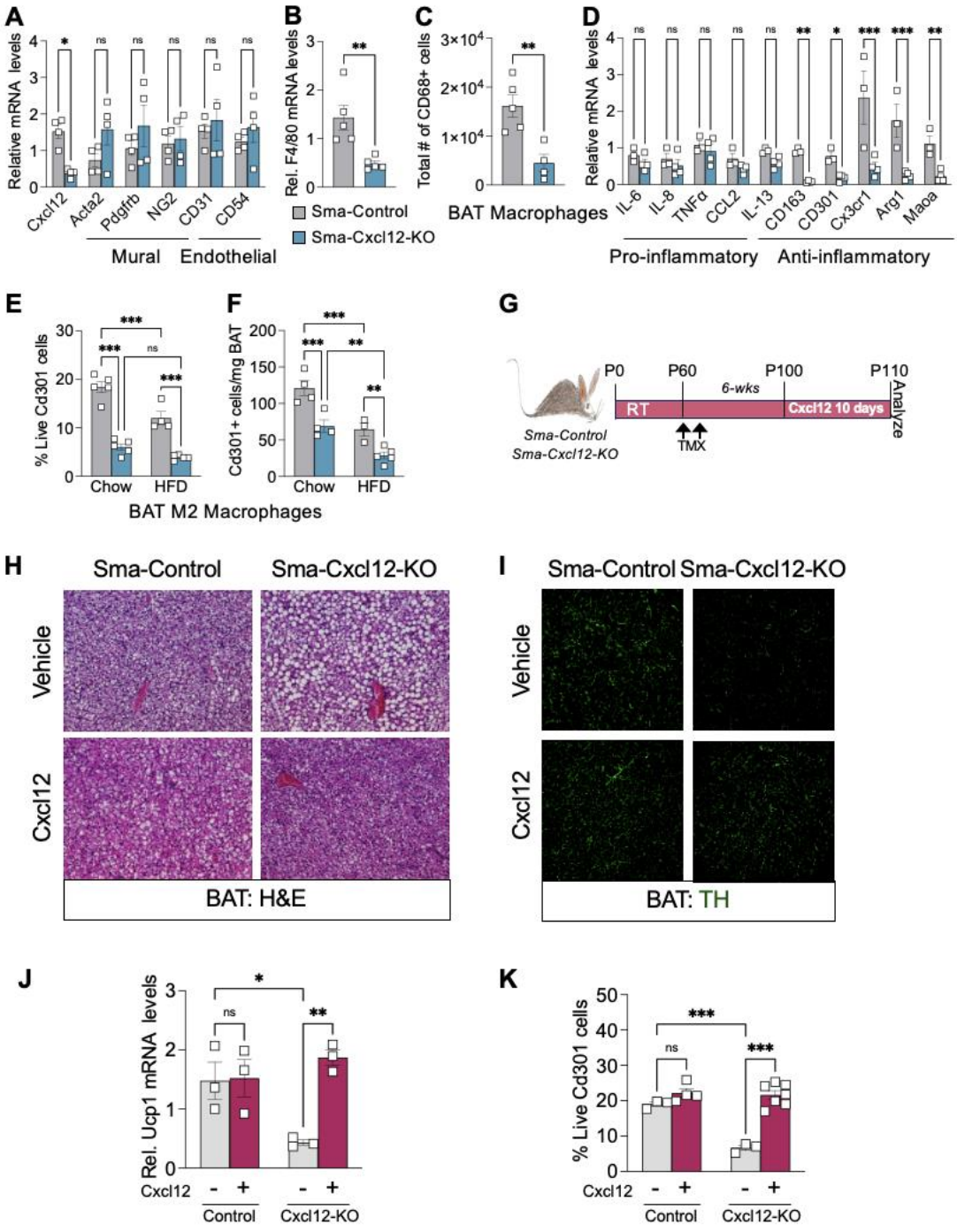

*Figure 15: CXCL12 is Sufficient for M2 Macrophage BAT Accrual. A) mRNA expression levels of denoted mural and endothelial cell markers within BAT of SMA-Control and Sma-Cxcl12-KO mice six-weeks post-TMX. *P ≤ 0.033 by ordinary one-way ANOVA. Data are mean ± s.e.m. n = 4-3 mice/group. B) mRNA expression levels of F4/80 within BAT of mice described in (A). n =5 mice/group. **P ≤ 0.002 by ordinary Students t-test. Data are mean ± s.e.m. C) Total number of CD68+ cells within BAT by FACS analysis. n = 5-4 mice/group. **P ≤ 0.002 by ordinary Students t-test. Data are mean ± s.e.m. D) mRNA expression levels of denoted pro-inflammatory and anti-*

*inflammatory markers within BAT from mice described in (A). *P ≤ 0.033; **P ≤ 0.002; ***P ≤ 0.001 by ordinary one-way ANOVA. Data are mean ± s.e.m. E) FACS analysis of CD301 frequency within BAT from mice described in (A) and from mice fed a HFD for 8 weeks beginning three weeks post-TMX. ***P ≤ 0.001 by ordinary one-way ANOVA. Data are mean ± s.e.m. F) FACS analysis of CD301 adundance within BAT from mice described in (A) and from mice fed a HFD for 8 weeks beginning three weeks post-TMX. ***P ≤ 0.001 by ordinary one-way ANOVA. Data are mean ± s.e.m. G) Experimental schema: Sma-Control and Sma-Cxcl12-KO mice were administered TMX at P60, chased for six-weeks then administered vehicle or Cxcl12 (100 ng/mouse) for 10 consecutive days. n = 3-7 mice/group H) Representative images of H&E staining from mice described in (F). I) Representative images of TH immunostaining from mice described in (F). J) mRNA expression levels of Ucp1 within BAT from mice described in (F). *P ≤ 0.033; **P ≤ 0.002 by ordinary one-way ANOVA. Data are mean ± s.e.m. K) FACS analysis of CD301+ cells within BAT from mice described in (F). ***P ≤ 0.001 by Students t-test. Data are mean ± s.e.m.*

CXCL12 promotes BAT innervation via macrophage accretion

Our data suggest that CXCL12 may regulate sympathetic innervation by controlling M2 macrophage accrual. Therefore, we hypothesized that CXCL12 might be sufficient to retain M2 macrophages to sustain BAT sympathetic innervation and raised the possibility that administering CXCL12 to SMA-CXCL12-KO mice might restore innervation, reducing brown adipocytes lipid accumulation. Towards this end, we administered CXCL12 for 10 consecutive days to TMX induced SMA-Control and SMA-CXCL12-KO mice (Figure 15F). By H&E staining, we observed that mutant mice receiving CXCL12 reduced lipid accumulation compared to vehicle-treated mutant mice (Figure 15G). Moreover, BAT TH immunostaining revealed restored innervation after CXCL12 administration in mutant mice compared to CXCL12-KO mice receiving vehicle (Figure 15H). Finally, we observed that treating SMA-CXCL12-KO mice with CXCL12 restored Cd301 macrophage numbers compared to vehicle-treated mice (Figure 15I). Overall, we find that CXCL12 is sufficient to drive Cd301 macrophage recruitment to restore sympathetic innervation of BAT.

2.4. Discussion

The generation of thermogenic fat cells (brown and beige) is clinically desirable due to their ability to futilely burn glucose and free fatty acids, generating heat rather than cellular energy (198). Accordingly, much attention has focused on fat cell-intrinsic factors controlling brown and beige adipocyte thermogenesis (236-238). However, a major obstacle has been the inability to examine niche regulatory factors that control the thermogenic process and BAT perdurance. Our findings have revealed an intricate function of BAT smooth muscle cells to secrete CXCL12 to support and retain local anti-inflammatory macrophages, which appear to be essential for maintaining BAT sympathetic innervation.

CXCL12/CXCR4 signaling is involved in several aspects of stem cell biology, hemopoiesis maturation, and embryonic tissue development and function. In addition, recent CXCL12/CXCR4 signaling research has extended beyond developmental regulation to suggest a role in adipose tissue biology and systemic metabolisms such as inflammation and insulin resistance (179). Yet, such regulatory functions of CXCL12 and CXCR4 have been suggested to emanate from mature adipocytes. Interestingly, our studies do not appear to support a role for CXCL12 expression within adipocytes, nor do our studies ascribe a functional role for CXCL12 in adipocyte biology. Using a variety of genetic and molecular approaches, we were unable to detect CXCL12 native expression within mature adipocytes under chow or HFD conditions. Also, we did not observe changes in adipogenic potential in vitro when APCs were treated with recombinant CXCL12. Unfortunately, the relative centimorgan proximity on chromosome 6 between PPARγ, the RosaR26 allele—used in fate mapping reporter systems—and CXCL12 loci prevents detailed genetic and fate mapping analyses of CXCL12 within the adipose lineage (84, 218, 239). Similarly, CXCR4 has been shown to regulate brown adipocyte lipid accumulation

(176, 216). However, at RT or upon cold temperature exposure, we could not detect physiological or morphological changes in response to CXCR4 brown adipocyte deletion. It is unclear what defines the differences in our studies compared to others. However, it may be related to the mouse strain background, vivarium conditions, gut microbiota, dietary stress, and in vitro cell lines used. Further assessment of CXCL12 and CXCR4 within the adipose lineage will be critical to understanding how this signaling pathway controls metabolism.

Several studies have suggested that BAT homeostasis and thermogenesis defects impair metabolic fitness in response to chronic overnutrition (240). Indeed, we observe subtle changes in glucose metabolism in response to CXCL12 deletion; however, we do not observe significant systemic metabolic effects, as previously demonstrated. Our observations may be due to timing and phenotypic evolution. For example, we administered HFD three weeks post CXCL12 deletion, which shows changes in BAT macrophage composition and innervation but may not be sufficient to exacerbate the metabolic phenotype in response to HFD. Thus, the degree and penetrance of the phenotype probably is a critical regulator of BAT metabolic perturbation and systemic metabolism in response to diet-induced obesity.

Our CXCR4 antagonism data demonstrate the involvement in CXCR4 mediated BAT innervation and brown adipocyte lipid homeostasis. Our studies identify that CXCR4 is expressed on Cd301+ M2 macrophages, yet how does CXCR4 function within these macrophages to regulate sympathetic innervation, and is CXCR4 required for Cd301 macrophage BAT retention? Recent work has suggested that Cx3Cr1+ BAT macrophages, an M2 macrophage subpopulation, can support BAT innervation through the regulation of Mecp2, a nuclear transcription regulator that is often mutated in Rett syndrome (241, 242). Genetic loss of Mecp2, within Cx3Cr1+ macrophages, causes an upregulation of Plexin A4, a protein involved in axon pruning and repulsion via

semaphorin receptor activity (243, 244). This hyper-interaction between Plexin A4 and semaphorin may be why these dysfunctional macrophages impede sympathetic innervation and lower norepinephrine tone (241). It will be interesting to determine if CXCL12/CXCR4 regulates the Mecp2-Plexin A4 pathway in Cd301+ macrophages to regulate BAT sympathetic tone. Moreover, other factors such as Slit3 have been shown to regulate sympathetic innervation of brown and beige thermogenic tissue via macrophages (245); thus, other pathways may exist to support macrophage accrual and sympathetic innervation.

Adipose tissue anti-inflammatory macrophages are critical for tissue homeostasis (246). However, these efforts have focused on conditions such as HFD induced obesity or cold challenge associated with local inflammatory changes (247). Regarding thermogenesis, these reports on inflammatory cells such as group 2 innate lymphocytes, leukocytes, and eosinophils, have centered around beige adipocyte development rather than brown adipocyte macrophage composition and function (212, 248-253). The metabolic changes induced in the absence of BAT Cd301+ macrophages reveal the critical physiological involvement in governing sympathetic innervation. Moreover, our data suggest an even deeper layer of complexity exists by demonstrating that BAT smooth muscle cells can control macrophage recruitment and retention. Our studies also demonstrate that the plasticity of smooth muscle cells dynamically changes the expression of CXCL12 in response to feeding conditions and temperature fluctuations. While our FACs studies suggest that SMA cells within BAT express CXCL12 other SMA+ cells in other tissues may be facilitating BAT macrophage accrual and sympathetic neuronal growth. In general, studies aimed at identifying and characterizing tissue reside vascular cells such as endothelial, smooth muscle, and adventitial fibroblasts will provide insight into unique regulating mechanisms governing tissue function and homeostasis. Additionally, more evidence directed at changes in other BAT niche

regulator cells could provide crucial insight into brown adipocyte thermogenesis and function (254).

In the SMA-CXCL12-KO mice, BAT function and thermogenesis are initially blunted; however, chronic cold temperature exposure can overcome the defects introduced by the lack of CXCL12. This suggests that compensatory mechanisms could exist to stimulate sympathetic innervation over extended periods of cold temperature exposure. Moreover, other cell types may facilitate Cd301+ macrophage recruitment to engage sympathetic nerve growth and norepinephrine release. This finding highlights the specialized functionality of macrophages but also the requirement of other chemokine networks that may facilitate BAT innervation and thermogenesis (255).

Collectively, we have established a previously unknown homeostatic function of BAT smooth muscle cells to retain a subset of macrophages that control BAT innervation and thermogenesis. Altered BAT innervation disrupts BAT homeostasis increasing lipid accumulation and impairing acute thermogenic responses, altering energy homeostasis. Our results identify a unique role for CXCL12/CXCR4 signaling to retain and support M2 macrophages within BAT to bolster sympathetic innervation to control BAT thermogenesis. Prospective studies aimed at other niche regulatory cells within BAT could uncover new avenues to regulate brown adipocyte thermogenesis. Finally, our data suggest that maintaining supportive BAT macrophages via CXCL12 signaling could be a mechanism to brown adipocyte perdurance and metabolic homeostasis.

Author Contributions:

BMS and AMB conducted animal husbandry, physiological measurements, pharmacological treatments, and histological analysis. BMS additionally conducted metabolic cage and in vitro cell culture experimentation. AMB additionally conducted flow cytometry and western blotting. DL and JF conducted histological analysis, immunostaining, and RNA isolation. DL additionally conducted qPCR analysis and tyrosine hydroxylase quantification. YJ and DCB designed experimentation, interpreted results, and wrote the manuscript. All authors discussed results and commented on the manuscript.

2.5. Materials and Methods

Mouse models: Mice were maintained on a 14:10-hour light/dark cycle with free access to food and water. *Sma-Cre^{ERT2}* mouse model was generously obtained from Drs. Pierre Chambon and Daniel Metzger (226). *Sma-Cre^{ERT2}* mice were combined with either R26-^{tdtomato} (stock #007914) or R26-^{mTmG} (stock #007676) mice from Jackson Laboratories. *Sma-Cre^{ERT2}* reporter mice were crossed with either *Pdgfrb*^{D849V} (stock #018435) or *Pdgfrb$^{fl/fl}$* (stock #010977) from Jackson Laboratories. AdipoTrak was previously created using the following genetic models: Pparg-tTA (stock #024755 Jackson Laboratories) and TRE-H2B-GFP (generously provided by Dr. Tudorita Tumbar)(84). Ucp1-Cre (stock #024670), Cxcl12fl/fl (stock #021773); Cxcl12-DsRed (stock #022458), Cxcr4fl/fl (stock #008767) were purchased from Jackson Laboratories. Offspring were intercrossed for six generations prior to experimentation and were maintained on mixed C57BL/6J-129SV background. To induce recombination, denoted mice were administered one dose of TMX (50 mg/Kg; Cayman Chemical: 13258) dissolved in sunflower seed oil (Sigma, item no: S5007) for two consecutive days via intraperitoneal (IP) injection. After the final TMX

injection, mice were maintained for seven days at room temperature prior to experimentation, as a TMX washout period. For cold temperature exposure, mice were housed in a 6.5ºC cold chamber (Power Scientific RIS70SD) or mice were maintained at RT (~22ºC). For thermoneutrality experiments, mice were house in a 30ºC chamber (Power Scientific RIS70SD). All animal experiments were performed on 3 or more mice per cohort and performed at least twice. All animal experiments were performed according to procedures approved by the Cornell University Institutional Animal Care and Use Committee under the auspices of protocol number 2017-0063.

Physiological measurements: Temperature was monitored daily (~18:00 EST) using a TH-5 ThermalertClinical Thermometer (Physitemp) attached to a RET-3 rectal probe for mice (Physitemp). Prior to insertion, the probe was lubricated with glycerol and was inserted 1/2 inch and temperature was measured once stabilized. Glucose monitoring: blood glucose levels were measured with a Contour glucometer (Bayer) and with Contour glucose strips.

Pharmacological treatments: For Cxcl12 treatments, mice at the denoted time points were administered one dose of vehicle (1X PBS with 1% BSA) or one dose of recombinant Cxcl12 (100 ng/mouse; PeproTech: 250-20A) dissolved in 1X PBS with 1% BSA for ten consecutive days via IP injection. For AMD 3100 experiments, mice were administered one dose of vehicle (1X PBS) or AMD 3100 (5mg/kg;) dissolved in 1X PBS 4x/week for four weeks via IP injection. For CL316 treatments, mice were administered one dose of vehicle (1X PBS) or one dose of Cl316 (1 mg/kg; 17499 Cayman Chemicals) by IP for 24 or 168hrs.

Metabolic cage analysis: Mice were singly housed in Promethion metabolic cages placed in an environmental chamber at 6am for 14 days with ad lib access to food (chow) and water. Environmental temperatures were set to 23ºC for the first 7 days. Mice were removed from the cages at 6am on day 8 and environmental temperatures were decreased to 6ºC. After

environmental temperatures were achieved (2pm), mice were placed back into their respective cages for the duration of the study. Following the total 14 days, mice were removed for analysis. Body mass, water intake, food intake, oxygen consumption, carbon dioxide production, energy expenditure, energy balance, respiratory exchange ratio, locomotor activity, pedestrian locomotion, and total distance traveled in the cage were measured by CalR software. Data analysis was conducted using the web based indirect calorimetry software (256).

Histological analysis:

Tissues were dissected and immediately placed in 10% formalin (neutralized with 1X PBS) for 24 hours. Tissues were processed using Thermo Scientific™ STP 120 Spin Tissue Processor with the following conditions: Bucket 1: 50% ethanol (45 minutes); Bucket 2: 70% ethanol (45 minutes) Bucket 3: 80% ethanol (45 minutes); Bucket 4 and 5: 95% ethanol (45 minutes); Bucket 6 and 7: 100% ethanol (45 minutes); Bucket 8-10: Xylene Substitute (45 minutes); Bucket 11 and 12: paraffin (4 hours each). Tissues were embedded into cassettes using a Histostar™ embedding station. Tissues were refrigerated for at least 24 hours prior to sectioning. 8-12-micron tissue sections were generated using a HM-325 microtome using low profile blades. Sections were placed in a 40 ºC water bath and positioned on microscope slides. Microscope slides with tissue sections were baked overnight at 55 ºC in an oven. Slides were rehydrated using the following protocol: xylene (3 mins 3x), 100% reagent alcohol (1 min 2x); 95% reagent alcohol (1 min 2x); water (1 min). Slides were stained in hematoxylin and eosin (H&E) staining for 2:30 minutes and 10 repeated submerges, respectively. Slides were dehydrated in the reverse order as the rehydration steps. Coverslips were mounted with cryoseal 60 mounting media. Brighfield images were acquired using a lecia DMi8 inverted microscope system.

Immunostaining:

Paraffin Sections: Slides were rehydrated using the following protocol: xylene (3 mins 3x), 100% reagent alcohol (1 min 2x); 95% reagent alcohol (1 min 2x); water (1 min). Slides were placed in an antigen retriever from Electron Microscopy Science (2100 Retriever). Antigen retrieval was performed using the 1x R-Buffer A solution (62706-10) at +120 ºC for 20 mins with a 2 hour cool down period. Sections were washed thrice with 1xTBS with a 5-minute incubation period between each wash. Slides were covered in 0.3% Sudan Black with 70% ethanol for 5 minutes, washed in 1X TBS for 5 minutes (3x), and 0.3% Triton X-100 with 1X TBS. Slides were left in Triton X-100 overnight to permeabilize. Slides were again washed with 1X TBS for 5 minutes and then blocked with 5% donkey serum for 30 minutes, washed with 1X TBS for 5 minutes and then enclosed with primary antibody in 1X TBS refrigerated overnight . The primary antibodies in this experiment are as follows: anti-Tubulin Beta 3 (1:200; 657404 BioLegend), goat anti-Perilipin (1:200; abcam: ab61682), rabbit anti-UCP1 (1:200; abcam: ab10983). Afterwards, the slides were washed with 1X TBS for 10 minutes and loaded with the appropriate secondary antibody from the following for 2 hours at RT: Texas Red donkey anti-rabbit (1:200; ThermoFisher Scientific: Alexa Fluor 568 A10042), 488 donkey anti-goat (1:200), Cy5 donkey anti-mouse (1:200; Jackson ImmunoResearch 715-175-150). For TH immunostaining, primary antibodies were refrigerated for 36 hours proceeded with a 1X TBS wash for 1 hour. Secondary antibodies were loaded onto the tissue for 4 hours at RT and washed with 1X TBS for 10 minutes. Tissues were exposed 0.1% Sudan Black in 70% ethanol for 5-10 minutes, washed with 1X TBS for 10 min (3x), and covered with 0.02% Tween20 in 1X TBS for 15 minutes(204, 209). At the end of staining, all slides were washed with 1X TBS for 10 minutes and stained with Hoescht in 1X TBS (1:1000; H3570; Life Technologies) for another 10 minutes. After another wash with 1X TBS for 5 minutes, slides were

mounted with Epredia™ Immu-Mount™ media and cover slipped. Snapshots of fluorescent images were obtained through a Leica DMi8 inverted microscope system.

RNA Isolation and qPCR: ~200 mg of BAT or iWAT tissue from each mice sample was placed into Precellys tubes that included ceramic beads and 1mL of TRIzol (ABI). Samples were placed into a Precellys 24 Lysis and Homogenization machine (Bertin Tecnhnologies) to homogenize and set at 3 pulses at 4500 rpm (30 sec) with 30 second rest periods in between each pulse and final rest period of 4 minutes. When utilizing cells, TRIzol was directly placed into the culture dish. RNA was isolated from samples using chloroform extraction and isopropanol precipitation. The quality and concentrations of RNA were established through a TECAN Infinite F-Nano^{+} spectrophotometer. With these concentrations, each sample was transformed into cDNA utilizing a high-capacity RNA to cDNA kit (Life Technologies #4368813) and thermal cycler. The converted sample was diluted to 1:10 solution using molecular grade H_2O for qPCR analysis. The diluted sample was then mixed with PowerUp™ SYBR™ Green Master Mix (Life Technologies A25742) and the necessary primer. Samples were placed into an Applied Biosystems QuantiStudio™ 3 Real-Time PCR system for qPCR analysis. The machine was set to collect data using the ΔΔ-CT method compared to the internal control Rn 18s. Each datum corresponds to a single mouse sample/culture and was executed in technical quadruplets.

Western Blot/Immunoblotting: BAT samples were collected from mice and homogenized using 200 µL RIPA Lysis Buffer. The appropriate standard curve and relative protein concentrations for samples were determined utilizing the protocol provided in a protein assay kit (Pierce™ BCA Protein Assay - ThermoScientific). Samples were then prepared based upon calculated protein concentrations with the appropriate ratios for SDS/DTT and lysis buffer. A 12% separating and stacking gel were constructed with a 10 well comb and allowed to solidify for 30 minutes before

loading. The solidified gel was placed into a Mini-PROTEAN Tetra Electrophoresis Cell chamber suspended in 1x running buffer. Prepared samples and protein ladder were maximally loaded into individual wells and allowed to run for 15-20 minutes at 90V followed by 120V for 2 hours. Gel was then transferred onto a nitrocellulose membrane sandwiched into a cassette containing filter papers and sponges. The cassette was immediately placed back into the gel chamber and submerged in fresh 1x transfer buffer and allowed to run overnight at 30V. The protein-containing membrane was removed and washed with 1x TBS-0.1% Tween20 (TBS-T) 3x for 5-10 minutes each time on a rocker. Membrane was then blocked with 5% BSA in 1X TBS-T for 1 hour, washed 3x for 5-10 minutes in 1x TBS-T each and covered in the appropriate primary antibody with loading control overnight. The primary antibodies in this experiment are as follows: rabbit anti-UCP1 (1:1000; abcam #ab10983); rabbit anti-tyrosine hydroxylase (1:1000; EMD Millipore: ab152); rabbit anti-beta-tubulin (1:1000; Cell Signaling: 15155); rabbit anti-GAPDH (1;1000; Cell Signaling: 2118). Membrane was washed again 4x in 1x TBS-T for 15 minutes each and covered in secondary antibody for 1 hour (1:10000; ThermoFisher Scientific: donkey anti-rabbit IgG (H+L) Cross-Adsorbed HRP 31458). Membrane was washed as previously mentioned and submerged in 1:1 solution of SuperSignal™ West Pico PLUS Chemiluminescent Substrate (ThermoScientific: 34580) for 2 minutes and then exposed utilizing a FlourChem E system (biotechne® proteinsimple).

Tyrosine Hydroxlyase (TH) Quantification: Fiji ImageJ software was used to trace individual lines of tyrosine hydroxylase and measure the respective lengths for each sample. Scale length was adjusted based on known image dimensions (3.0667 pixels/µm). Traced TH neurons under 10 µm were excluded from data analysis.

SV cell isolation:

WAT: Fat pads were removed and a pair of inguinal adipose depots from a single mouse were minced and placed in 10 ml of isolation buffer (0.1 M HEPES, 0.12 M NaCl, 50 mM KCl, 5 mM D-glucose, 1.5% BSA, 1 mM $CaCl_2$) supplemented with collagenase type I (10,000 units) and incubated in a 37ºC incubator with gentle agitation for ~1 hour (257). Serum free Dulbecco's Modified Eagle's Medium Nutrient Mixture F-12 Ham (Sigma, cat. no. D8900 and D6421) (DMEM/F12) media was added to the digested tissue and strained through a 100 µm cell strainer. Samples were spun (Eppendorf at 200 X g for 10 minutes. The supernatant was removed, and the pellet was resuspended in 10 ml of erythrocyte lysis buffer (155 mM NH_4Cl, 10 mM $KHCO_3$, 0.1 mM EDTA). After a 5-minute incubation period, growth media (DMEM/F12 supplemented with 10% fetal bovine serum (FBS) was added, mixed, and strained through a 40 µm cell strainer. Samples were then spun at 200 X g for 5 minutes. Supernatant was removed and the cell pellet was resuspended growth media and cells were plated. After ~12 hours, growth media was removed and replenished.

BAT: Mice were dissected and SV cells were isolated from brown fat lobes. Briefly, tissue was minced and digested for half an hour with vortexing every ten minutes in 5 ml isolation buffer containing collagenase II (50,000 units) at 37°C. 5 ml DMEM/F12 was then added and the suspension filtered through a 70 µm basket. Suspension was then spun at 200 x G for 10 minutes and the supernatant aspirated off. The pellet was then resuspended in 10 ml erythrocyte lysis buffer (155 mMNH4Cl, 10 mMKHCO3, 0.1 496mM EDTA) for 5 minutes. 15 ml of DMEM/F12 supplemented with 10% FBS was added, the suspension filtered through a 40 µm basket, and spun at 200 x G for 5 minutes. Isolated SV cells were resuspended and cultured in DMEM/F12 supplemented with 10% FBS. The following day, growth media was removed and replenished.

Adipogenesis:

White adipogenesis: Isolated SV cells were grown to confluency. Two days post confluency white adipogenic media one (DMEM/F12 supplemented with 5% FBS 10 µg/ml insulin, 1µM Dexamethasone, 250 µM 3-Isobutyl-1-methylxanthine) for 48 hours. At 48 hours, white adipogenic media one was removed and replaced with white adipogenic media two (DMEM/F12 supplemented with 10% FBS, 10 ug/ml insulin) was added for 120 hours but replaced every 48 hours. Differentiation was assessed by LipidTox™ staining and mRNA expression.

Brown adipogenesis: Isolated SV cells were grown to confluency. Two days post confluency beige adipogenic media one (DMEM/F12 supplemented with 5% FBS 10 µg/ml insulin, 1µM Dexamethasone, 250 µM 3-Isobutyl-1-methylxanthine, 2 nM Triiodothyronine (T3); 250 nM Indomethycin) for 48 hours. At 48 hours, beige adipogenic media one was removed and replaced with beige adipogenic media two (DMEM/F12 supplemented with 10% FBS 10 ug/ml insulin, 2 nM T3) was added for 120 hours but replaced every 48 hours. Differentiation was assessed by LipidTox™ staining and mRNA expression.

LipidTox staining: At the end of differentiation, media was aspirated, and adipocytes were fixed with 4% paraformaldehyde for 45 minutes. Adipocytes were washed thrice with 1xTBS with a 5-minute incubation between each wash. Adipocytes were permeabilized using 0.3% TritonX-100 in 1XTBS for 30 minutes. Adipocytes were washed as previously described. Adipocytes were incubated with either HSC LipidTox-green or HSC LipidTox-deep red at 1/1000 in 1xTBS. Adipocytes were then washed twice with 1xTBS with a 3-minute incubation between each wash. Adipocytes were then stained with Hoechst (1 µg/ml in 1XTBS) for 10 minutes. Adipocytes were washed twice with 1xTBS with a 3-minute incubation between each wash. Fluorescent images were collected on a Leica DMi8 inverted microscope system.

Flow Cytometry: White and brown adipose SV cells were isolated as previously described. Cells were resuspended in 1X PBS. Cells were then pelleted (200 x G for 10 minutes) and resuspended in 0.3-0.5 ml of FACS buffer (2.5% horse serum; 2 mM EDTA in 1xPBS with 1X phosphatase inhibitor cocktail) and pipetted through 5 ml cell-strainer capped FACS tube (BD Falcon). Cell sorting was performed on a BD Biosciences FACS Aria Fusion. Cells were analyzed on a Thermo-Fisher Attune NxT cytometry. Viable cells were gated by singlet forward and side scatter pattern and GFP+ and RFP+ viable cells were either analyzed or sorted. Alternatively, cells were stained for CD45 (1:200; 103151 Biolegend), CD301 (1:200 145705 Biolegend), Cxcr4 (1:200; 146507 Biolegend), or CD68 (1:200 137003 Biolegend) antibodies and analyzed for their respective conjugated fluorophore.

CHAPTER 3

A CXCL12/CXCR4 SIGNALING AXIS CONTROLS WHITE ADIPOGENESIS VIA ESTROGEN RECEPTOR TRANSCRIPTIONAL ACTIVATION

Benjamin M. Steiner[1], Derek Lee[1], Yuwei Jiang[2], and Daniel C. Berry[1, 3]

[1]Division of Nutritional Sciences, Cornell University, Ithaca, NY 14853

[2]Department of Physiology and Biophysics, University of Illinois at Chicago, Chicago IL 60612 USA

[3]Lead contact: dcb37@cornell.edu

Pending journal submission as of dissertation completion

3.1. Abstract:

White adipose tissue (WAT) plays a myriad of roles in the body such as the regulation of metabolism and reproduction. Formed throughout the lifecycle, adipocytes are thought to take up residency in their respective fat pad through CXCL12/CXCR4 homing. Once migrated to the fat pads, physiological regulators such as estrogen are then responsible for adipocyte function such as lipid accumulation and lipolysis. However, we have found another potential role of CXCR4 within the adipocyte. Here we show that deletion of CXCR4 within the adipocyte lineage impairs adipocyte differentiation in females, but not males. Additionally, high fat diet studies failed to induce hypertrophic WAT expansion in females lacking CXCR4 within the adipose lineage. In vitro studies showed a complete lack of adipogenesis in CXCR4-deficient female cells, though the addition of an estrogen inhibitor yielded a full recovery. Supporting these findings, in vitro studies

using CXCR4-deficient male cells displayed the same phenotype when treated with estrogen. In vivo ovariectomy studies using CXCR4-deficient female mice showed a full recovery on adipogenesis. This sexually dimorphic phenotype suggests that while estrogen is controlling adipogenesis, CXCR4 is playing a role in the regulation of estrogen signaling. Overall, our studies suggest that targeting CXCR4 could be a new therapy to combat WAT expansion in women.

3.2. Introduction:

Obesity can give rise to a host of metabolic disorders such as type 2 diabetes, cardiovascular disease, atherosclerosis, and certain types of cancer (258). At the crux of metabolic imbalance is the uncontrolled pathophysiological expansion of WAT. WAT expansion occurs either through hypertrophy (enlarged adipocytes) or hyperplasia (increased number of adipocytes) (94, 259). Hypertrophy has been deemed as metabolically unhealthy due to hypoxia (78), fibrosis, chronic inflammation (260), and insulin resistance (261, 262). Hyperplasia, on the other hand, is considered to be metabolically healthy. Multiple studies have shown that obese individuals with higher proportions of small adipocytes are insulin sensitive while exhibiting normal metabolic parameters (263, 264). By causing adiposity to develop through hyperplasia, many complications such as type 2 diabetes and metabolic syndrome may be alleviated due to reduced inflammation (265). Increasing the number of adipocytes for hyperplastic tissue expansion can only be accomplished through the activation of the stem cell compartment. However, other factors such as location of the adipose tissue also play a role in metabolic health.

Anatomical location of WAT is a clear determinate of metabolic health in obesity as intra-abdominal accumulation, visceral fat, leads to significant risk of developing metabolic disease due to hypertrophic inflammation (266). However, expansion via subcutaneous fat happens via hyperplasia and plays a protective role against trauma and cold (267, 268). Men typically store fat

in the viscera, which puts them at a greater risk for type 2 diabetes and coronary artery disease (269). Women have a higher percentage of body fat than men but it tends to be positioned, anatomically, in the hips and thighs as subcutaneous fat (270) as estrogen is thought to increase subcutaneous depots (271). However, menopause, which is characterized by ovarian inactivity, decreases estrogen levels which yields more visceral adiposity. This places post-menopausal women at a greater risk for the same ailments that obese men face (272-274), as the decrease in estrogen allows for redistribution of body fat and metabolic dysregulation (123). The question then becomes how to stimulate hyperplastic adipose tissue growth. Though the answer is multifaceted, the crux of hyperplasia is the stem cell compartment.

Stem cells reside in specialized microenvironments throughout the body which modulate tissue maintenance and function. These microenvironments, termed the stem cell niche, communicate with the resident stem cells through signaling pathways causing proliferation, migration, chemotaxis, and differentiation. While many have been identified, specific pathways such as vascular endothelial growth factor (Vegf), platelet derived growth factor (Pdgf), and the chemokine CXCL12 pathways have been of heightened interest due to their cellular responses (90, 94, 275, 276). While pathways such as Vegf and Pdgf are responsible for fate determination, maintenance, and function (277), CXCL12 has been of interest due to its ability to induce cellular chemotaxis (278). Initially identified as a pre-B cell growth-stimulating factor, CXCL12 functions in the recruitment of vascular progenitor cells from bone-marrow to neoangiogenic locations through its G protein-coupled receptor C-X-C chemokine receptor 4 (CXCR4) (165, 279). Previous research has suggested that the CXCL12/CXCR4 pathway also plays a role in adipose tissue biology (178). Due to these findings, it could be postulated that the CXCL12/CXCR4 signaling pathway is also responsible for recruitment of APCs to fat pads. However, each tissue is

different, and these organ-specific interactions have just begun to be explored in adipose tissue biology.

By communicating with the stem cell compartment, the niche is ultimately responsible for the homeostasis and the organ-specific function of the tissue (280-282). Stem cells have been extensively characterized in various tissues such as blood and skin (283). Understanding the stem cell progression into progenitors (committed to differentiation) and, ultimately terminally differentiated cells, leads to direct testing of cells in response to injury, diseases, regeneration, and so on (284). WAT has been shown to generate new adipocytes in both homeostatic and obesogenic conditions via the stem/progenitor cell compartment, mirroring the classical stem cell examples (285). Residing along the vasculature within the WAT, APCs appear to resemble smooth muscle cells, express a bevy of smooth muscle genes (69), and can be marked by several smooth muscle cell genetic tools (α-SMA, PDGFRβ). These cells can be further delineated based on their expression of the master regulator of adipogenesis, peroxisome proliferator activated receptor gamma (PPARγ) (54, 286, 287). However, beyond their discovery much remains unknown about the cellular signaling pathways regulating their adipogenic trajectory. The limited knowledge of characterization within the adipose lineage represents a major hurdle when understanding metabolic issues such as obesity and diabetes. Discovering these characteristics will yield insight to both maintenance and repair within adipose tissue as well as clinical potential regarding targeted therapy for reduction of adiposity in an obesogenic state.

Responsible for cellular chemotaxis, CXCL12 and its cell surface receptor CXCR4 are ideal for investigation to uncover adipose tissue niche signaling. Our data suggests that CXCL12 is secreted by the niche, which then causes a signaling cascade within the adipocyte through CXCR4. By using genetic and pharmacological necessity tests, we have identified that CXCR4

plays a critical role in female adipogenesis as CXCR4-KO (mutant) mice show a drastic reduction of adiposity, upwards of 70%. Male mice, on the other hand, have minimal reductions in adiposity with the deletion of CXCR4. Interestingly, CXCR4-deficient female mice cannot be adipogenically rescued with a high-fat diet (60% kcal from fat). Furthermore, in vitro adipogenesis has identified that mutant cells are not only more sensitive to estrogen but can overcome lipodystrophy when given estrogen receptor inhibitors. This sexual dimorphism suggests that estrogen receptor (Esr1) transcriptional activation in conjunction with the CXCL12/CXCR4 signaling pathway is playing a major role in adipogenic potential.

3.3. Results:

CXCL12/CXCR4 expression in adipocytes.

Adult APCs reside on the vasculature within the niche after WAT development and bud off to form adipocytes around postnatal day 30 (69). To identify factors mediating vascular homing and niche residence, our studies focused on CXCL12/CXCR4 signaling. Previous research focused on the hematopoietic stem cell model pointed to the CXCL12/CXCR4 pathway being responsible for niche retention, which fueled this idea. Our genetic studies of APCs demonstrated enrichment of CXCR4 while CXCL12 was expressed in the surrounding niche. APCs were FACs isolated from the adipose lineage tracking model, AdipoTrak. This genetic system incorporates a PPARγ-tTA knock-in allele along with inducible marking and tracking tools such as TRE-H2B-GFP allowing for lineage tracing and APC dynamics. We first assessed CXCR4 mRNA expression which was found to be enriched in both subcutaneous and visceral APC populations as well as mature adipocytes, but not in the surrounding stroma. It appears that anatomical location of the fat pads plays a role in CXCR4 enrichment as visceral APCs had an eight-fold increase in expression when compared to subcutaneous APCs. However, CXCL12 mRNA expression was only enriched in the non-GFP cells, and wasn't detected in mature adipocytes, indicating that the adipose lineage is not producing CXCL12. Previously, we showed that CXCL12 was not expressed

in the adipocyte lineage through the AT-CXCL12-dsRed mouse model, thus confirming these findings. We further validated these findings through immunostaining adipose tissue as co-localization of CXCL12 and the adipocyte marker, perilipin, was not observable. In vitro models further support these findings as CXCR4 mRNA expression increased while CXCL12 decreased when cells were given adipogenic induction media. Furthermore, antibody staining of in vitro differentiated adipocytes confirmed CXCR4 positivity. These findings suggest that while CXCR4 is expressed in the adipose lineage, CXCL12 is being expressed in the surrounding tissues, maintaining adipocyte residency, and decreasing ectopic lipid distribution.

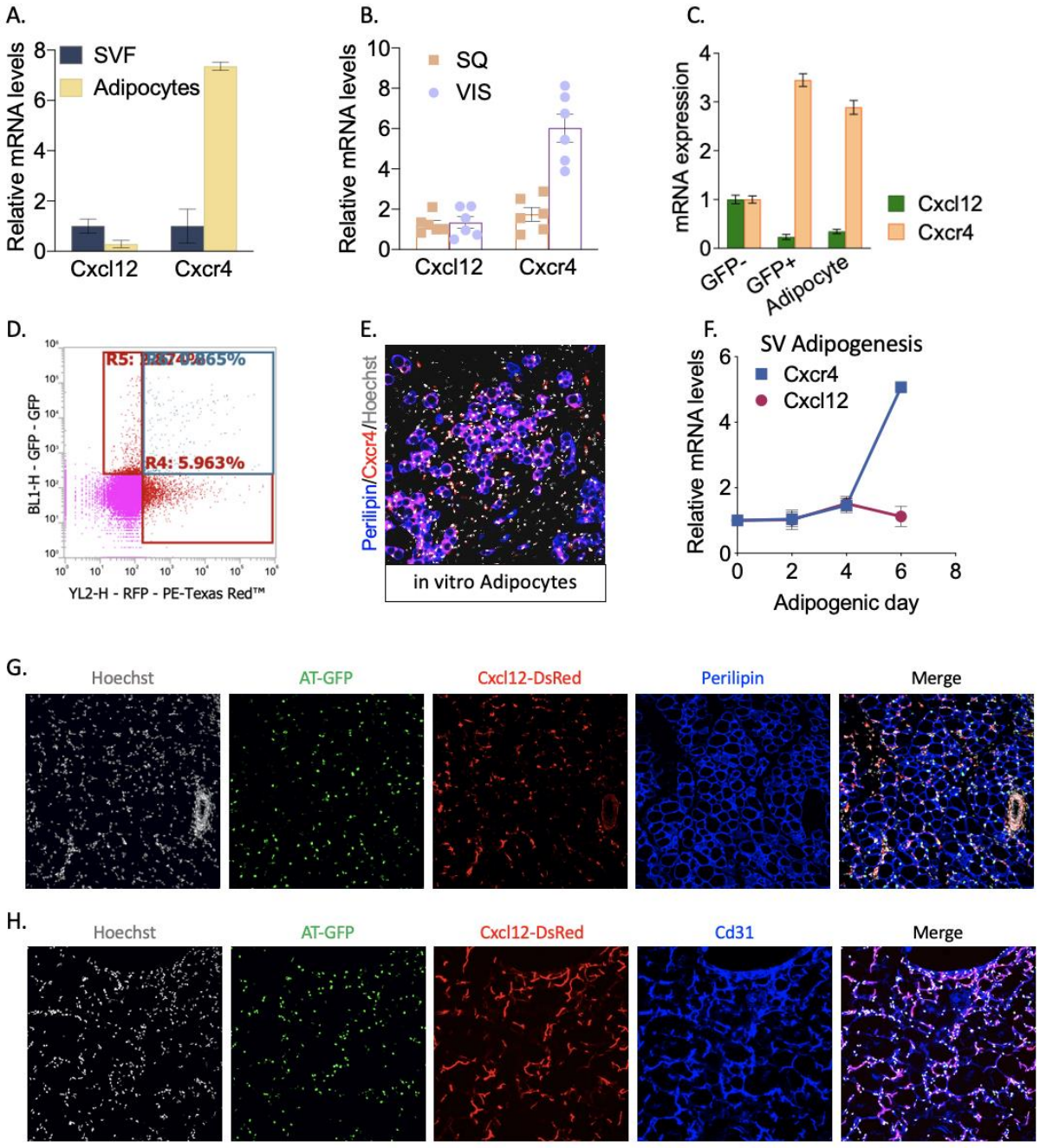

Figure 16: CXCL12/CXCR4 expression in adipocytes. A) Experimental schema: At P60, SV and mature adipocytes were removed and mRNA expression was measured for CXCL12 and CXCR4. B) Depot mRNA expression for CXCL12 and CXCR4 was measured from mice described in (A). C) mRNA expression of CXCL12 and CXCR4 was measured on FACs sorted SV cells and mature adipocytes. D) FACs analysis on SV cells expressing GFP (PPARγ+) and/or dsRed (CXCL12+). E) Immunostaining in vitro adipocytes against perilipin (lipids) shown in blue and CXCR4 shown in red. F) mRNA expression of CXCL12 and CXCR4 in vitro throughout APC adipogenesis to mature adipocytes. G) Representative images of GFP and dsRed colocalization within perilipin immunostained iWAT depots. Hoechst was used to visualize nuclei. H) Representative images of

GFP and dsRed colocalization within CD31 (vascular) immunostained iWAT depots. Hoechst was used to visualize nuclei.

CXCR4 deletion impairs adipogenic expansion of WAT

In order to further probe the role of the CXCL12/CXCR4 signaling pathway in the adipose lineage, we next aimed to delete CXCR4 within APCs and, consequently, mature adipocytes. To address this, we combined a $CXCR4^{fl/fl}$ conditional mouse model with the AdipoTrak (PPARγ-tTA; TRE-Cre; TRE-H2B-GFP) system to generate AT-CXCR4-KO mice. Adipose tissue development appeared normal in both male and female mice. However, by sexual maturity (postnatal day 60), male mice had approximately 10-20% reduction in fat content while female mice saw a 50-70% reduction in fat mass. Interestingly, this loss of adiposity did not correlate with impaired insulin sensitivity as glucose tolerance testing did not show significant changes between control and mutant mice, regardless of sex. Furthermore, food intake nor APC population did not vary between controls and mutants, regardless of sex. Female mice did not demonstrate hepatic steatosis, as assessed by tissue weight and hematoxylin and eosin (H&E) staining. H&E staining of WAT did reveal disrupted adipose tissue architecture and hypertrophic adipocytes in males. Female mice WAT, on the other hand, showed a complete lack of adipocytes as the tissue was engulfed with fibrotic tissue, as assessed by Sirius red staining. Additionally, mRNA analysis of female WAT demonstrated reduced adipogenic genes with an increase in fibrotic and inflammatory markers. To confirm these findings of a reduced adipogenic potential, stromal vascular (SV) cells were isolated from control and mutant female mice and cultured in adipogenic media. While female control cells differentiated into mature adipocytes, female mutant cells failed to undergo adipogenesis as assessed by lipid staining and mRNA analysis of adipocyte markers.

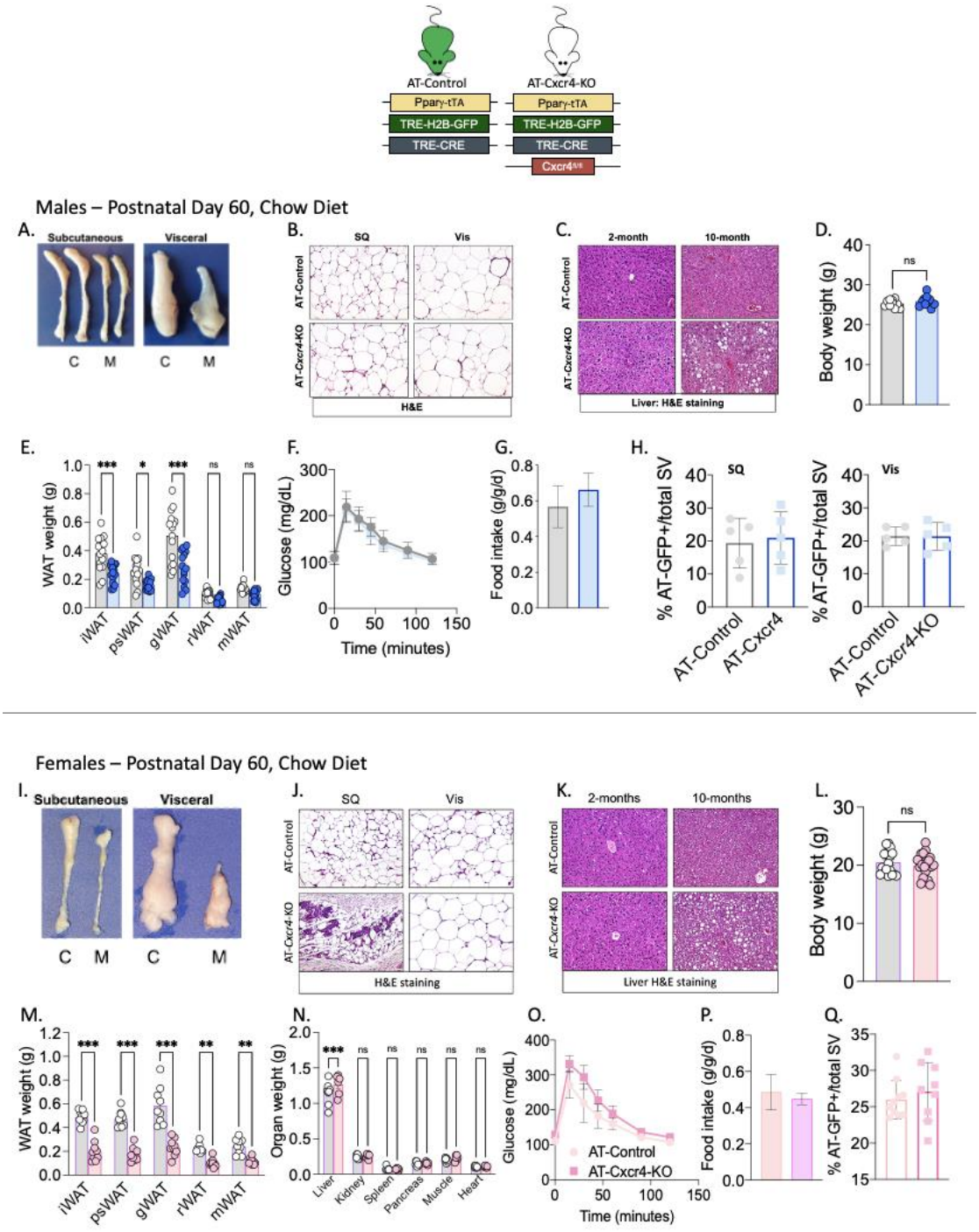

Figure 17: CXCR4 is crucial for homeostasis of female WAT. A) Representative images of male subcutaneous and visceral fat depots from AT-Control and AT-CXCR4-KO mice at P60. B) Representative images of H&E staining of subcutaneous and visceral fat depot sections from mice described in (A) C) Representative images of H&E staining of liver from mice described in (A). D) Body weight from mice described in (A). E) Individual adipose depot weights from mice described in (A). F) Glucose tolerance tests from mice described in (A). G) Food intake levels over 1 week from mice described in (A). H) Comparative percentage of APCs (GFP+) in both SQ and

VIS from mice described in (A). I) Representative images of female subcutaneous and visceral fat depots from AT-Control and AT-CXCR4-KO mice at P60. J) Representative images of H&E staining of subcutaneous and visceral fat depot sections from mice described in (I) K) Representative images of H&E staining of liver from mice described in (I). L) Body weight from mice described in (I) M) Individual adipose depot weights from mice described in (I). N) Individual organ weights from mice described in (I). O) Glucose tolerance tests from mice described in (I). P) Food intake levels over 1 week from mice described in (I). Q) Comparative percentage of APCs (GFP+) in both SQ and VIS from mice described in (I).

Obesogenic conditions fail to restore adipogenesis in AT-CXCR4-KO females

APCs can be stressed into forming adipocytes through administering a high-fat diet (HFD). Therefore, we sought to challenge CXCR4-deficient APCs by feeding adult (postnatal day 60) control and mutant mice a HFD for 12 weeks to identify if CXCR4 is required for in vivo adipogenic induction. Control male mice increased in adiposity and decreased insulin sensitivity as expected, and mutant male mice increased fat mass to equal that of the HFD control males. Both control and mutant males exhibited similar glucose sensitivity impairment, adipose tissue weight, adipose tissue histology, and adipocyte marker expression. However, female mice saw strikingly different results. Mutant female mice resisted HFD-induced adipogenesis and maintained their lipodystrophic phenotype. Histological staining of WAT in the female mutant HFD mice showed the same lack of adipose tissue with fibrotic replacement as seen in the female mutant mice fed a chow diet. Additionally, mRNA analysis from female mutant WAT showed a lack of adipocyte and endothelial blood vessel markers while demonstrating an increase in inflammatory genes when compared with their female control HFD counterparts. These data suggest that CXCL12/CXCR4 signaling is critical for female-induced fat mass accumulation.

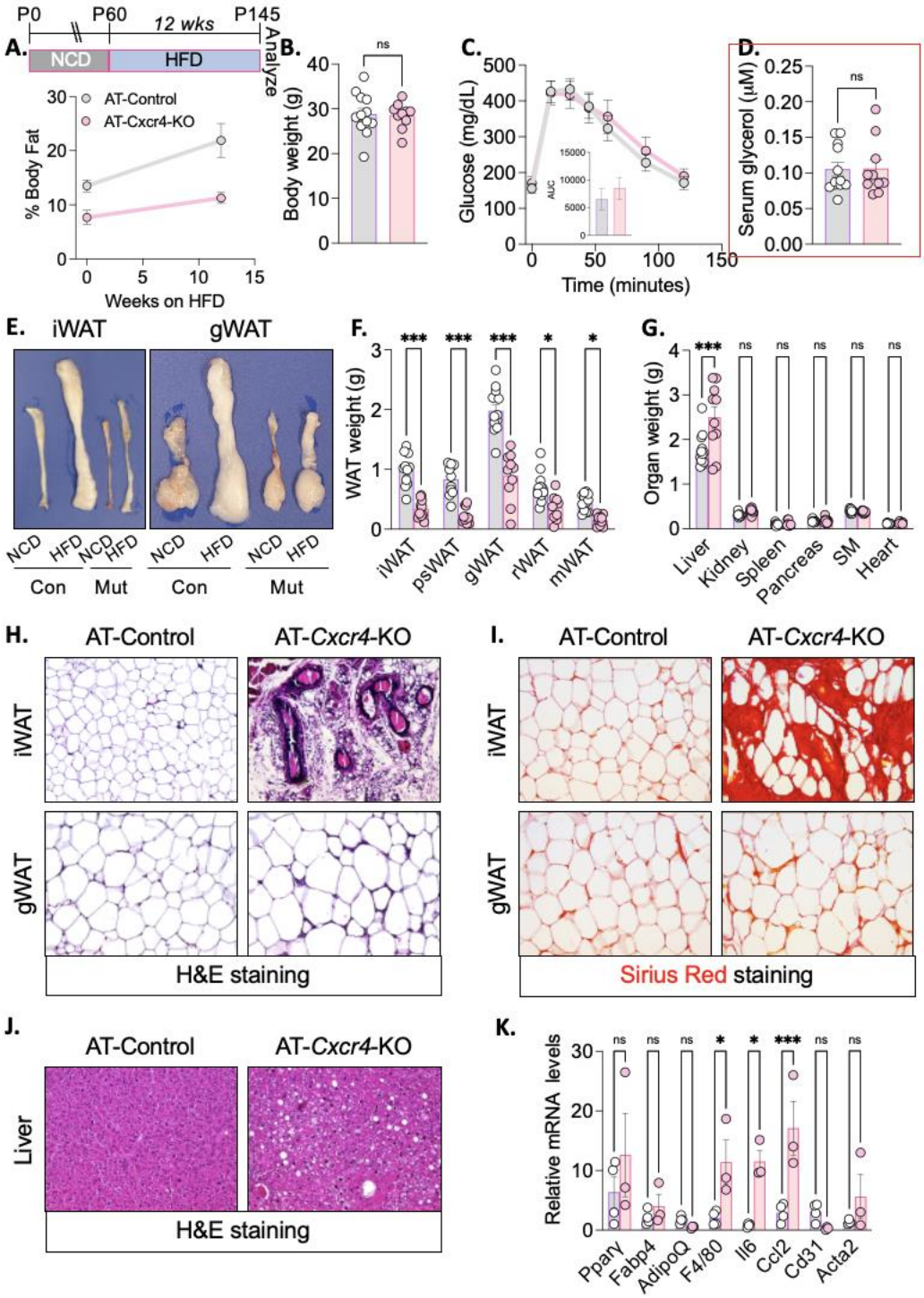

Figure 18: HFD does not recover phenotype in CXCR4-deficient female WAT. A) Experimental schema: Female AT-Control and AT-CXCR4-KO mice were dox suppressed from conception until P60. At P60, mice were placed on HFD for 12 weeks before analysis. B) Body weight upon analysis from mice described in (A). C) Glucose tolerance tests from mice described in (A). D) Serum glycerol levels from mice described in (A). E) Representative images of female subcutaneous and visceral fat depots from AT-Control and AT-CXCR4-KO mice at time of analysis (P145). F)

Individual adipose depot weights from mice described in (A). G) Individual organ weights from mice described in (A). H) Representative images of H&E staining of subcutaneous and visceral fat depot sections from mice described in (A) I) Representative images of Sirius red (fibrotic) staining of subcutaneous and visceral fat depot sections from mice described in (A). J) Representative images of H&E staining of liver sections from mice described in (A). K) Relative mRNA levels of inflammation from mice described in (A).

Adipogenic failure in females is due to the deletion of CXCR4 in the adult APC population

We then hypothesized that WAT integrity might be compromised resulting in an impaired adipogenic action. Due to adipose tissue development normality in both male and female controls and mutants, we aimed to induce CXCR4 deletion solely within the adult APC population. By utilizing the AT system, we doxycycline-suppressed control and mutant mice from conception until postnatal day 30. We then removed doxycycline (Dox) and examined fat content and glucose sensitivity 6 weeks later. Upon examination, male mice exhibited little difference between adipose tissue mass and glucose sensitivity. Histological analysis of male control and mutant mice showed normal adipose tissue architecture and gene expression. While female controls followed a similar phenotype to the males, female mutant mice revealed a stagnation in fat content. Interestingly, there was no difference in glucose sensitivity between female control and mutant mice. To validate these findings, we specifically challenged the adult APC population by doxycycline-suppressing the CXCR4 deletion until postnatal day 60, followed by HFD for 6 weeks. Female control mice saw an increase in fat content and a decrease in glucose sensitivity. However, female mutant mice resisted weight gain, though the tissue did not exhibit excessive fibrosis as with previous experiments. These findings suggested that deletion of CXCR4 within the female adult APC population results in stunted adipogenesis. Furthermore, this sexually dimorphic phenotype suggests that the CXCL12/CXCR4 signaling pathway is regulating female sex steroid action on adipogenesis.

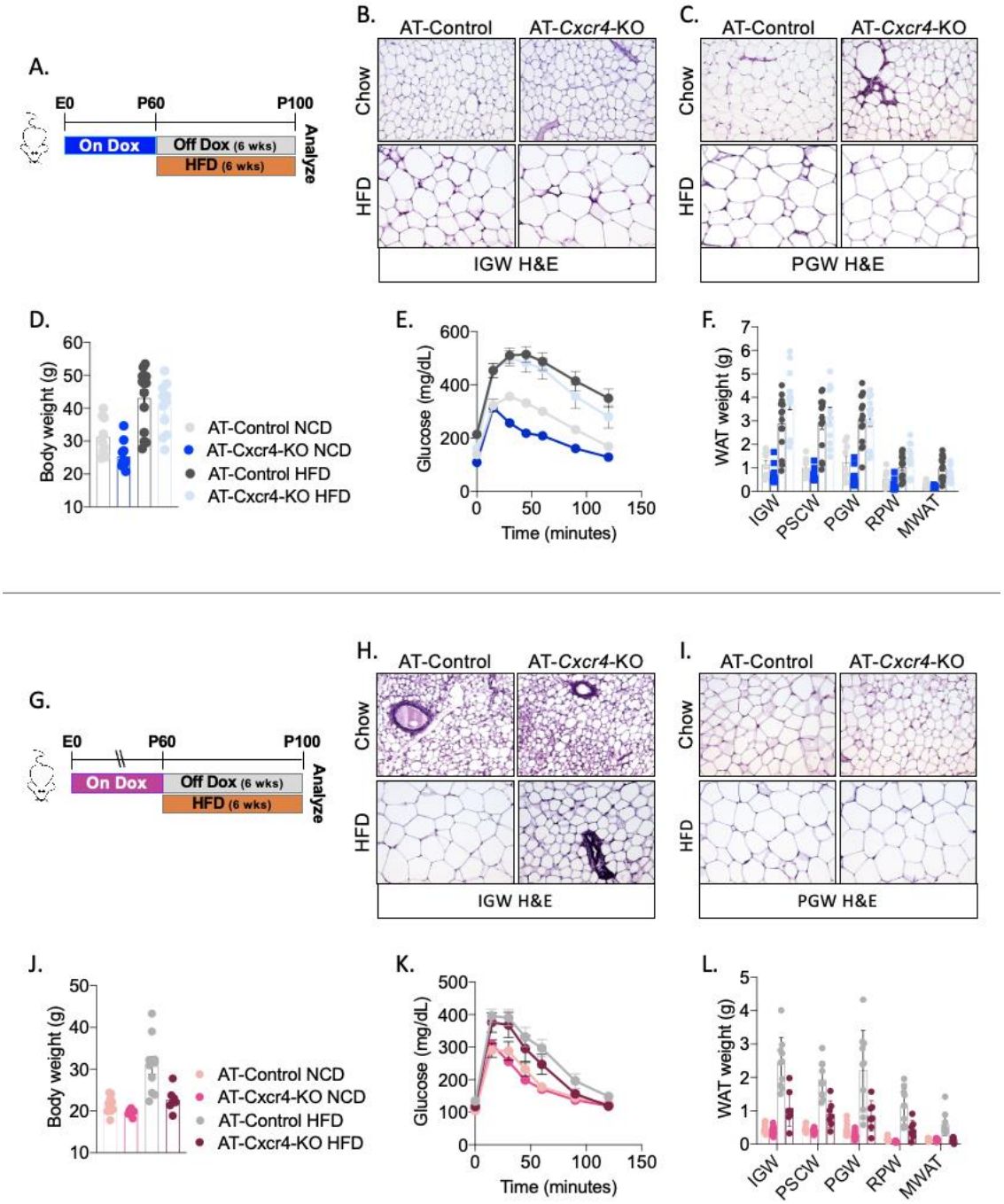

Figure 19: CXCR4 deletion within the adult APC population results in adipogenic blockade. A) Experimental schema: Male AT-Control and AT-CXCR4-KO mice were dox suppressed from conception until P60. At P60, mice were placed on HFD or chow for an additional 6 weeks. B) Representative images of subcutaneous fat depots from mice described in (A). C) Representative images of visceral fat depots from mice described in (A). D) Body weight at time of analysis from mice described in (A). E) Glucose tolerance tests 1 day prior to analysis on mice described in (A). F) Individual adipose depot weights from mice described in (A). G) Experimental schema: Female

AT-Control and AT-CXCR4-KO mice were dox suppressed from conception until P60. At P60, mice were placed on HFD or chow for an additional 6 weeks. H) Representative images of subcutaneous fat depots from mice described in (G) I) Representative images of visceral fat depots from mice described in (G) J) Body weight at time of analysis from mice described in (G). K) Glucose tolerance tests 1 day prior to analysis on mice described in (G). L) Individual adipose depot weights from mice described in (G).

Estrogen inhibits adipogenesis in WAT

To identify potential differences of sex steroid levels between sexually mature female mutant and control adipose tissue, mRNA expression of both Esr1 and Esr2 along with g-protein estrogen receptor-1 was measured revealing that only Esr1 was upregulated in the absence of CXCR4. To validate these findings, SV cells from WAT were isolated and plated in adipogenic media for 48 hours then stained for estrogen receptor 1 (Esr1) in order to visually identify regulatory changes caused by the presence or absence of CXCR4. In accordance with mRNA data, female mutant cells showed an increase in Esr1 mRNA expression when compared to the female control cells. To assess the impact of increased Esr1 on adipogenic potential, sexually mature female control and mutant SV cells were isolated, plated in adipogenic media, and given the Esr1 inhibitor fulvestrant throughout differentiation. The control SV cells showed no differences in adipogenesis, with or without Esr1 inhibition. However, the mutant SV cells demonstrated normal adipogenic potential with Esr1 inhibition as they mirrored control cells. These data suggest that Esr1 is inhibiting adipogenesis and that the CXCL12/CXCR4 pathway is potentially regulating Esr1 activity. To validate these findings, SV cells were isolated from sexually mature male control and mutant mice. The cells, once plated and confluent, were given 17β-estradiol at various concentrations throughout differentiation. While both control and mutant cells given a vehicle demonstrated typical adipogenesis, the administration of 17β-estradiol showed hindered adipogenesis in mutants at all concentrations. These findings suggested that cells deficient in CXCR4 have an increased sensitivity to estradiol.

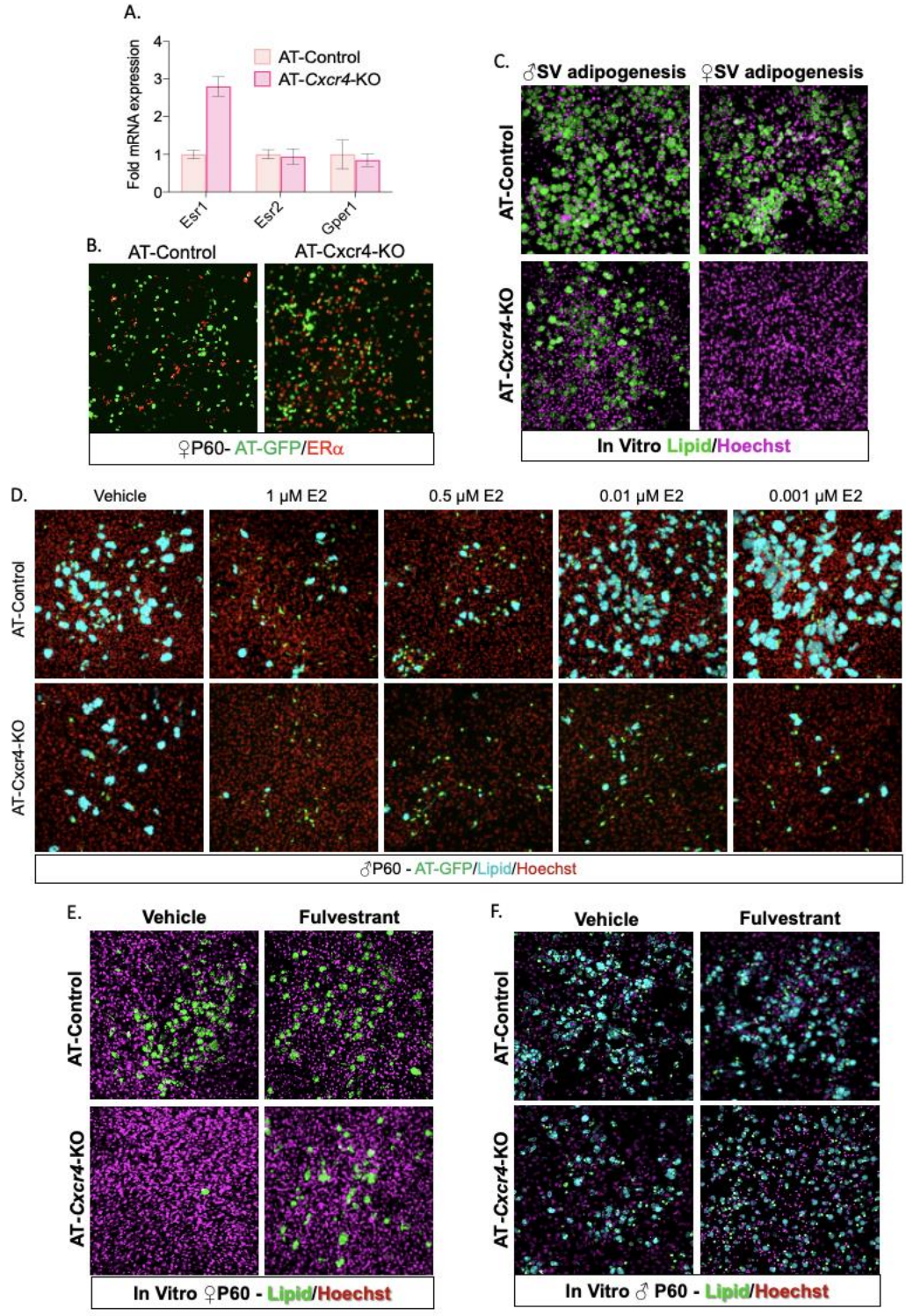

Figure 20: CXCR4-deficient APCs are sensitive to estrogen-induced adipogenic blockade. A) Experimental schema: At P60, SV cells from female AT-Control and AT-CXCR4-KO mice were removed and mRNA expression was measured for Esr1, Esr2, and GPER1. B) SV cells from mice described in (A) were cultured and immunostained for ERα. C) At P60, both male and female SV

cells were isolated from AT-Control and AT-CXCR4-KO mice. After confluent, they were stained for lipids to identify adipocytes and Hoechst to identify all nuclei (cells) in the field of view. D) At P60, SV cells were isolated from male AT-Control and AT-CXCR4-KO mice. During differentiation, the cells were treated with estradiol at various concentrations daily until terminally differentiated. E) At P60, SV cells were isolated from female AT-Control and AT-CXCR4-KO mice. During differentiation, the cells were treated with the anti-estrogen compound fulvestrant daily until terminally differentiated. F) At P60, SV cells were isolated from male AT-Control and AT-CXCR4-KO mice. During differentiation, the cells were treated with the anti-estrogen compound fulvestrant daily until terminally differentiated.

Estrogen depletion by ovariectomies restores WAT expansion in mutant female mice

To explore Esr1's ability to inhibit adipogenesis we turned to our mouse model. Ovariectomy surgeries were performed on control and mutant female mice to block Esr1 activity through E2 hinderance. While removal of ovaries does not reduce circulating E2 levels to zero, it has been shown to diminish circulating E2 by 98% in rodents (288). Therefore, ovariectomies are a prime surgical target for studying the effects of E2 and Esr1 on all tissues including, in our case, WAT. Once the surgeries were completed, the mice were aged for 30 days to allow phenotypic results to take place, as hyperplasia and rapid weight gain associated with ovariectomies takes place for approximately one month before WAT expansion is maintained (289, 290). Upon analysis, sham controls and mutants saw the same phenotypic results as seen in Figure 17. Ovariectomized controls had significant tissue expansion, as expected when comparing to well-established research (123, 291). However, ovariectomized mutants saw a robust increase in WAT as they surpassed both sham controls and mutants. In fact, the ovariectomized mutant WAT expanded to the size of the ovariectomized controls, indicating a full recovery. To further investigate these findings, histological examination was conducted which indicated that ovariectomized mutant WAT expanded through hyperplasia while ovariectomized control WAT underwent hypertrophy. These findings suggest that mutant WAT underwent adipogenesis due to the absence of E2, indicating that Esr1 is stopping adipogenesis.

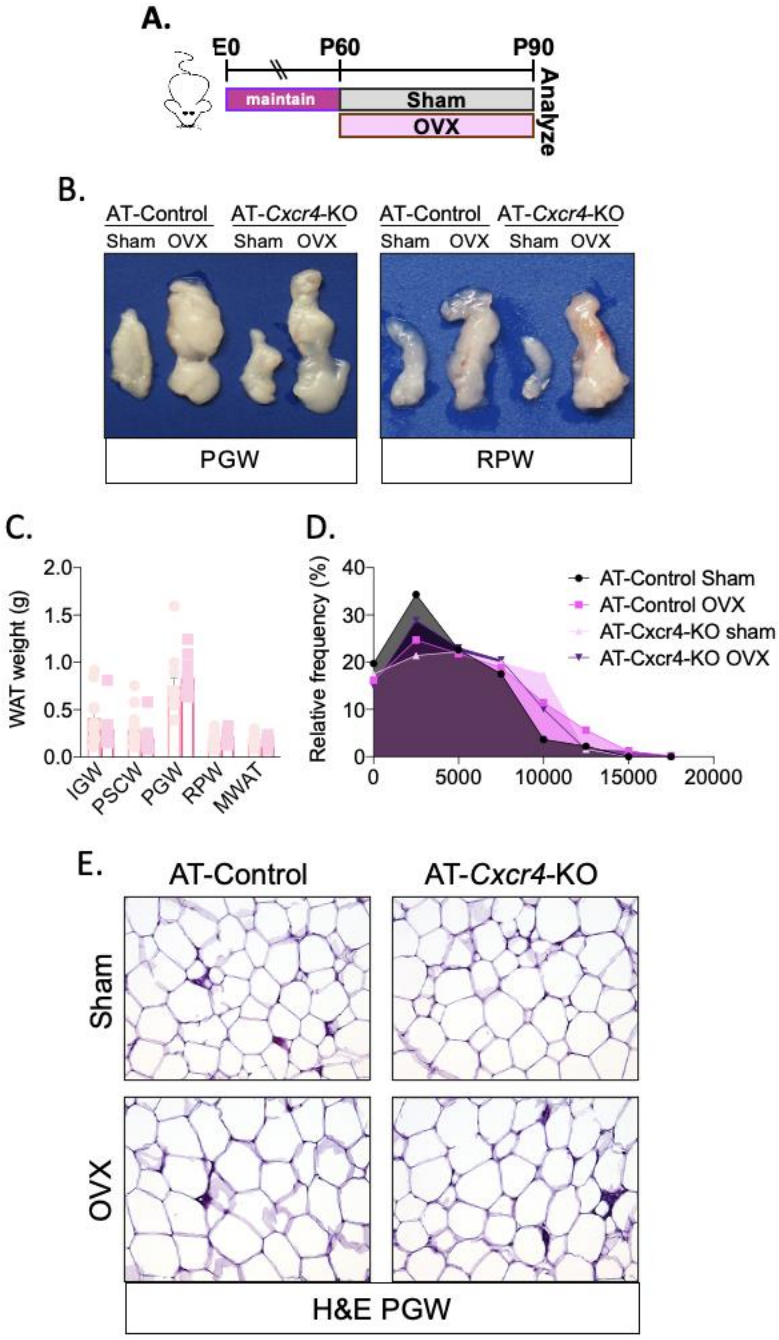

Figure 21: Estrogen depletion by ovariectomies restores WAT expansion in CXCR4-deleted female WAT. A) Experimental schema: Female AT-Control and AT-CXCR4-KO mice were maintained until P60. At P60, these mice underwent either ovariectomy or sham surgeries and were allowed 30 days before analysis (P90). B) Representative images of visceral fat pads described in (A). C) Individual adipose depot weights from mice described in (A). Percentage of relative frequency and adipocyte number in mice described in (A). E) Representative images of H&E staining of mice described in (A).

3.4. Discussion:

Obesity and its associated metabolic diseases such as type 2 diabetes and coronary heart disease are leading health problems around the world (292-296). Interestingly, body fat distribution plays a major role in determining metabolic health and is linked to sex (297). While males tend to accumulate body fat in the viscera, females accumulate body fat in the waist, hips, and buttocks (116). Due to visceral adiposity, males are at a higher risk for metabolic imbalance and develop obesity-related comorbidities such as non-alcoholic fatty liver disease. However, the depletion of circulating estrogen in post-menopausal women causes a body fat distribution shift resulting in increased visceral adiposity, increasing their risk for metabolic dysfunction (298). Beyond our understanding of sex steroid-induced body fat distribution much remains unknown regarding factors influencing body fat placement. Here we identified that the stromal-derived factor CXCL12 influences CXCR4 signaling in APCs and adipocytes to regulate ER activity. The presence of CXCL12/CXCR4 signaling represses ER transcriptional activity, thus promoting adipogenic action. Alternatively, the absence of CXCL12/CXCR signaling increases ER transcriptional activity leading to a reduction in APC differentiation and mature adipocytes.

Regulating healthy WAT expansion is dependent on APC differentiation and migration to the fat pad. The CXCL12/CXCR4 signaling axis has been demonstrated to mediate this process through both in vivo and in vitro studies (177, 299). Once WAT residency has been acquired, adipose tissue maintenance is mediated by sex steroids (300). However, the influence of CXCR4 signaling on estrogenic responses remains elusive. Our data shows for the first time that CXCR4 regulates estrogen's antiadipogenic role within WAT.

The CXCL12/CXCR4 signaling pathway has been shown to be of upmost importance in stem/progenitor migration and chemotaxis. As the sole ligand for CXCR4, CXCL12 is produced

by many cell types to induce stem/progenitor mobilization for repair, maintenance, and development of tissues. Often produced by the stem cell niche, CXCL12 has been reported to be produced by adipocytes themselves, thus resulting in APC migration to the fat pad and hyperplastic WAT growth (179). However, here we showed that while CXCR4 is enriched in APCs, CXCL12 is not being expressed in the adipose lineage. This difference could be due to adipocyte isolation techniques or cellular contaminants interfering with expression profiles. Our data suggests that endothelial cells secrete CXCL12, though the primary source of WAT CXCL12 remains to be determined. We further showed that while CXCR4 is being expressed by APCs and mature adipocytes, CXCL12 expression is observed within the surrounding tissues, thus anchoring adipocytes to the fat pads. These findings are supported through previous studies showing ablation of CXCR4 within the adipose lineage results in ectopic lipid deposition within skeletal muscle (178). However, the roles of CXCR4 in the adipose lineage have yet to be fully explored beyond cellular homing.

G coupled-protein receptor crosstalk with estrogen has been identified through the $G\alpha_i$ protein/Src/PI3K pathway (182). In breast cancer, Esr1 activates the CXCR4 pathway and regulates CXCL12 expression (183, 301). While these findings suggest a synergistic relationship between CXCR4 and Esr1, no clear findings have surfaced within adipose tissue. For the first time, we have found that CXCR4 activity acts as a sex-dependent regulator of adiposity. Our findings show that deletion of CXCR4 in adipose lineage causes lipodystrophy in females but not in males. Looking exclusively at females, it appears that CXCR4 is indeed responsible for APC migration as adipocytes are unable to take up residency in the fat pad. This idea can be further supported through the use of HFD feedings and the inability for APCs to be forced into adipogenesis. However, these findings are subject only to sexually mature females. As CXCR4 deletion does not

produce similar lipodystrophic results in male populations nor the developmental WAT population in either sex, sex steroids must be playing a role. This notion was the validated through upregulation of Esr1 expression in CXCR4-deficient female SV cells. Furthering these findings, deletion of CXCR4 in either sex resulted in an increased sensitivity to estradiol-mediated adipogenic inhibition while depleting circulating estrogen levels through ovariectomies restores adiposity in CXCR4-deficient female mice. This indicates that estrogen is negatively affecting adipogenesis and ablation of estrogen results in expansion of fat pads. Furthermore, CXCR4 is playing a regulating role in estrogen's influence on adipogenesis. Through these findings, we found that CXCR4 signaling blocks estrogen receptor activity to promote adipocyte differentiation.

The results of the present study show that deletion of CXCR4 in female mice leads to a depletion of adipose tissue accompanied by fibrotic tissue, macrophage infiltration, and upregulation of Esr1 signaling. These data provide a rationale for the function of CXCR4 in regulating energy balance through Esr1 suppression within the adipocyte and suggest that CXCR4 could be a potential target for combating obesity in premenopausal women.

CXCR4 is only part of the equation. Identifying CXCR4's ligand, CXCL12, is critical for understanding the signaling axis. We have identified CXCL12 expression to be taking place in CD31+ endothelial cells, but what signals are stimulating CXCL12 expression in these cells? Does this signaling pathway play a role in beige fat development? If so, what critical signals are determining CXCL12 release and CXCR4 activation? While studies in other tissues such as the hematopoietic field have demonstrated that CXCL12 is being expressed in multiple cell types, adipose tissue CXCL12 expression is undefined. Furthermore, is CXCL12 expression within

adipose tissue occurring in a sex-dependent manner? With many questions to be answered, the study of adipose tissue biology is not finished yet.

3.5. Limitations:

A limitation to our study is the incomplete mechanistic understanding of how CXCR4 is regulating ER transcriptional activity. Our studies demonstrate CXCR4's influence to negatively control ER's ability to regulate adipogenic action. However, CXCR4 and ER have been shown to cooperate in a positive feedback loop driving oncogenic activity in breast cancer. Additionally, our studies do not distinguish between G-protein estrogenic receptor (GPER) and nuclear ER activity. Both activated by estrogen, GPER has non-genomic functions and responds to ligand activation within minutes while ER acts on gene transcription. Our studies do not examine which ER is at play, which in itself could provide novel ideas regarding estrogen's control over adiposity.

Author Contributions:

BMS conducted animal husbandry, physiological measurements, pharmacological treatments, histological analysis, in vitro cell culture experimentation, tissue assessment, and immunostaining. DL conducted histological analysis and immunostaining. YJ and DCB designed experimentation, interpreted results, and wrote the manuscript. All authors discussed results and commented on the manuscript.

3.6. Materials and Methods:

Materials. For cell culture experimentation: High glucose Dulbecco's Modified Eagle Media (Sigma) and Ham's F-12 Nutrient Mixture (Gibco) (DMEM/F12); L-Glutamine 200mM, Pen Strep, Sodium Pyruvate 100mM (Gibco); Fetal bovine serum (Corning), Collagenase (Roche

Diagnostics GmbH), Fulvestrant (Sigma), Insulin (Sigma), IBMX (Sigma), Dexamethasone (Sigma), Doxycycline (Cayman), Tamoxifen (Cayman), 17β Estradiol (Cayman), Imatinib (Cayman), Rosiglitazone (Cayman), Forskolin (Cayman), and Trizol Reagent (Ambion). Tissues were processed for embedding using a ThermoScientific STP120 tissue processor and Thermoscientific HistoStar imbedding station before sectioning using a ThermoScientific HM325 Microtome. Reagents for H&E staining consisted of alcohols (Fisher Brand, HistoPrep, 95% and 100%), xylene (ThermoScientific), and Gill 2 Hematoxylin and Eosin (Epredia). Primary antibodies for immunostaining at 1:200 dilutions: PECAM-1 (CD31) rat anti-mouse (BD Pharmingen), Anti-Estrogen Receptor alpha rabbit monoclonal antibody [E115] (abcam), Anti-Parilipin-1 goat polyclonal (abcam), Anti-UCP1 rabbit polyclonal (abcam), Anti-GFP chicken polyclonal (abcam), and CXCR4 rabbit polyclonal (ThermoFisher Scientific). Secondary antibodies at 1:200 dilutions from Jackson ImmunoResearch Laboratories: Cy3-conjugated Donkey Anti-Rabbit IgG, Cy3-conjugated Donkey Anti-Mouse IgG, Cy5-conjugated Donkey Anti-Mouse IgG, Cy5-conjugated Donkey Anti-Rat IgG, Cy5-conjugated Donkey Anti-Goat IgG, Alexa Fluor 488-conjugated Donkey Anti-Rabbit IgG, and Alexa Fluor 488-conjugated Donkey Anti-Chicken IgG. LipidTox staining was performed at 1:500 dilution (Invitrogen). Microscopes used for imaging were Leica DMi8 and Leica M205 FA. Gene expression was conducted using a RT-qPCR (ThermoScientific Applied BioSystems, QuantStudio3) and a thermocycler (BioRad T100 Thermal Cycler). Mice were given one of the following diets: High fat diet (Research Diets, 60% kcal from fat), Doxycycline diet (Bio-Serv, 600mg/kg), or standard chow diet (Envigo, 5.8% fat).

Animals. The PPARγ-tTA and TRE-Cre mouse models were purchased from Jackson Laboratories. Mice were crossed and recombined mice were mated with TRE-H2B-GFP mice

generously provided by Dr. Todrita Tumbar. The three allelic combination creates the AdipoTrak mouse model. AdipoTrak offspring were intermated for three generations before being combined with the CXCR4fl/fl conditional mouse model purchased from Jackson Laboratories. Offspring were intercrossed for three generations prior to experimentation. Mice were housed in a 14:10 light:dark cycle and chow (19.1% protein, 5.8% fat, and 4.3% carbohydrates) and water were provided ad libitum. For high fat diet (60% fat), mice were fed chow until P60 then given HFD ad libitum until analysis. To suppress genetic deletion, mice were fed doxycycline food during mating and the offspring continued doxycycline food consumption until the appropriate timeframe where they then received either chow or HFD food until analysis. To assess food intake, mice were singly housed and given a set weight of food which was then measured daily.

Glucose Tolerance Testing. Mice were placed in omega bedding and fasted for 6 hours before administering a glucose tolerance test. In short, a 0.69 molar glucose solution was made using 1xPBS. After fasting, baseline glucose levels were measured before IP glucose injection of 1.25 milligrams of glucose per gram of body weight. Blood glucose levels were then measured every 15 minutes for the first hour followed by 30-minute measurements for the second hour using an UltraTouch meter. Mice were then given food following testing.

SV Fractionation. SV cells were isolated from pooled WAT depots (inguinal or perigonadal) through mincing WAT into fine pieces (2-5mm^2). The minced WAT was then digested in adipocyte isolation buffer (0.1M HEPES pH 7.4, 120mM NaCl, 50mM KCl, 1mM $CaCl_2$, 1.5% bovine serum albumin, and 5mM D-glucose) containing 1mg/mL collagenase at 37ºC under agitation for 1 hour. Digestion was then stopped by adding DMEM/F12 to the digested solution. The digested solution was then passed through a 100-micron basket to remove undigested clumps. The effluent was then centrifuged at 50 rcf for 5 minutes. After centrifugation, the infranatant was

collected while supernatant and precipitate were discarded. The infranatant was then centrifuged for 10 minutes at 200 rcf to pellet the SV before adding red blood cell lysis buffer (10mM $KHCO_3$, 155mM NH_4CL, and 0.1mM EDTA), re-pelleting, resuspension in DMEM/F12 with 10% fetal bovine serum, and finally plating.

Cell Culture. Adipose SV cells were isolated (SV fractionation) and cultured in Dulbecco's Modified Eagle Media/Hams Nutrient Mixture F12 (DMEM/F12) with 10% fetal bovine serum (FBS). After reaching confluency, the cells were given fresh DMEM/F12 with 10% FBS and the media was spiked with 10uL/mL IBMX, 1uL/mL dexamethasone, and 1uL/mL insulin to induce adipogenic differentiation. 3 days later, fresh DMEM/F12 with 10% FBS was given again with only 1uL/mL insulin for nutrient uptake into the adipocytes. After an additional 3 days (6 days post initial induction) cells were analyzed. For in vitro pharmacological testing, drugs were given during the 6-day differentiation period.

RNA Extraction, cDNA Synthesis, and qPCR. Briefly, total RNA from cells were extracted using Trizol as the manufacturer suggested. RNA was treated with DNase-1 and reverse transcribed using random primers and reverse transcriptase. qPCR was conducted using Power-Up SYBR Green PCR Master Mix. Values were normalized against 18S expression.

Tissue Processing. Whole tissues were placed in 10% formalin for 24-48 hours. 4 μm sections were then removed from the sample and placed into pre-labeled cassettes. The cassettes were then placed into the tissue processor and ran overnight in various concentrations of alcohol and paraffin. Next, the cassettes were removed, and the tissue was imbedded in paraffin, placed into a 4°C refrigerator for 12 hours, then sectioned. After sectioning, the tissue was transferred onto microscope slides before being baked for 12 hours at 37°C.

Hematoxylin and Eosin Staining. Once processed, slides were stained using standard H&E protocols. In brief, slides were placed into xylene followed by alcohol before hematoxylin staining. Next, slides were rinsed before eosin staining. Following dehydration by alcohol and clearing through xylene, slides were cover slipped and allowed to cure for 12 hours before microscopy.

Sirius Red Staining. Once processed, slides were stained following H&E protocols through hematoxylin steps. Following hematoxylin, slides were rinsed for 10 minutes before exposure to Sirius Red dye for 45 minutes before final dehydration, clearing, and cover slipping.

Immunostaining. Immunostaining in vitro cells was performed on either adhered stromovascular cells or mature adipocytes using standard methods. Tissue sampled were immunostained following tissue processing and sectioned between 5-12 μm, dependent on tissue type. In short, samples were probed with antibodies indicated in the figures before detection through conjugated secondary antibodies. Controls for immunostaining included either no primary or no secondary antibody.

CHAPTER 4

GENERAL DISCUSSION

4.1. Overall Summary:

The goal of this research has been to gain insight on the role of the CXCL12/CXCR4 signaling pathway in adipose tissue maintenance and expansion. BAT is controlled by sympathetic innervation which regulates adaptive thermogenesis in exposure to cold environments. However, BAT innervation remains poorly understood. Here, we have shown that smooth muscle cell expression of CXCL12 is regulating BAT lipid accumulation, though not directly regulating thermogenic function. Indirectly, the loss of CXCL12 within BAT smooth muscle cells causes a reduction in BAT innervation which then increases whitening of BAT while reducing thermogenic responses to cold stimuli. The loss of CXCL12 limits the amount of CXCR4+/CD301 macrophages that contribute to neuronal maintenance. These findings suggest a smooth muscle cell chemokine-dependent mechanism linking immune cell infiltration and sympathetic neuronal presence. Moreover, we wanted to understand the role of CXCL12/CXCR4 signaling in adipogenesis. Adipose tissue expands through two mechanisms; hypertrophy, the swelling of adipocytes through continuously increased lipid accumulation, or hyperplasia, the generation of new adipocytes to accommodate excess lipid uptake. Both types of adipose tissue expansion are the result of an increased energy intake and reduced energy expenditure. It has been previously reported that CXCR4 downregulates adipogenesis and deletion results in weight gain. However, our lab has shown that deletion of CXCR4 within the adipose lineage results in a lipodystrophic phenotype in females and is only recovered through ablation of estrogen via ovariectomies or pharmacological inhibition of estrogen. Further, we have shown that the deletion of CXCR4 increases Esr1 expression within adipocytes, suggesting a possible mechanism of CXCR4 that has

previously gone unreported. These findings highlight the importance of CXCR4 beyond cellular chemotaxis and show a new regulatory role on sex steroids.

4.2. Future Direction:

Short Term Direction:

Our findings indicate that within BAT, SMA cells are responsible for the secretion of CXCL12 which influences sympathetic innervation. However, these findings are limited to SMA+ cells exclusive to BAT. Other surrounding tissues expressing SMA could also be playing a role in BAT macrophage retention and, thus, sympathetic neuronal growth. These tissues such as endothelial vascular and smooth muscle cells could potentially provide further insight regarding the mechanisms responsible for BAT function and homeostasis. If these surrounding tissues are contributing to CXCL12 expression driving BAT function, they could be targeted therapeutically to combat metabolic dysregulations associated with obesity such as hypertriglyceridemia through increased fatty acid oxidation. Additionally, looking into other regulatory cells within BAT could potentially give rise to additional pharmacological targets to improve metabolic health.

Our phenotypic profiles indicate that deletion of CXCR4 in WAT does not impact body temperature, overall body weight, nor glucose tolerance. However, our studies have shown that deletion of CXCR4 within female WAT results in reduced adiposity. Through suppression of the deletion until sexual maturity, we were able to identify a CXCR4 deletion-driven reduction in the volume of mature adipocytes, indicating that lipids were either being utilized for energy or being introduced into circulation. In order to identify whether lipid metabolism or hypertriglyceridemia is taking place, triglyceride accumulation assays should be utilized to measure lipid levels in both the serum and fat pads of these mice.

While we have suggested a mechanism by which CXCL12/CXCR4 regulates Esr1 through mRNA expression and cell culture experimentation, a more detailed investigation is crucial to understand sex steroid-induced APC dynamics. Our data demonstrated that ablating CXCR4 within the adipose lineage results in a sexually dimorphic lipodystrophic phenotype. That is, female mice lacking CXCR4 within the adipose lineage have reduced adiposity. CXCR4-deficient APCs cannot be rescued in response to HFD feeding. However, reducing circulating estrogen levels through ovariectomies leads to restored adiposity in CXCR4-deficient female cells. Complimentary to these findings, treating CXCR4-deficient APCs with the anti-estrogen fulvestrant fully restores adipogenic potential. While these findings propose a regulatory role of CXCR4 on Esr1, the mechanism remains unclear. To test if CXCR4 alters Esr1 transcriptional activity, several experiments should be explored such as luciferase assays on estrogen DNA response elements, western blotting of a known downstream signaling molecule for both Esr1 and CXCR4, and chromatin immunoprecipitation sequencing on wildtype and CXCR4-deficient adipose tissues. These experiments would both confirm CXCR4's influence on Esr1 signaling as well as identify potential mechanisms governing estrogen-mediated WAT homeostasis.

Long Term Direction:

Our data has indicated that CXCL12 can successfully restore BAT innervation. By administration of CXCL12 over a truncated time point (daily, 1 week), lipid accumulation within BAT is reduced and the brown adipocyte becomes multiloculated, indicative of lipid-burning thermogenesis. To this effect, administration of CXCL12 can potentially serve as a therapeutic approach to combat metabolic dysfunction associated with obesity. Therefore, it is plausible to suggest clinical trials of CXCL12 administration for the reduction of hypertriglyceridemia coupled with increased BAT activation in adults. What's more, our studies indicate that targeting CXCR4

plays no role in BAT activation. Therefore, administration of both CXCR4 inhibitors and CXCL12 should be investigated in both pre and postmenopausal women to combat obesity and obesity-related diseases.

The data presented in the second study suggests the notion that CXCR4 can be an efficacious therapeutic target to reverse the effects of diet induced obesity in premenopausal women. Furthermore, targeting CXCR4 as previously suggested can potentially play an important role in blunting visceral adiposity in postmenopausal women. Our research suggests that CXCR4 is downregulating estrogenic effects on WAT homeostasis. Beside regulating body fat distribution, estrogen has been shown to have beneficial roles on metabolism. Hormone replacement therapy (HRT) has been shown to decrease fasting glucose levels while significantly lowering the instances of diabetes in postmenopausal women (302). Furthermore, HRT elevates high density lipoproteins (HDL) while reducing low density lipoproteins (LDL), resulting in healthier blood lipid profiles and lowering the risk for coronary heart disease (303, 304). Postmenopausal women receiving HRT showed a decrease in visceral adiposity, further reducing the risk of cardiovascular disease (305). Clearly, the addition of estrogen in postmenopausal women has positive health implications. By adding a CXCR4 inhibitor such as AMD3100 in conjunction with HRT, estrogenic effects could potentially be elevated. Furthermore, healthy premenopausal females do not require HRT. It is estimated by the National Health and Nutrition Examination Survey that ~42% of women aged 20-59 years old are overweight or obese in the US. While women within this age range typically do not require estrogen treatments, AMD3100 could be a potential therapeutic agent for weight loss by inhibiting CXCR4's downregulation of estrogenic effects. While AMD3100 has been utilized in clinical trials for HIV and cancer patients, its effects on adiposity have yet to be

explored. The findings in our research suggest a possible therapeutic target for premenopausal women suffering from obesity as well as postmenopausal women taking HRT treatments.

APPENDIX:

CHAPTER 2

Supplemental Figures

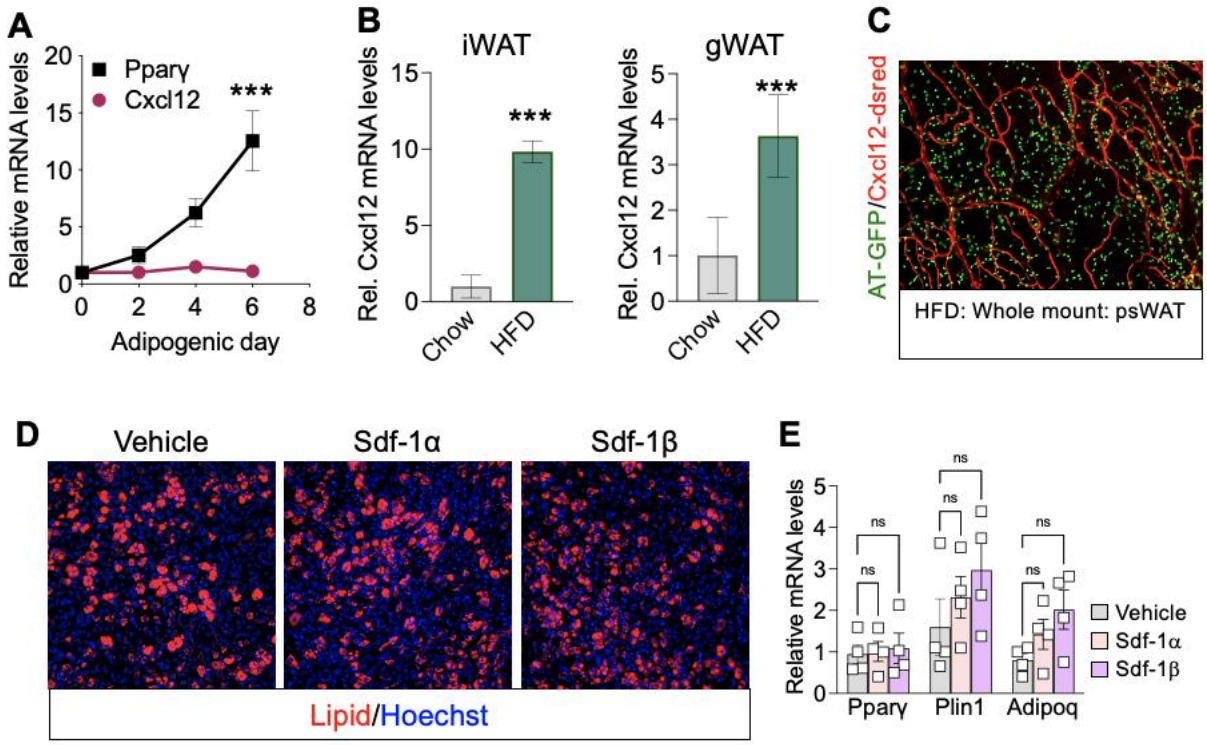

*Figure 22: Supplemental Figure 1, Related to Figure 9. A) mRNA expression of Pparg and Cxcl12 in response to adipogenic media. SV cells were isolated from iWAT depots and induced to differentiate. ***P ≤ 0.001 by Students t-test. Data are mean ± s.e.m. B) mRNA expression levels of Cxcl12 within iWAT or gWAT depots while mice were maintained on chow or HFD for eight-weeks. ***P ≤ 0.001 by Students t-test. Data are mean ± s.e.m. n = 4/group. C) Representative images of whole mount fluorescence microscopy (GFP and RFP) of periscapular WAT (psWAT) from AT-Cxc12-DsRed mice. D) Representative images of lipid staining of in vitro derived white adipocytes from isolated iWAT SV cells treated with vehicle, Sd1-a, or Sdf-1b. E) mRNA expression levels of denoted adipocyte markers from adipocytes described in (D)*

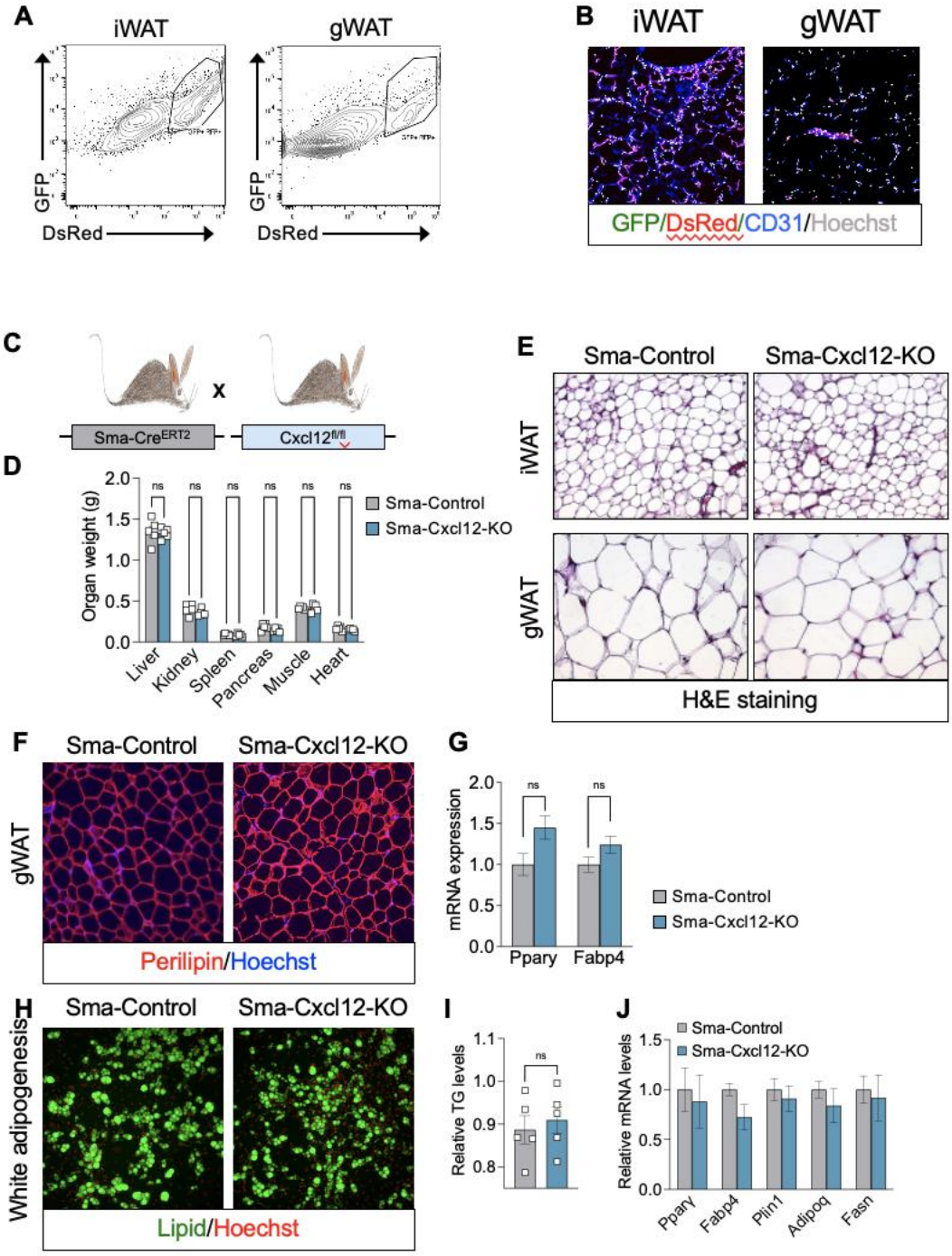

Figure 23: Supplemental Figure 2, Related to Figure 10. A) Representative flow plots demonstrating gating strategizes for colocalization between GFP and DsRed for iWAT and gWAT. B) Representative images of GFP, DsRed, and CD31 immunostaining of iWAT and gWAT sections from AT-Cxcl12-DsRed mice. C) Genetic schema: Sma-CreERT2 mice were combined with Cxcl12fl/fl mice to create (Sma-Cxcl12-KO) D) Sma-Control (Sma-CreERT2; or Cxcl12fl/fl) and Sma-Cxcl12-KO (Sma-CreERT2; Cxcl12fl/fl) mice were administered tamoxifen (TMX) at P60 and chased for six-weeks at room temperature (RT). Organ weight was assessed. E) Representative images of H&E staining from iWAT and gWAT depots from mice described in (D) F)

Representative images of Plin1 staining of gWAT sections from mice described in (D). G) mRNA expression levels of adipocyte markers from iWAT depots of mice described in (D). H) Representative images of lipid staining of in vitro derived adipocytes from iWAT SV cells from mice described in (D). I) Relative triglyceride accumulation of in vitro derived adipocyte cultures (H) from mice described in (D). J) mRNA expression levels of denoted adipocyte markers from in vitro derived adipocyte cultures (H) from mice described in (D).

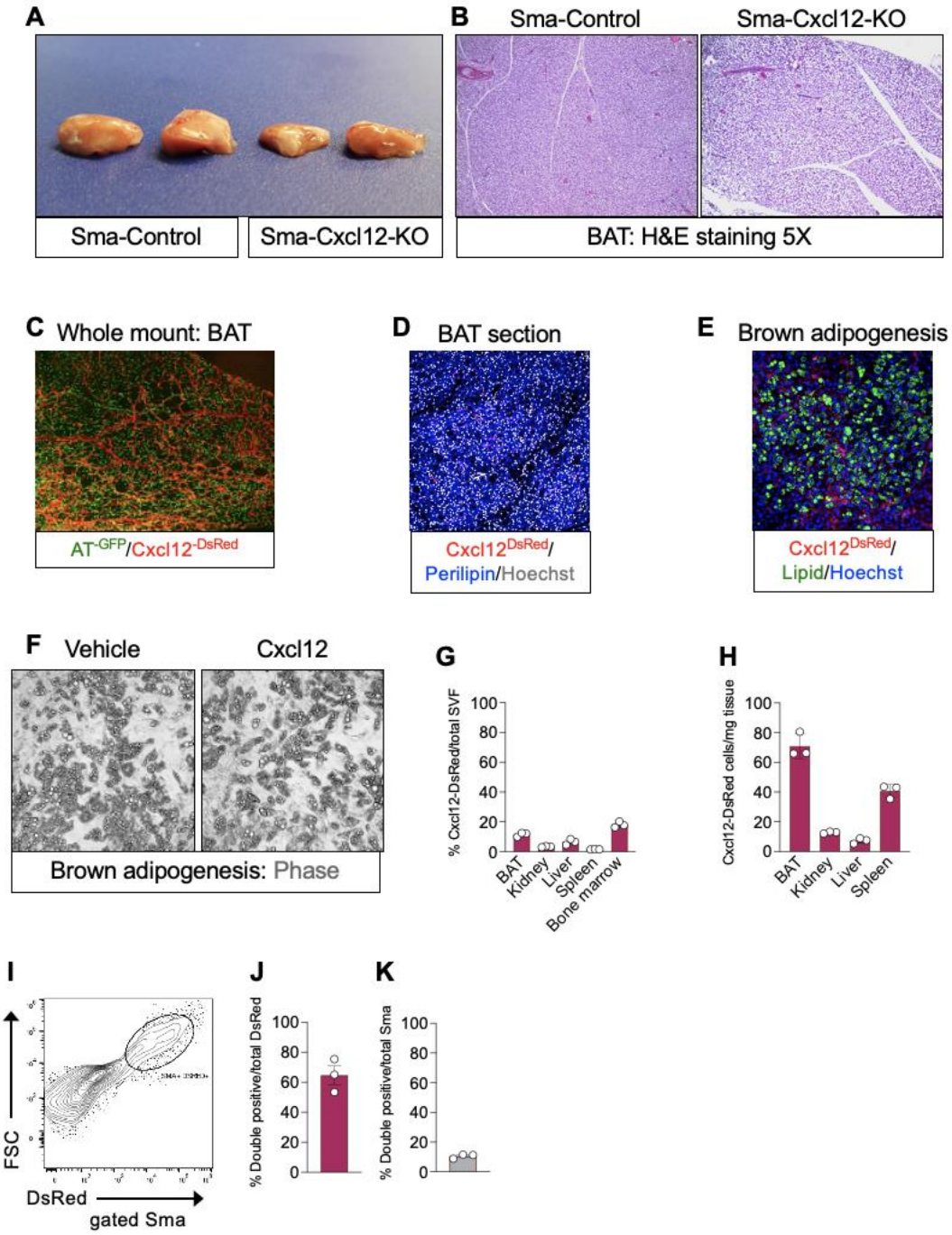

Figure 24: Supplemental Figure 3, Related to Figure 11. A) Sma-Control (Sma-CreERT2; or Cxcl12fl/fl) and Sma-Cxcl12-KO (Sma-CreERT2; Cxcl12fl/fl) mice were administered tamoxifen (TMX) at P60 and chased for six-weeks at room temperature (RT). Representative images of brown adipose depots. B) Representative images of H&E staining from mice described in (A) at 5x magnification. C) Representative images of whole mount fluorescence microscopy (GFP and RFP) of BAT from AT-Cxc12-DsRed mice. D) Representative images of DsRed and Plin1 staining from BAT sections from Cxc12-DsRed mice. E) Representative images of lipid staining of in vitro derived brown adipocytes from BAT SV cells isolated from Cxcl12-DsRed mice. F) Experimental schema: BAT SV cells were isolated from Sma-Control mice and cultured in the presence of vehicle

or Cxcl12 (50 ng/ml) and adipogenic media. Differentiation was assessed by micrographs. G) SV cells were isolated from BAT, kidney, liver, spleen, and bone marrow. Total cellular composition was assessed for Cxcl12-DsRed expression by flow cytometry. H) Relative abundance was calculated from FACS analyzed cells described in (G), expect bone marrow. I) Representative FACS plot for gating for DsRed and Sma colocalization in BAT. J) Quantification of colocalization between DsRed and Sma compared to the total number of Cxcl12-DsRed+ cells from FACS analysis described in (I). K) Quantification of colocalization between DsRed and Sma compared to the total number of Sma+ cells. L) Representative images of Plin1 staining of gWAT sections from mice described in (D).

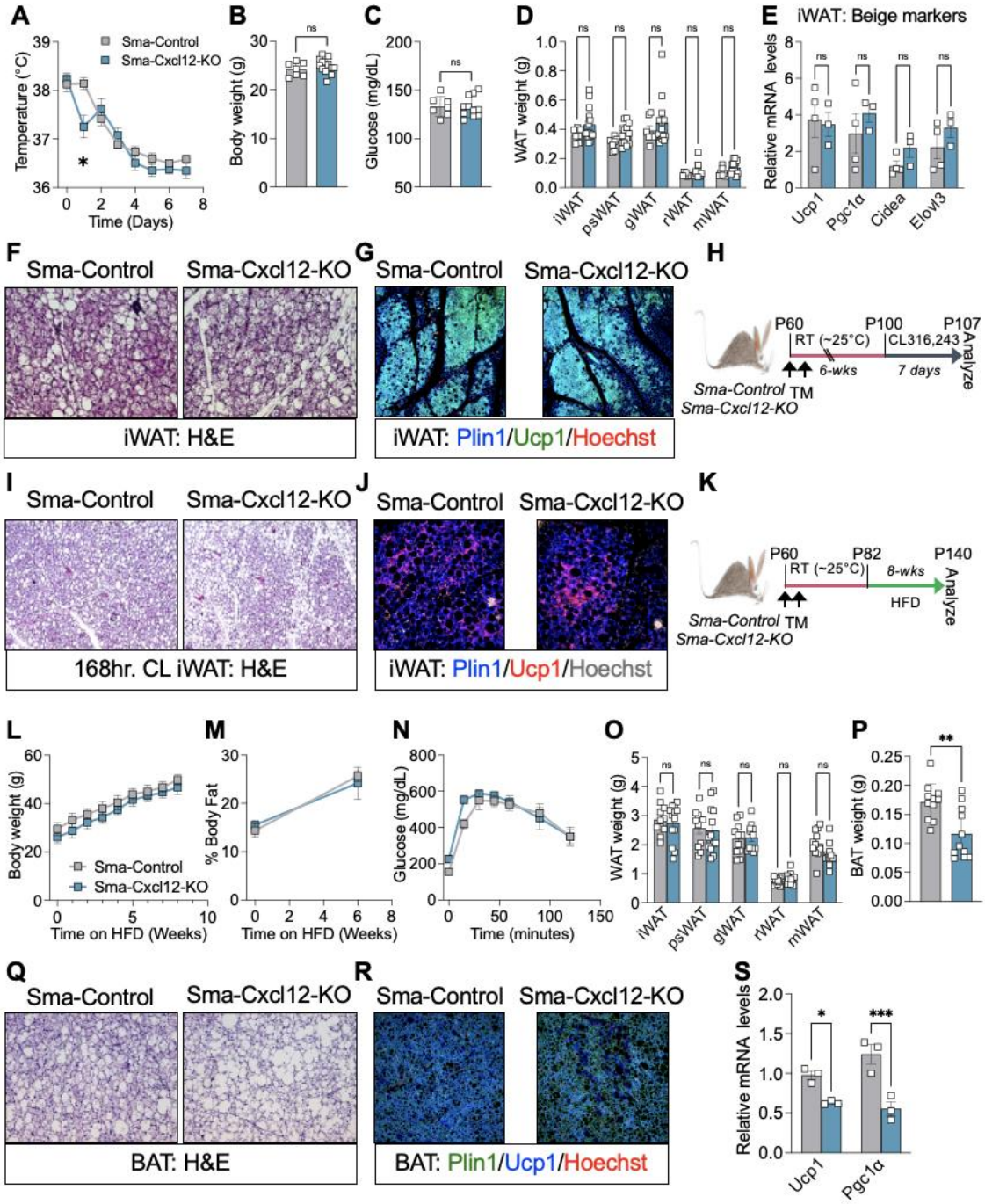

*Figure 25: Supplemental Figure 4, Related to Figure 12. A-E) Sma-Control (Sma-CreERT2; or Cxcl12fl/fl) and Sma-Cxcl12-KO (Sma-CreERT2; Cxcl12fl/fl) mice were administered tamoxifen (TMX) at P60 and chased for six-weeks at room temperature (RT). Mice were then cold exposed up to seven days. Rectal temperatures (A), bodyweight (B), blood glucose (C), WAT weight (D), and mRNA expression of thermogenic markers (E) were assessed. *P ≤ 0.001 by Students t-test. Data are mean ± s.e.m. n = 7-11 mice/group. F-G) Representative images of H&E staining and Plin1 and Ucp1 immunostaining of iWAT sections from seven-day cold exposed mice described in (A) H) Experimental schema: Sma-Control and Sma-Cxcl12-KO mice were administered TMX at P60 and chased for six weeks at RT and then administered CL316,243 (1 mg/Kg) for seven days.*

*I-J) Representative images of H&E staining and Plin1 and Ucp1 immunostaining of iWAT sections from mice described in (H) K) Experimental schema: Sma-Control and Sma-Cxcl12-KO mice were administered TMX at P60 and chased for three weeks at RT and then administered HFD for eight-weeks. n = 9-12 mice/group. L-P) Body weight (L), % body fat (M), glucose tolerance test (N), and WAT (O) and BAT (P) weight was assessed from mice described in (K). **P ≤ 0.002 by Students t-test. Data are mean ± s.e.m. Q-R) Representative images of H&E staining and Plin1 and Ucp1 immunostaining of BAT sections from HFD fed mice described in (K) S) mRNA expression levels of Ucp1 and Pgc1a within BAT depots from HFD mice described in (K). *P ≤0.033; **P ≤ 0.001 by Students t-test. Data are mean ± s.e.m. n = 3 mice/group.*

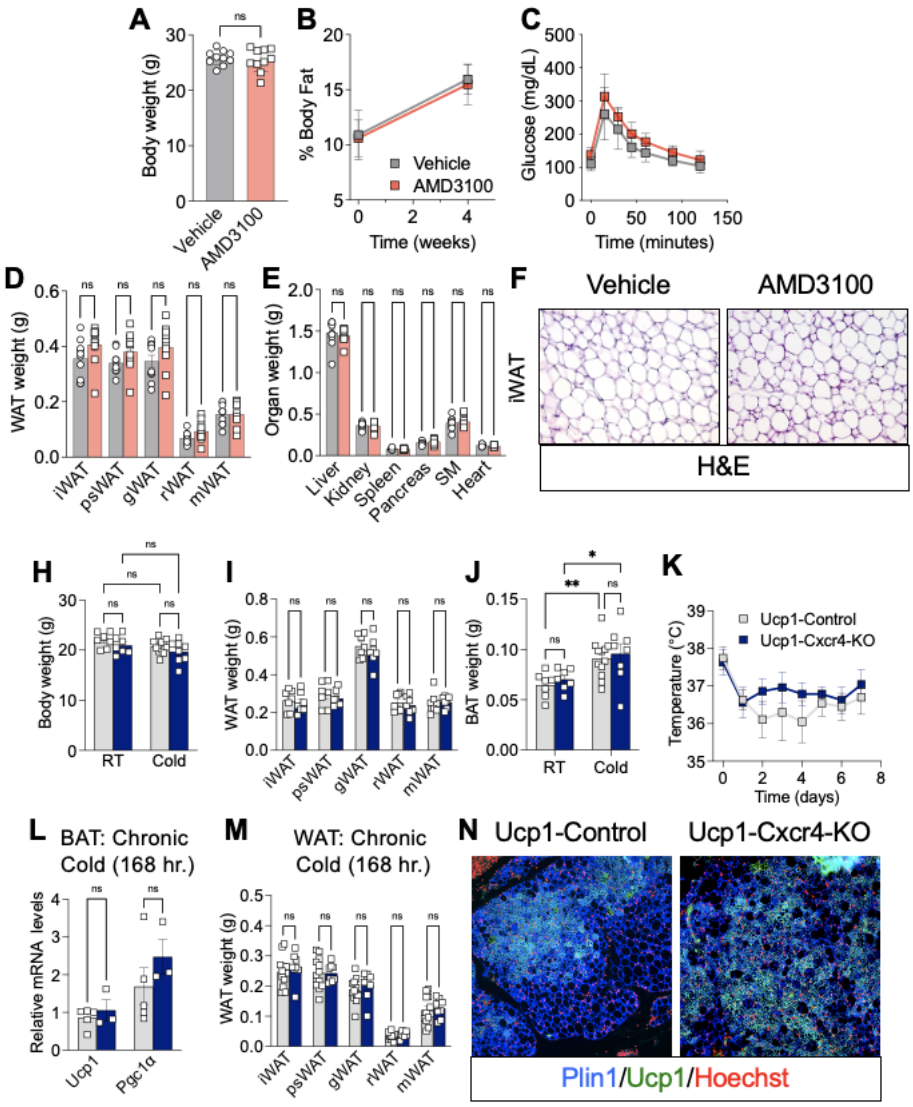

Figure 26: Supplemental Figure 5, Related to Figure 13. A-E) At P60, Sma-Control were administered vehicle (PBS) or AMD3100 (5mg/Kg IP 4x/week for four weeks). n = 10 mice/group. Body weight (A), %body fat (B), glucose tolerance test (C), WAT weight (D), and organ weight (E) were assessed. F) Representative images of H&E staining of iWAT depots from mice described in (A). H-M) Ucp1-Control (Ucp1-Cre) and Ucp1-Cxcr4-KO (Ucp1-Cre; Cxcr4$^{fl/fl}$) were

maintained at RT until P60; subsequently, mice were cold exposure seven days (168 hrs. chronic). n = 9-10 mice/group. Body weight (H), WAT weight RT (I), and BAT weight (J), rectal temperature (K), thermogenic gene expression-cold (L), and WAT weight cold (M) were assessed. N) Representative images of Plin1 and Ucp1 immunostaining of iWAT sections from mice described in (H).

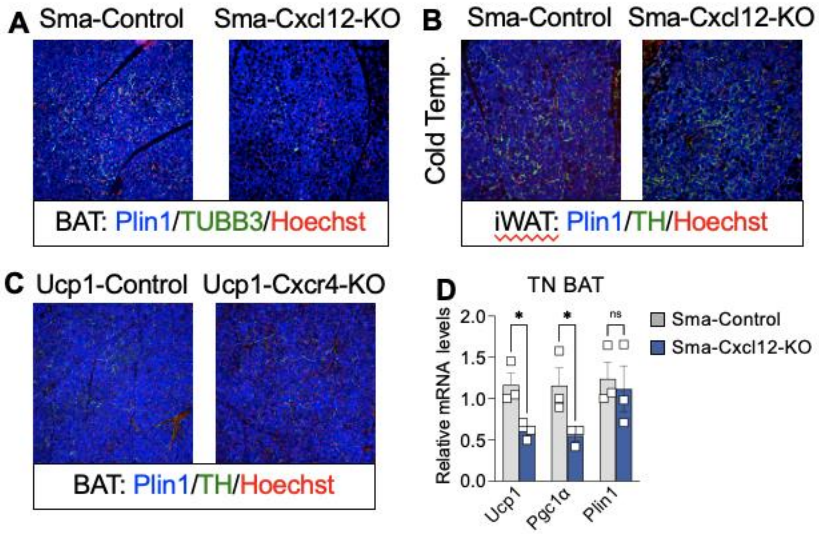

*Figure 27: Supplemental Figure 6, Related to Figure 14. A) Representative images of Plin1 and TUBB3 immunostaining from BAT sections from Sma-Control and Sma-Cxcl12-KO mice post TMX six-weeks. B) Representative images of Plin1 and TH immunostaining from iWAT sections from Sma-Control and Sma-Cxcl12-KO mice post TMX six weeks cold exposed for seven days. C) Representative images of Plin1 and TH immunostaining from BAT sections from Ucp1-Control and Ucp1-Cxcr4-KO mice at P60 maintained at RT. D) mRNA expression levels of denoted genes within BAT depots from Sma-Control and Sma-Cxcl12-KO mice maintained at TN six weeks post TMX. *P ≤0.033 by ordinary one-way ANOVA; n = 3 mice/group.*

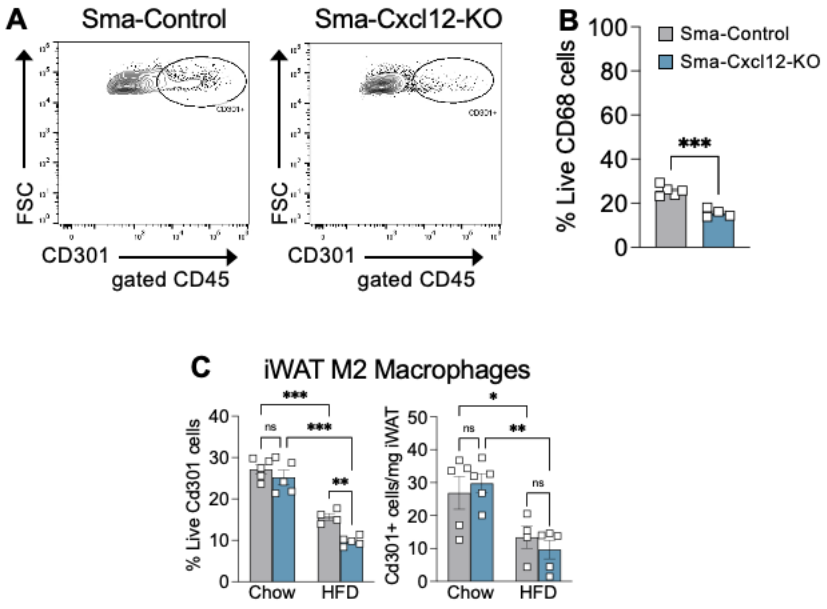

*Figure 28: Supplemental Figure 7, Related to Figure 15. A) Representative FACS plot for gating of CD301 cellular populations within BAT from Sma-Control and Sma-Cxcl12-KO mice post TMX six-weeks. B) Relative percentage of live CD68+ within BAT depots from Sma-Control and Sma-Cxcl12-KO mice. ***P ≤0.001 by Student t-test; n = 5 mice/group. C) Relative frequency and abundance of CD301+ cells with iWAT depots from Sma-Control and Sma-Cxcl12-KO mice fed a chow or HFD (8-weeks). *P ≤ 0.033; **P ≤ 0.002; ***P ≤ 0.001 by ordinary one-way ANOVA. Data are mean ± s.e.m. n = 4-6 mice/group.*

CHAPTER 3

Supplemental Figures

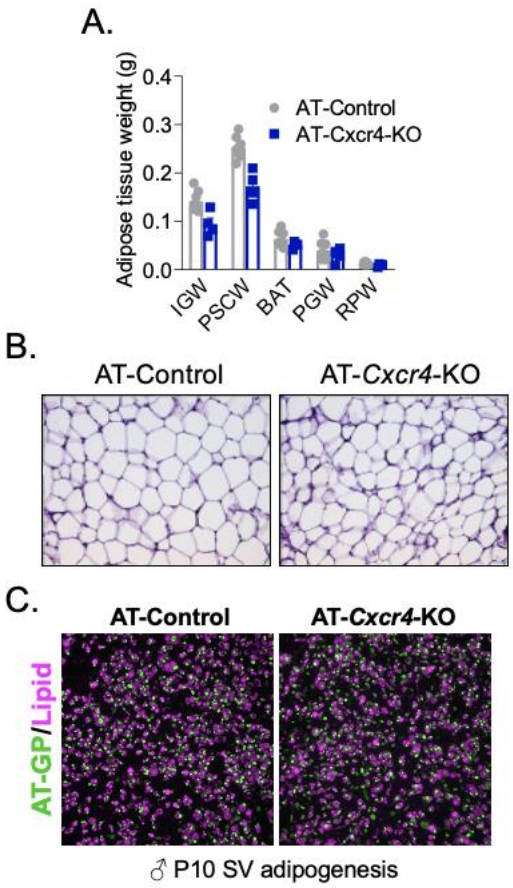

Figure 29: Supplemental Figure 8, Related to Figure 17. A) Individual adipose depot weights for AT-Control and AT-CXCR4-KO mice at P10. B) Representative images of H&E staining of subcutaneous fat depots on mice described in (A). C) Representative images of in vitro lipid staining after terminal differentiation on mice described in (A).

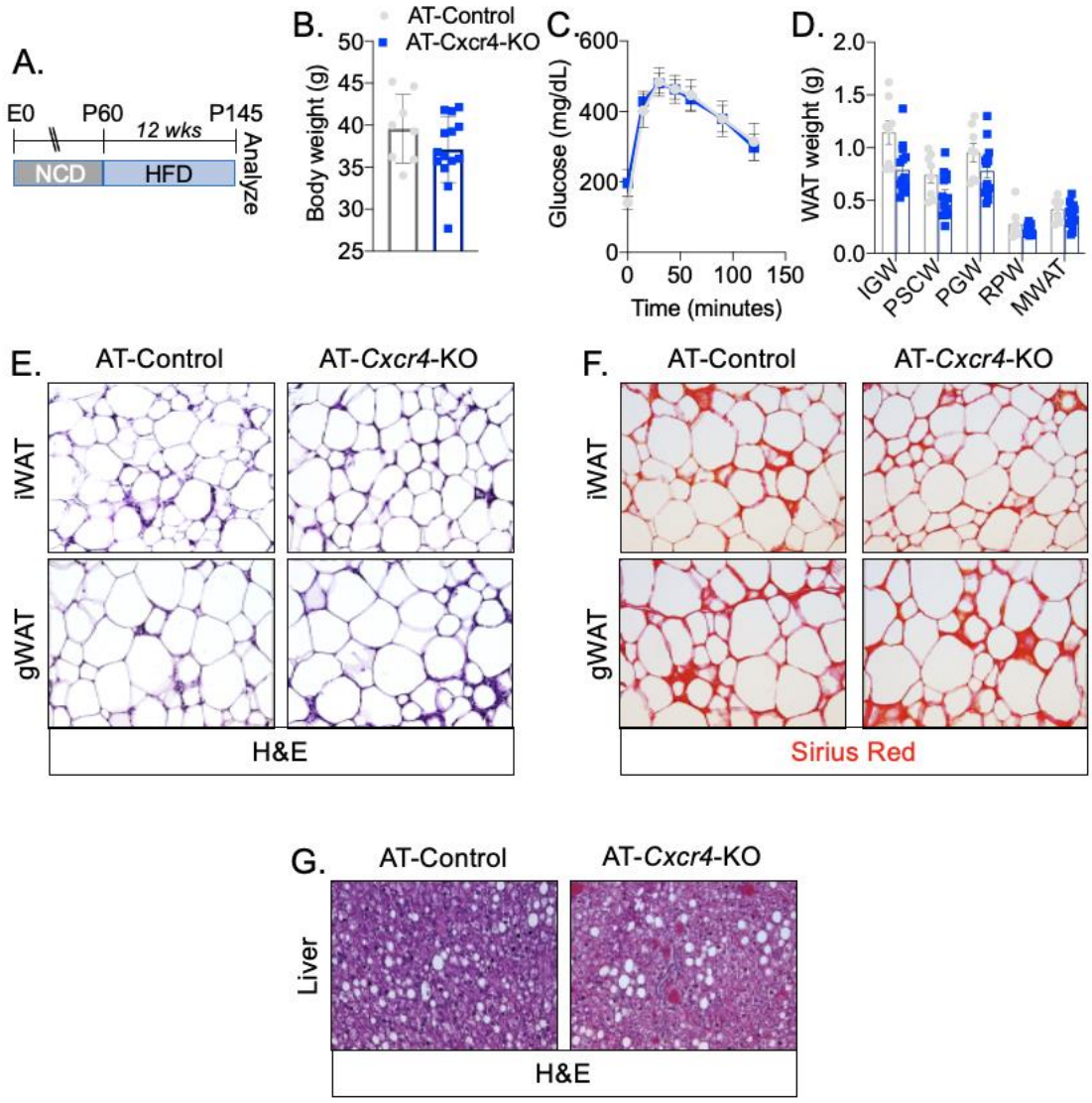

Figure 30: Supplemental Figure 9, Related to Figure 18. A) Experimental schema: Male AT-Control and AT-CXCR4-KO mice were placed on chow diet from conception until P60. At P60, mice were placed on HFD for 12 weeks before analysis. B) Body weight upon analysis from mice described in (A). C) Glucose tolerance tests from mice described in (A). D) Individual adipose depot weights from mice described in (A). E) Representative images of H&E staining of subcutaneous and visceral fat depot sections from mice described in (A) I) Representative images of Sirius red (fibrotic) staining of subcutaneous and visceral fat depot sections from mice described in (A). J) Representative images of H&E staining of liver sections from mice described in (A).

References:

1. Spalding KL, Bernard S, Naslund E, Salehpour M, Possnert G, Appelsved L, Fu KY, Alkass K, Druid H, Thorell A, Ryden M, Arner P. Impact of fat mass and distribution on lipid turnover in human adipose tissue. Nat Commun. 2017;8:15253. Epub 2017/05/24. doi: 10.1038/ncomms15253. PubMed PMID: 28534500; PMCID: PMC5457499.
2. Gil A, Maria Aguilera C, Gil-Campos M, Canete R. Altered signalling and gene expression associated with the immune system and the inflammatory response in obesity. Br J Nutr. 2007;98 Suppl 1:S121-6. Epub 2007/11/21. doi: 10.1017/S0007114507838050. PubMed PMID: 17922949.
3. Kusminski CM, Shetty S, Orci L, Unger RH, Scherer PE. Diabetes and apoptosis: lipotoxicity. Apoptosis. 2009;14(12):1484-95. Epub 2009/05/08. doi: 10.1007/s10495-009-0352-8. PubMed PMID: 19421860.
4. Rahmani S, Turton P, Shaaban A, Dall B. Overview of gynecomastia in the modern era and the Leeds Gynaecomastia Investigation algorithm. Breast J. 2011;17(3):246-55. Epub 2011/04/12. doi: 10.1111/j.1524-4741.2011.01080.x. PubMed PMID: 21477170.
5. Jensen MD. Role of body fat distribution and the metabolic complications of obesity. J Clin Endocrinol Metab. 2008;93(11 Suppl 1):S57-63. Epub 2008/12/04. doi: 10.1210/jc.2008-1585. PubMed PMID: 18987271; PMCID: PMC2585758.
6. Rodriguez A, Catalan V, Gomez-Ambrosi J, Fruhbeck G. Visceral and subcutaneous adiposity: are both potential therapeutic targets for tackling the metabolic syndrome? Curr Pharm Des. 2007;13(21):2169-75. Epub 2007/07/14. doi: 10.2174/138161207781039599. PubMed PMID: 17627548.
7. Ibrahim MM. Subcutaneous and visceral adipose tissue: structural and functional differences. Obes Rev. 2010;11(1):11-8. Epub 2009/08/07. doi: 10.1111/j.1467-789X.2009.00623.x. PubMed PMID: 19656312.
8. Fruhbeck G, Gomez-Ambrosi J. Rationale for the existence of additional adipostatic hormones. FASEB J. 2001;15(11):1996-2006. Epub 2001/09/05. doi: 10.1096/fj.00-0829hyp. PubMed PMID: 11532980.
9. Fruhbeck G, Gomez-Ambrosi J. Control of body weight: a physiologic and transgenic perspective. Diabetologia. 2003;46(2):143-72. Epub 2003/03/11. doi: 10.1007/s00125-003-1053-4. PubMed PMID: 12627314.
10. Rodriguez A, Ezquerro S, Mendez-Gimenez L, Becerril S, Fruhbeck G. Revisiting the adipocyte: a model for integration of cytokine signaling in the regulation of energy metabolism. Am J Physiol Endocrinol Metab. 2015;309(8):E691-714. Epub 2015/09/04. doi: 10.1152/ajpendo.00297.2015. PubMed PMID: 26330344.
11. Ahima RS, Prabakaran D, Mantzoros C, Qu D, Lowell B, Maratos-Flier E, Flier JS. Role of leptin in the neuroendocrine response to fasting. Nature. 1996;382(6588):250-2. Epub 1996/07/18. doi: 10.1038/382250a0. PubMed PMID: 8717038.
12. Oh DK, Ciaraldi T, Henry RR. Adiponectin in health and disease. Diabetes Obes Metab. 2007;9(3):282-9. Epub 2007/03/30. doi: 10.1111/j.1463-1326.2006.00610.x. PubMed PMID: 17391153.

13. Qatanani M, Szwergold NR, Greaves DR, Ahima RS, Lazar MA. Macrophage-derived human resistin exacerbates adipose tissue inflammation and insulin resistance in mice. J Clin Invest. 2009;119(3):531-9. Epub 2009/02/04. doi: 10.1172/JCI37273. PubMed PMID: 19188682; PMCID: PMC2648673.
14. Bokarewa M, Nagaev I, Dahlberg L, Smith U, Tarkowski A. Resistin, an adipokine with potent proinflammatory properties. J Immunol. 2005;174(9):5789-95. Epub 2005/04/22. doi: 10.4049/jimmunol.174.9.5789. PubMed PMID: 15843582.
15. Goerdt S, Politz O, Schledzewski K, Birk R, Gratchev A, Guillot P, Hakiy N, Klemke CD, Dippel E, Kodelja V, Orfanos CE. Alternative versus classical activation of macrophages. Pathobiology. 1999;67(5-6):222-6. Epub 2000/03/22. doi: 10.1159/000028096. PubMed PMID: 10725788.
16. Moschen AR, Gerner R, Schroll A, Fritz T, Kaser A, Tilg H. A key role for Pre-B cell colony-enhancing factor in experimental hepatitis. Hepatology. 2011;54(2):675-86. Epub 2011/05/14. doi: 10.1002/hep.24416. PubMed PMID: 21567435.
17. Romacho T, Azcutia V, Vazquez-Bella M, Matesanz N, Cercas E, Nevado J, Carraro R, Rodriguez-Manas L, Sanchez-Ferrer CF, Peiro C. Extracellular PBEF/NAMPT/visfatin activates pro-inflammatory signalling in human vascular smooth muscle cells through nicotinamide phosphoribosyltransferase activity. Diabetologia. 2009;52(11):2455-63. Epub 2009/09/04. doi: 10.1007/s00125-009-1509-2. PubMed PMID: 19727662.
18. Lee SA, Yuen JJ, Jiang H, Kahn BB, Blaner WS. Adipocyte-specific overexpression of retinol-binding protein 4 causes hepatic steatosis in mice. Hepatology. 2016;64(5):1534-46. Epub 2016/10/22. doi: 10.1002/hep.28659. PubMed PMID: 27227735; PMCID: PMC5074895.
19. Wang QA, Tao C, Gupta RK, Scherer PE. Tracking adipogenesis during white adipose tissue development, expansion and regeneration. Nat Med. 2013;19(10):1338-44. Epub 2013/09/03. doi: 10.1038/nm.3324. PubMed PMID: 23995282; PMCID: PMC4075943.
20. Sun K, Tordjman J, Clement K, Scherer PE. Fibrosis and adipose tissue dysfunction. Cell Metab. 2013;18(4):470-7. Epub 2013/08/21. doi: 10.1016/j.cmet.2013.06.016. PubMed PMID: 23954640; PMCID: PMC3795900.
21. Ouchi N, Parker JL, Lugus JJ, Walsh K. Adipokines in inflammation and metabolic disease. Nat Rev Immunol. 2011;11(2):85-97. Epub 2011/01/22. doi: 10.1038/nri2921. PubMed PMID: 21252989; PMCID: PMC3518031.
22. Gesta S, Tseng YH, Kahn CR. Developmental origin of fat: tracking obesity to its source. Cell. 2007;131(2):242-56. Epub 2007/10/25. doi: 10.1016/j.cell.2007.10.004. PubMed PMID: 17956727.
23. Canavoso LE, Wells MA. Role of lipid transfer particle in delivery of diacylglycerol from midgut to lipophorin in larval Manduca sexta. Insect Biochem Mol Biol. 2001;31(8):783-90. Epub 2001/05/30. doi: 10.1016/s0965-1748(00)00183-1. PubMed PMID: 11378413.
24. Arner P. Differences in lipolysis between human subcutaneous and omental adipose tissues. Ann Med. 1995;27(4):435-8. Epub 1995/08/01. doi: 10.3109/07853899709002451. PubMed PMID: 8519504.
25. Dawkins MJ, Hull D. The Production of Heat by Fat. Sci Am. 1965;213:62-7. Epub 1965/08/01. doi: 10.1038/scientificamerican0865-62. PubMed PMID: 14319024.
26. Himms-Hagen J, Melnyk A, Zingaretti MC, Ceresi E, Barbatelli G, Cinti S. Multilocular fat cells in WAT of CL-316243-treated rats derive directly from white adipocytes. Am J Physiol Cell

Physiol. 2000;279(3):C670-81. Epub 2000/08/16. doi: 10.1152/ajpcell.2000.279.3.C670. PubMed PMID: 10942717.
27. Vitali A, Murano I, Zingaretti MC, Frontini A, Ricquier D, Cinti S. The adipose organ of obesity-prone C57BL/6J mice is composed of mixed white and brown adipocytes. J Lipid Res. 2012;53(4):619-29. Epub 2012/01/25. doi: 10.1194/jlr.M018846. PubMed PMID: 22271685; PMCID: PMC3307639.
28. Petrovic N, Walden TB, Shabalina IG, Timmons JA, Cannon B, Nedergaard J. Chronic peroxisome proliferator-activated receptor gamma (PPARgamma) activation of epididymally derived white adipocyte cultures reveals a population of thermogenically competent, UCP1-containing adipocytes molecularly distinct from classic brown adipocytes. J Biol Chem. 2010;285(10):7153-64. Epub 2009/12/24. doi: 10.1074/jbc.M109.053942. PubMed PMID: 20028987; PMCID: PMC2844165.
29. Wu J, Cohen P, Spiegelman BM. Adaptive thermogenesis in adipocytes: is beige the new brown? Genes Dev. 2013;27(3):234-50. Epub 2013/02/08. doi: 10.1101/gad.211649.112. PubMed PMID: 23388824; PMCID: PMC3576510.
30. Rosenwald M, Perdikari A, Rulicke T, Wolfrum C. Bi-directional interconversion of brite and white adipocytes. Nat Cell Biol. 2013;15(6):659-67. Epub 2013/04/30. doi: 10.1038/ncb2740. PubMed PMID: 23624403.
31. Barbatelli G, Murano I, Madsen L, Hao Q, Jimenez M, Kristiansen K, Giacobino JP, De Matteis R, Cinti S. The emergence of cold-induced brown adipocytes in mouse white fat depots is determined predominantly by white to brown adipocyte transdifferentiation. Am J Physiol Endocrinol Metab. 2010;298(6):E1244-53. Epub 2010/04/01. doi: 10.1152/ajpendo.00600.2009. PubMed PMID: 20354155.
32. Murano I, Barbatelli G, Giordano A, Cinti S. Noradrenergic parenchymal nerve fiber branching after cold acclimatisation correlates with brown adipocyte density in mouse adipose organ. J Anat. 2009;214(1):171-8. Epub 2008/11/21. doi: 10.1111/j.1469-7580.2008.01001.x. PubMed PMID: 19018882; PMCID: PMC2667925.
33. Bukowiecki L, Collet AJ, Follea N, Guay G, Jahjah L. Brown adipose tissue hyperplasia: a fundamental mechanism of adaptation to cold and hyperphagia. Am J Physiol. 1982;242(6):E353-9. Epub 1982/06/01. doi: 10.1152/ajpendo.1982.242.6.E353. PubMed PMID: 6953766.
34. Cannon B, Nedergaard J. Brown adipose tissue: function and physiological significance. Physiol Rev. 2004;84(1):277-359. Epub 2004/01/13. doi: 10.1152/physrev.00015.2003. PubMed PMID: 14715917.
35. Bagchi M, Kim LA, Boucher J, Walshe TE, Kahn CR, D'Amore PA. Vascular endothelial growth factor is important for brown adipose tissue development and maintenance. FASEB J. 2013;27(8):3257-71. Epub 2013/05/18. doi: 10.1096/fj.12-221812. PubMed PMID: 23682123; PMCID: PMC3714576.
36. Kajimura S, Seale P, Tomaru T, Erdjument-Bromage H, Cooper MP, Ruas JL, Chin S, Tempst P, Lazar MA, Spiegelman BM. Regulation of the brown and white fat gene programs through a PRDM16/CtBP transcriptional complex. Genes Dev. 2008;22(10):1397-409. Epub 2008/05/17. doi: 10.1101/gad.1666108. PubMed PMID: 18483224; PMCID: PMC2377193.
37. Seale P, Bjork B, Yang W, Kajimura S, Chin S, Kuang S, Scime A, Devarakonda S, Conroe HM, Erdjument-Bromage H, Tempst P, Rudnicki MA, Beier DR, Spiegelman BM. PRDM16

controls a brown fat/skeletal muscle switch. Nature. 2008;454(7207):961-7. Epub 2008/08/23. doi: 10.1038/nature07182. PubMed PMID: 18719582; PMCID: PMC2583329.
38. Takahashi A, Shimazu T, Maruyama Y. Importance of sympathetic nerves for the stimulatory effect of cold exposure on glucose utilization in brown adipose tissue. Jpn J Physiol. 1992;42(4):653-64. Epub 1992/01/01. doi: 10.2170/jjphysiol.42.653. PubMed PMID: 1474682.
39. Trayhurn P, Milner RE. A commentary on the interpretation of in vitro biochemical measures of brown adipose tissue thermogenesis. Can J Physiol Pharmacol. 1989;67(8):811-9. Epub 1989/08/01. doi: 10.1139/y89-128. PubMed PMID: 2688850.
40. Ghorbani M, Claus TH, Himms-Hagen J. Hypertrophy of brown adipocytes in brown and white adipose tissues and reversal of diet-induced obesity in rats treated with a beta3-adrenoceptor agonist. Biochem Pharmacol. 1997;54(1):121-31. Epub 1997/07/01. doi: 10.1016/s0006-2952(97)00162-7. PubMed PMID: 9296358.
41. Guerra C, Navarro P, Valverde AM, Arribas M, Bruning J, Kozak LP, Kahn CR, Benito M. Brown adipose tissue-specific insulin receptor knockout shows diabetic phenotype without insulin resistance. J Clin Invest. 2001;108(8):1205-13. Epub 2001/10/17. doi: 10.1172/JCI13103. PubMed PMID: 11602628; PMCID: PMC209529.
42. Bartelt A, Bruns OT, Reimer R, Hohenberg H, Ittrich H, Peldschus K, Kaul MG, Tromsdorf UI, Weller H, Waurisch C, Eychmuller A, Gordts PL, Rinninger F, Bruegelmann K, Freund B, Nielsen P, Merkel M, Heeren J. Brown adipose tissue activity controls triglyceride clearance. Nat Med. 2011;17(2):200-5. Epub 2011/01/25. doi: 10.1038/nm.2297. PubMed PMID: 21258337.
43. Fredriksson JM, Nikami H, Nedergaard J. Cold-induced expression of the VEGF gene in brown adipose tissue is independent of thermogenic oxygen consumption. FEBS Lett. 2005;579(25):5680-4. Epub 2005/10/13. doi: 10.1016/j.febslet.2005.09.044. PubMed PMID: 16219308.
44. Mitchell JR, Jacobsson A, Kirchgessner TG, Schotz MC, Cannon B, Nedergaard J. Regulation of expression of the lipoprotein lipase gene in brown adipose tissue. Am J Physiol. 1992;263(3 Pt 1):E500-6. Epub 1992/09/01. doi: 10.1152/ajpendo.1992.263.3.E500. PubMed PMID: 1415530.
45. Ouellet V, Labbe SM, Blondin DP, Phoenix S, Guerin B, Haman F, Turcotte EE, Richard D, Carpentier AC. Brown adipose tissue oxidative metabolism contributes to energy expenditure during acute cold exposure in humans. J Clin Invest. 2012;122(2):545-52. Epub 2012/01/25. doi: 10.1172/JCI60433. PubMed PMID: 22269323; PMCID: PMC3266793.
46. Shabalina IG, Jacobsson A, Cannon B, Nedergaard J. Native UCP1 displays simple competitive kinetics between the regulators purine nucleotides and fatty acids. J Biol Chem. 2004;279(37):38236-48. Epub 2004/06/23. doi: 10.1074/jbc.M402375200. PubMed PMID: 15208325.
47. Spalding KL, Arner E, Westermark PO, Bernard S, Buchholz BA, Bergmann O, Blomqvist L, Hoffstedt J, Naslund E, Britton T, Concha H, Hassan M, Ryden M, Frisen J, Arner P. Dynamics of fat cell turnover in humans. Nature. 2008;453(7196):783-7. Epub 2008/05/06. doi: 10.1038/nature06902. PubMed PMID: 18454136.
48. Farmer SR. Transcriptional control of adipocyte formation. Cell Metab. 2006;4(4):263-73. Epub 2006/10/03. doi: 10.1016/j.cmet.2006.07.001. PubMed PMID: 17011499; PMCID: PMC1958996.

49. Foulkes NS, Borrelli E, Sassone-Corsi P. CREM gene: use of alternative DNA-binding domains generates multiple antagonists of cAMP-induced transcription. Cell. 1991;64(4):739-49. Epub 1991/02/22. doi: 10.1016/0092-8674(91)90503-q. PubMed PMID: 1847666.
50. Tang QQ, Gronborg M, Huang H, Kim JW, Otto TC, Pandey A, Lane MD. Sequential phosphorylation of CCAAT enhancer-binding protein beta by MAPK and glycogen synthase kinase 3beta is required for adipogenesis. Proc Natl Acad Sci U S A. 2005;102(28):9766-71. Epub 2005/06/30. doi: 10.1073/pnas.0503891102. PubMed PMID: 15985551; PMCID: PMC1175002.
51. Wang GL, Shi X, Salisbury E, Sun Y, Albrecht JH, Smith RG, Timchenko NA. Cyclin D3 maintains growth-inhibitory activity of C/EBPalpha by stabilizing C/EBPalpha-cdk2 and C/EBPalpha-Brm complexes. Mol Cell Biol. 2006;26(7):2570-82. Epub 2006/03/16. doi: 10.1128/MCB.26.7.2570-2582.2006. PubMed PMID: 16537903; PMCID: PMC1430318.
52. Tontonoz P, Spiegelman BM. Fat and beyond: the diverse biology of PPARgamma. Annu Rev Biochem. 2008;77:289-312. Epub 2008/06/04. doi: 10.1146/annurev.biochem.77.061307.091829. PubMed PMID: 18518822.
53. Massague J, Seoane J, Wotton D. Smad transcription factors. Genes Dev. 2005;19(23):2783-810. Epub 2005/12/03. doi: 10.1101/gad.1350705. PubMed PMID: 16322555.
54. Tontonoz P, Hu E, Graves RA, Budavari AI, Spiegelman BM. mPPAR gamma 2: tissue-specific regulator of an adipocyte enhancer. Genes Dev. 1994;8(10):1224-34. Epub 1994/05/15. doi: 10.1101/gad.8.10.1224. PubMed PMID: 7926726.
55. Rosen ED, MacDougald OA. Adipocyte differentiation from the inside out. Nat Rev Mol Cell Biol. 2006;7(12):885-96. Epub 2006/12/02. doi: 10.1038/nrm2066. PubMed PMID: 17139329.
56. Qiu Z, Wei Y, Chen N, Jiang M, Wu J, Liao K. DNA synthesis and mitotic clonal expansion is not a required step for 3T3-L1 preadipocyte differentiation into adipocytes. J Biol Chem. 2001;276(15):11988-95. Epub 2001/03/30. doi: 10.1074/jbc.M011729200. PubMed PMID: 11278974.
57. Janderova L, McNeil M, Murrell AN, Mynatt RL, Smith SR. Human mesenchymal stem cells as an in vitro model for human adipogenesis. Obes Res. 2003;11(1):65-74. Epub 2003/01/17. doi: 10.1038/oby.2003.11. PubMed PMID: 12529487.
58. Kim SP, Ha JM, Yun SJ, Kim EK, Chung SW, Hong KW, Kim CD, Bae SS. Transcriptional activation of peroxisome proliferator-activated receptor-gamma requires activation of both protein kinase A and Akt during adipocyte differentiation. Biochem Biophys Res Commun. 2010;399(1):55-9. Epub 2010/07/20. doi: 10.1016/j.bbrc.2010.07.038. PubMed PMID: 20638365.
59. Salasznyk RM, Klees RF, Westcott AM, Vandenberg S, Bennett K, Plopper GE. Focusing of gene expression as the basis of stem cell differentiation. Stem Cells Dev. 2005;14(6):608-20. Epub 2006/01/26. doi: 10.1089/scd.2005.14.608. PubMed PMID: 16433616.
60. Gurriaran-Rodriguez U, Al-Massadi O, Roca-Rivada A, Crujeiras AB, Gallego R, Pardo M, Seoane LM, Pazos Y, Casanueva FF, Camina JP. Obestatin as a regulator of adipocyte metabolism and adipogenesis. J Cell Mol Med. 2011;15(9):1927-40. Epub 2010/10/30. doi: 10.1111/j.1582-4934.2010.01192.x. PubMed PMID: 21029370; PMCID: PMC3918048.

61. Cao Z, Umek RM, McKnight SL. Regulated expression of three C/EBP isoforms during adipose conversion of 3T3-L1 cells. Genes Dev. 1991;5(9):1538-52. Epub 1991/09/01. doi: 10.1101/gad.5.9.1538. PubMed PMID: 1840554.
62. Corvera S. Cellular Heterogeneity in Adipose Tissues. Annu Rev Physiol. 2021;83:257-78. Epub 2021/02/11. doi: 10.1146/annurev-physiol-031620-095446. PubMed PMID: 33566675; PMCID: PMC8091658.
63. Berry R, Rodeheffer MS. Characterization of the adipocyte cellular lineage in vivo. Nat Cell Biol. 2013;15(3):302-8. Epub 2013/02/26. doi: 10.1038/ncb2696. PubMed PMID: 23434825; PMCID: PMC3721064.
64. Rodeheffer MS, Birsoy K, Friedman JM. Identification of white adipocyte progenitor cells in vivo. Cell. 2008;135(2):240-9. Epub 2008/10/07. doi: 10.1016/j.cell.2008.09.036. PubMed PMID: 18835024.
65. Warming S, Rachel RA, Jenkins NA, Copeland NG. Zfp423 is required for normal cerebellar development. Mol Cell Biol. 2006;26(18):6913-22. Epub 2006/09/01. doi: 10.1128/MCB.02255-05. PubMed PMID: 16943432; PMCID: PMC1592861.
66. Bond HM, Scicchitano S, Chiarella E, Amodio N, Lucchino V, Aloisio A, Montalcini Y, Mesuraca M, Morrone G. ZNF423: A New Player in Estrogen Receptor-Positive Breast Cancer. Front Endocrinol (Lausanne). 2018;9:255. Epub 2018/06/06. doi: 10.3389/fendo.2018.00255. PubMed PMID: 29867779; PMCID: PMC5968090.
67. Alcaraz WA, Gold DA, Raponi E, Gent PM, Concepcion D, Hamilton BA. Zfp423 controls proliferation and differentiation of neural precursors in cerebellar vermis formation. Proc Natl Acad Sci U S A. 2006;103(51):19424-9. Epub 2006/12/08. doi: 10.1073/pnas.0609184103. PubMed PMID: 17151198; PMCID: PMC1748242.
68. Addison WN, Hall KC, Kokabu S, Matsubara T, Fu MM, Gori F, Baron R. Zfp423 Regulates Skeletal Muscle Regeneration and Proliferation. Mol Cell Biol. 2019;39(8). Epub 2019/01/30. doi: 10.1128/MCB.00447-18. PubMed PMID: 30692273; PMCID: PMC6447414.
69. Shin S, Pang Y, Park J, Liu L, Lukas BE, Kim SH, Kim KW, Xu P, Berry DC, Jiang Y. Dynamic control of adipose tissue development and adult tissue homeostasis by platelet-derived growth factor receptor alpha. Elife. 2020;9. Epub 2020/06/20. doi: 10.7554/eLife.56189. PubMed PMID: 32553115; PMCID: PMC7338051.
70. Bachmeier M, Loffler G. Influence of growth factors on growth and differentiation of 3T3-L1 preadipocytes in serum-free conditions. Eur J Cell Biol. 1995;68(3):323-9. Epub 1995/11/01. PubMed PMID: 8603685.
71. Fitter S, Vandyke K, Gronthos S, Zannettino AC. Suppression of PDGF-induced PI3 kinase activity by imatinib promotes adipogenesis and adiponectin secretion. J Mol Endocrinol. 2012;48(3):229-40. Epub 2012/04/05. doi: 10.1530/JME-12-0003. PubMed PMID: 22474082.
72. Sanchez-Gurmaches J, Guertin DA. Adipocytes arise from multiple lineages that are heterogeneously and dynamically distributed. Nat Commun. 2014;5:4099. Epub 2014/06/20. doi: 10.1038/ncomms5099. PubMed PMID: 24942009; PMCID: PMC4066194.
73. Silva KR, Cortes I, Liechocki S, Carneiro JR, Souza AA, Borojevic R, Maya-Monteiro CM, Baptista LS. Characterization of stromal vascular fraction and adipose stem cells from subcutaneous, preperitoneal and visceral morbidly obese human adipose tissue depots. PLoS One. 2017;12(3):e0174115. Epub 2017/03/23. doi: 10.1371/journal.pone.0174115. PubMed PMID: 28323901; PMCID: PMC5360317.

74. Brosnihan KB, Li P, Ferrario CM. Angiotensin-(1-7) dilates canine coronary arteries through kinins and nitric oxide. Hypertension. 1996;27(3 Pt 2):523-8. Epub 1996/03/01. doi: 10.1161/01.hyp.27.3.523. PubMed PMID: 8613197.
75. Giacchetti G, Faloia E, Sardu C, Camilloni MA, Mariniello B, Gatti C, Garrapa GG, Guerrieri M, Mantero F. Gene expression of angiotensinogen in adipose tissue of obese patients. Int J Obes Relat Metab Disord. 2000;24 Suppl 2:S142-3. Epub 2000/09/21. doi: 10.1038/sj.ijo.0801305. PubMed PMID: 10997636.
76. Burke GL, Bertoni AG, Shea S, Tracy R, Watson KE, Blumenthal RS, Chung H, Carnethon MR. The impact of obesity on cardiovascular disease risk factors and subclinical vascular disease: the Multi-Ethnic Study of Atherosclerosis. Arch Intern Med. 2008;168(9):928-35. Epub 2008/05/14. doi: 10.1001/archinte.168.9.928. PubMed PMID: 18474756; PMCID: PMC2931579.
77. Virtanen KA, Lonnroth P, Parkkola R, Peltoniemi P, Asola M, Viljanen T, Tolvanen T, Knuuti J, Ronnemaa T, Huupponen R, Nuutila P. Glucose uptake and perfusion in subcutaneous and visceral adipose tissue during insulin stimulation in nonobese and obese humans. J Clin Endocrinol Metab. 2002;87(8):3902-10. Epub 2002/08/06. doi: 10.1210/jcem.87.8.8761. PubMed PMID: 12161530.
78. Trayhurn P. Hypoxia and adipose tissue function and dysfunction in obesity. Physiol Rev. 2013;93(1):1-21. Epub 2013/01/11. doi: 10.1152/physrev.00017.2012. PubMed PMID: 23303904.
79. Trayhurn P, Wood IS. Adipokines: inflammation and the pleiotropic role of white adipose tissue. Br J Nutr. 2004;92(3):347-55. Epub 2004/10/08. doi: 10.1079/bjn20041213. PubMed PMID: 15469638.
80. Vengellur A, Woods BG, Ryan HE, Johnson RS, LaPres JJ. Gene expression profiling of the hypoxia signaling pathway in hypoxia-inducible factor 1alpha null mouse embryonic fibroblasts. Gene Expr. 2003;11(3-4):181-97. Epub 2003/12/23. doi: 10.3727/000000003108749062. PubMed PMID: 14686790; PMCID: PMC5991159.
81. Owens GK. Regulation of differentiation of vascular smooth muscle cells. Physiol Rev. 1995;75(3):487-517. Epub 1995/07/01. doi: 10.1152/physrev.1995.75.3.487. PubMed PMID: 7624392.
82. El Akoum S, Cloutier I, Tanguay JF. Vascular smooth muscle cell alterations triggered by mice adipocytes: role of high-fat diet. J Atheroscler Thromb. 2012;19(12):1128-41. Epub 2012/10/11. doi: 10.5551/jat.13482. PubMed PMID: 23047600.
83. Hu Y, Zhang Z, Torsney E, Afzal AR, Davison F, Metzler B, Xu Q. Abundant progenitor cells in the adventitia contribute to atherosclerosis of vein grafts in ApoE-deficient mice. J Clin Invest. 2004;113(9):1258-65. Epub 2004/05/05. doi: 10.1172/JCI19628. PubMed PMID: 15124016; PMCID: PMC398426.
84. Tang W, Zeve D, Suh JM, Bosnakovski D, Kyba M, Hammer RE, Tallquist MD, Graff JM. White fat progenitor cells reside in the adipose vasculature. Science. 2008;322(5901):583-6. Epub 2008/09/20. doi: 10.1126/science.1156232. PubMed PMID: 18801968; PMCID: PMC2597101.
85. Schack LM, Buettner M, Wirth A, Neunaber C, Krettek C, Hoffmann A, Noack S. Expression of CD24 in Human Bone Marrow-Derived Mesenchymal Stromal Cells Is Regulated by TGFbeta3 and Induces a Myofibroblast-Like Genotype. Stem Cells Int. 2016;2016:1319578.

Epub 2016/01/21. doi: 10.1155/2016/1319578. PubMed PMID: 26788063; PMCID: PMC4691640.
86. Smith NC, Fairbridge NA, Pallegar NK, Christian SL. Dynamic upregulation of CD24 in pre-adipocytes promotes adipogenesis. Adipocyte. 2015;4(2):89-100. Epub 2015/07/15. doi: 10.4161/21623945.2014.985015. PubMed PMID: 26167413; PMCID: PMC4496983.
87. Joshi PA, Waterhouse PD, Kasaian K, Fang H, Gulyaeva O, Sul HS, Boutros PC, Khokha R. PDGFRalpha(+) stromal adipocyte progenitors transition into epithelial cells during lobulo-alveologenesis in the murine mammary gland. Nat Commun. 2019;10(1):1760. Epub 2019/04/17. doi: 10.1038/s41467-019-09748-z. PubMed PMID: 30988300; PMCID: PMC6465250.
88. Sun C, Sakashita H, Kim J, Tang Z, Upchurch GM, Yao L, Berry WL, Griffin TM, Olson LE. Mosaic Mutant Analysis Identifies PDGFRalpha/PDGFRbeta as Negative Regulators of Adipogenesis. Cell Stem Cell. 2020;26(5):707-21 e5. Epub 2020/04/02. doi: 10.1016/j.stem.2020.03.004. PubMed PMID: 32229310; PMCID: PMC7214206.
89. Yamamoto N, Akamatsu H, Hasegawa S, Yamada T, Nakata S, Ohkuma M, Miyachi E, Marunouchi T, Matsunaga K. Isolation of multipotent stem cells from mouse adipose tissue. J Dermatol Sci. 2007;48(1):43-52. Epub 2007/07/24. doi: 10.1016/j.jdermsci.2007.05.015. PubMed PMID: 17644316.
90. Jiang Y, Berry DC, Jo A, Tang W, Arpke RW, Kyba M, Graff JM. A PPARgamma transcriptional cascade directs adipose progenitor cell-niche interaction and niche expansion. Nat Commun. 2017;8:15926. Epub 2017/06/27. doi: 10.1038/ncomms15926. PubMed PMID: 28649987; PMCID: PMC5490270.
91. Shao M, Vishvanath L, Busbuso NC, Hepler C, Shan B, Sharma AX, Chen S, Yu X, An YA, Zhu Y, Holland WL, Gupta RK. De novo adipocyte differentiation from Pdgfrbeta(+) preadipocytes protects against pathologic visceral adipose expansion in obesity. Nat Commun. 2018;9(1):890. Epub 2018/03/03. doi: 10.1038/s41467-018-03196-x. PubMed PMID: 29497032; PMCID: PMC5832777.
92. Jiang Y, Berry DC, Tang W, Graff JM. Independent stem cell lineages regulate adipose organogenesis and adipose homeostasis. Cell Rep. 2014;9(3):1007-22. Epub 2014/12/02. doi: 10.1016/j.celrep.2014.09.049. PubMed PMID: 25437556; PMCID: PMC4250841.
93. Su X, Lyu Y, Wang W, Zhang Y, Li D, Wei S, Du C, Geng B, Sztalryd C, Xu G. Fascia Origin of Adipose Cells. Stem Cells. 2016;34(5):1407-19. Epub 2016/02/13. doi: 10.1002/stem.2338. PubMed PMID: 26867029.
94. Merrick D, Sakers A, Irgebay Z, Okada C, Calvert C, Morley MP, Percec I, Seale P. Identification of a mesenchymal progenitor cell hierarchy in adipose tissue. Science. 2019;364(6438). Epub 2019/04/27. doi: 10.1126/science.aav2501. PubMed PMID: 31023895; PMCID: PMC6816238.
95. Cawthorn WP, Scheller EL, MacDougald OA. Adipose tissue stem cells meet preadipocyte commitment: going back to the future. J Lipid Res. 2012;53(2):227-46. Epub 2011/12/06. doi: 10.1194/jlr.R021089. PubMed PMID: 22140268; PMCID: PMC3269153.
96. Michalik L, Wahli W. Involvement of PPAR nuclear receptors in tissue injury and wound repair. J Clin Invest. 2006;116(3):598-606. Epub 2006/03/03. doi: 10.1172/JCI27958. PubMed PMID: 16511592; PMCID: PMC1386118.

97. Fajas L, Auboeuf D, Raspe E, Schoonjans K, Lefebvre AM, Saladin R, Najib J, Laville M, Fruchart JC, Deeb S, Vidal-Puig A, Flier J, Briggs MR, Staels B, Vidal H, Auwerx J. The organization, promoter analysis, and expression of the human PPARgamma gene. J Biol Chem. 1997;272(30):18779-89. Epub 1997/07/25. doi: 10.1074/jbc.272.30.18779. PubMed PMID: 9228052.
98. Lehmann JM, Moore LB, Smith-Oliver TA, Wilkison WO, Willson TM, Kliewer SA. An antidiabetic thiazolidinedione is a high affinity ligand for peroxisome proliferator-activated receptor gamma (PPAR gamma). J Biol Chem. 1995;270(22):12953-6. Epub 1995/06/02. doi: 10.1074/jbc.270.22.12953. PubMed PMID: 7768881.
99. Ferre P. The biology of peroxisome proliferator-activated receptors: relationship with lipid metabolism and insulin sensitivity. Diabetes. 2004;53 Suppl 1:S43-50. Epub 2004/01/30. doi: 10.2337/diabetes.53.2007.s43. PubMed PMID: 14749265.
100. Abbott BD, Wood CR, Watkins AM, Das KP, Lau CS. Peroxisome proliferator-activated receptors alpha, Beta, and gamma mRNA and protein expression in human fetal tissues. PPAR Res. 2010;2010. Epub 2010/08/14. doi: 10.1155/2010/690907. PubMed PMID: 20706641; PMCID: PMC2913814.
101. Desoye G, Herrera E. Adipose tissue development and lipid metabolism in the human fetus: The 2020 perspective focusing on maternal diabetes and obesity. Prog Lipid Res. 2021;81:101082. Epub 2021/01/01. doi: 10.1016/j.plipres.2020.101082. PubMed PMID: 33383022.
102. Johnson MH, Day ML. Egg timers: how is developmental time measured in the early vertebrate embryo? Bioessays. 2000;22(1):57-63. Epub 2000/01/29. doi: 10.1002/(SICI)1521-1878(200001)22:1<57::AID-BIES10>3.0.CO;2-L. PubMed PMID: 10649291.
103. Whitten WK, Biggers JD. Complete development in vitro of the pre-implantation stages of the mouse in a simple chemically defined medium. J Reprod Fertil. 1968;17(2):399-401. Epub 1968/11/01. doi: 10.1530/jrf.0.0170399. PubMed PMID: 5749384.
104. Tam PP, Williams EA, Chan WY. Gastrulation in the mouse embryo: ultrastructural and molecular aspects of germ layer morphogenesis. Microsc Res Tech. 1993;26(4):301-28. Epub 1993/11/01. doi: 10.1002/jemt.1070260405. PubMed PMID: 8305722.
105. Snow MH, Bennett D. Gastrulation in the mouse: assessment of cell populations in the epiblast of tw18/tw18 embryos. J Embryol Exp Morphol. 1978;47:39-52. Epub 1978/10/01. PubMed PMID: 722232.
106. Hatada Y, Stern CD. A fate map of the epiblast of the early chick embryo. Development. 1994;120(10):2879-89. Epub 1994/10/01. doi: 10.1242/dev.120.10.2879. PubMed PMID: 7607078.
107. Lawson SN, Waddell PJ. Soma neurofilament immunoreactivity is related to cell size and fibre conduction velocity in rat primary sensory neurons. J Physiol. 1991;435:41-63. Epub 1991/04/01. doi: 10.1113/jphysiol.1991.sp018497. PubMed PMID: 1770443; PMCID: PMC1181449.
108. Tam PP, Loebel DA. Gene function in mouse embryogenesis: get set for gastrulation. Nat Rev Genet. 2007;8(5):368-81. Epub 2007/03/28. doi: 10.1038/nrg2084. PubMed PMID: 17387317.

109. Sebo ZL, Rodeheffer MS. Assembling the adipose organ: adipocyte lineage segregation and adipogenesis in vivo. Development. 2019;146(7). Epub 2019/04/06. doi: 10.1242/dev.172098. PubMed PMID: 30948523; PMCID: PMC6467474.
110. Tajbakhsh S, Sporle R. Somite development: constructing the vertebrate body. Cell. 1998;92(1):9-16. Epub 1998/03/07. doi: 10.1016/s0092-8674(00)80894-6. PubMed PMID: 9489695.
111. Sebo ZL, Jeffery E, Holtrup B, Rodeheffer MS. A mesodermal fate map for adipose tissue. Development. 2018;145(17). Epub 2018/07/27. doi: 10.1242/dev.166801. PubMed PMID: 30045918; PMCID: PMC6141776.
112. Lepper C, Fan CM. Inducible lineage tracing of Pax7-descendant cells reveals embryonic origin of adult satellite cells. Genesis. 2010;48(7):424-36. Epub 2010/07/20. doi: 10.1002/dvg.20630. PubMed PMID: 20641127; PMCID: PMC3113517.
113. Atit R, Sgaier SK, Mohamed OA, Taketo MM, Dufort D, Joyner AL, Niswander L, Conlon RA. Beta-catenin activation is necessary and sufficient to specify the dorsal dermal fate in the mouse. Dev Biol. 2006;296(1):164-76. Epub 2006/05/30. doi: 10.1016/j.ydbio.2006.04.449. PubMed PMID: 16730693.
114. Gavin KM, Cooper EE, Raymer DK, Hickner RC. Estradiol effects on subcutaneous adipose tissue lipolysis in premenopausal women are adipose tissue depot specific and treatment dependent. Am J Physiol Endocrinol Metab. 2013;304(11):E1167-74. Epub 2013/03/28. doi: 10.1152/ajpendo.00023.2013. PubMed PMID: 23531620.
115. Van Pelt RE, Gozansky WS, Hickner RC, Schwartz RS, Kohrt WM. Acute modulation of adipose tissue lipolysis by intravenous estrogens. Obesity (Silver Spring). 2006;14(12):2163-72. Epub 2006/12/26. doi: 10.1038/oby.2006.253. PubMed PMID: 17189542; PMCID: PMC2832608.
116. Kautzky-Willer A, Harreiter J, Pacini G. Sex and Gender Differences in Risk, Pathophysiology and Complications of Type 2 Diabetes Mellitus. Endocr Rev. 2016;37(3):278-316. Epub 2016/05/10. doi: 10.1210/er.2015-1137. PubMed PMID: 27159875; PMCID: PMC4890267.
117. Khosla S, Atkinson EJ, Melton LJ, 3rd, Riggs BL. Effects of age and estrogen status on serum parathyroid hormone levels and biochemical markers of bone turnover in women: a population-based study. J Clin Endocrinol Metab. 1997;82(5):1522-7. Epub 1997/05/01. doi: 10.1210/jcem.82.5.3946. PubMed PMID: 9141544.
118. Haarbo J, Marslew U, Gotfredsen A, Christiansen C. Postmenopausal hormone replacement therapy prevents central distribution of body fat after menopause. Metabolism. 1991;40(12):1323-6. Epub 1991/12/01. doi: 10.1016/0026-0495(91)90037-w. PubMed PMID: 1961129.
119. Grumbach MM, Auchus RJ. Estrogen: consequences and implications of human mutations in synthesis and action. J Clin Endocrinol Metab. 1999;84(12):4677-94. Epub 1999/12/22. doi: 10.1210/jcem.84.12.6290. PubMed PMID: 10599737.
120. Jones ME, Thorburn AW, Britt KL, Hewitt KN, Wreford NG, Proietto J, Oz OK, Leury BJ, Robertson KM, Yao S, Simpson ER. Aromatase-deficient (ArKO) mice have a phenotype of increased adiposity. Proc Natl Acad Sci U S A. 2000;97(23):12735-40. Epub 2000/11/09. doi: 10.1073/pnas.97.23.12735. PubMed PMID: 11070087; PMCID: PMC18833.

121. Heine PA, Taylor JA, Iwamoto GA, Lubahn DB, Cooke PS. Increased adipose tissue in male and female estrogen receptor-alpha knockout mice. Proc Natl Acad Sci U S A. 2000;97(23):12729-34. Epub 2000/11/09. doi: 10.1073/pnas.97.23.12729. PubMed PMID: 11070086; PMCID: PMC18832.
122. Keller C, Larkey L, Distefano JK, Boehm-Smith E, Records K, Robillard A, Veres S, Al-Zadjali M, O'Brian AM. Perimenopausal obesity. J Womens Health (Larchmt). 2010;19(5):987-96. Epub 2010/04/13. doi: 10.1089/jwh.2009.1547. PubMed PMID: 20380578.
123. Newell-Fugate AE. The role of sex steroids in white adipose tissue adipocyte function. Reproduction. 2017;153(4):R133-R49. Epub 2017/01/25. doi: 10.1530/REP-16-0417. PubMed PMID: 28115579.
124. D'Eon TM, Souza SC, Aronovitz M, Obin MS, Fried SK, Greenberg AS. Estrogen regulation of adiposity and fuel partitioning. Evidence of genomic and non-genomic regulation of lipogenic and oxidative pathways. J Biol Chem. 2005;280(43):35983-91. Epub 2005/08/20. doi: 10.1074/jbc.M507339200. PubMed PMID: 16109719.
125. Foryst-Ludwig A, Clemenz M, Hohmann S, Hartge M, Sprang C, Frost N, Krikov M, Bhanot S, Barros R, Morani A, Gustafsson JA, Unger T, Kintscher U. Metabolic actions of estrogen receptor beta (ERbeta) are mediated by a negative cross-talk with PPARgamma. PLoS Genet. 2008;4(6):e1000108. Epub 2008/06/28. doi: 10.1371/journal.pgen.1000108. PubMed PMID: 18584035; PMCID: PMC2432036 Pharmaceuticals, Carlsbad, California, United States of America.
126. Lapid K, Lim A, Clegg DJ, Zeve D, Graff JM. Oestrogen signalling in white adipose progenitor cells inhibits differentiation into brown adipose and smooth muscle cells. Nat Commun. 2014;5:5196. Epub 2014/10/22. doi: 10.1038/ncomms6196. PubMed PMID: 25330806; PMCID: PMC4770882.
127. Santos RS, Frank AP, Fatima LA, Palmer BF, Oz OK, Clegg DJ. Activation of estrogen receptor alpha induces beiging of adipocytes. Mol Metab. 2018;18:51-9. Epub 2018/10/03. doi: 10.1016/j.molmet.2018.09.002. PubMed PMID: 30270132; PMCID: PMC6309577.
128. Davis KE, M DN, Sun K, W MS, J DB, J AZ, Zeve D, L DH, D WC, L MG, Xu Y, Z VW, S AK, Clegg DJ. The sexually dimorphic role of adipose and adipocyte estrogen receptors in modulating adipose tissue expansion, inflammation, and fibrosis. Mol Metab. 2013;2(3):227-42. Epub 2013/09/21. doi: 10.1016/j.molmet.2013.05.006. PubMed PMID: 24049737; PMCID: PMC3773827.
129. Gao Q, Horvath TL. Cross-talk between estrogen and leptin signaling in the hypothalamus. Am J Physiol Endocrinol Metab. 2008;294(5):E817-26. Epub 2008/03/13. doi: 10.1152/ajpendo.00733.2007. PubMed PMID: 18334610.
130. Ainslie DA, Morris MJ, Wittert G, Turnbull H, Proietto J, Thorburn AW. Estrogen deficiency causes central leptin insensitivity and increased hypothalamic neuropeptide Y. Int J Obes Relat Metab Disord. 2001;25(11):1680-8. Epub 2001/12/26. doi: 10.1038/sj.ijo.0801806. PubMed PMID: 11753591.
131. Shughrue PJ, Lane MV, Merchenthaler I. Comparative distribution of estrogen receptor-alpha and -beta mRNA in the rat central nervous system. J Comp Neurol. 1997;388(4):507-25. Epub 1997/12/05. doi: 10.1002/(sici)1096-9861(19971201)388:4<507::aid-cne1>3.0.co;2-6. PubMed PMID: 9388012.

132. Gonzalez-Garcia I, Contreras C, Estevez-Salguero A, Ruiz-Pino F, Colsh B, Pensado I, Linares-Pose L, Rial-Pensado E, Martinez de Morentin PB, Ferno J, Dieguez C, Nogueiras R, Le Stunff H, Magnan C, Tena-Sempere M, Lopez M. Estradiol Regulates Energy Balance by Ameliorating Hypothalamic Ceramide-Induced ER Stress. Cell Rep. 2018;25(2):413-23 e5. Epub 2018/10/12. doi: 10.1016/j.celrep.2018.09.038. PubMed PMID: 30304681; PMCID: PMC6198289.
133. Fatima LA, Campello RS, Santos RS, Freitas HS, Frank AP, Machado UF, Clegg DJ. Estrogen receptor 1 (ESR1) regulates VEGFA in adipose tissue. Sci Rep. 2017;7(1):16716. Epub 2017/12/03. doi: 10.1038/s41598-017-16686-7. PubMed PMID: 29196658; PMCID: PMC5711936.
134. Yamasaki H, Douchi T, Yamamoto S, Oki T, Kuwahata R, Nagata Y. Body fat distribution and body composition during GnRH agonist therapy. Obstet Gynecol. 2001;97(3):338-42. Epub 2001/03/10. doi: 10.1016/s0029-7844(00)01181-9. PubMed PMID: 11239633.
135. Blouin K, Boivin A, Tchernof A. Androgens and body fat distribution. J Steroid Biochem Mol Biol. 2008;108(3-5):272-80. Epub 2007/10/20. doi: 10.1016/j.jsbmb.2007.09.001. PubMed PMID: 17945484.
136. Evans DJ, Barth JH, Burke CW. Body fat topography in women with androgen excess. Int J Obes. 1988;12(2):157-62. Epub 1988/01/01. PubMed PMID: 3384560.
137. Dunaif A. Insulin resistance and the polycystic ovary syndrome: mechanism and implications for pathogenesis. Endocr Rev. 1997;18(6):774-800. Epub 1997/12/31. doi: 10.1210/edrv.18.6.0318. PubMed PMID: 9408743.
138. Varlamov O, Chu MP, McGee WK, Cameron JL, O'Rourke RW, Meyer KA, Bishop CV, Stouffer RL, Roberts CT, Jr. Ovarian cycle-specific regulation of adipose tissue lipid storage by testosterone in female nonhuman primates. Endocrinology. 2013;154(11):4126-35. Epub 2013/09/07. doi: 10.1210/en.2013-1428. PubMed PMID: 24008344; PMCID: PMC3800767.
139. Woodhouse LJ, Gupta N, Bhasin M, Singh AB, Ross R, Phillips J, Bhasin S. Dose-dependent effects of testosterone on regional adipose tissue distribution in healthy young men. J Clin Endocrinol Metab. 2004;89(2):718-26. Epub 2004/02/07. doi: 10.1210/jc.2003-031492. PubMed PMID: 14764787.
140. Tsai EC, Matsumoto AM, Fujimoto WY, Boyko EJ. Association of bioavailable, free, and total testosterone with insulin resistance: influence of sex hormone-binding globulin and body fat. Diabetes Care. 2004;27(4):861-8. Epub 2004/03/30. doi: 10.2337/diacare.27.4.861. PubMed PMID: 15047639.
141. Chazenbalk G, Singh P, Irge D, Shah A, Abbott DH, Dumesic DA. Androgens inhibit adipogenesis during human adipose stem cell commitment to preadipocyte formation. Steroids. 2013;78(9):920-6. Epub 2013/05/28. doi: 10.1016/j.steroids.2013.05.001. PubMed PMID: 23707571; PMCID: PMC3951890.
142. Tchernof A, Labrie F, Belanger A, Prud'homme D, Bouchard C, Tremblay A, Nadeau A, Despres JP. Androstane-3alpha,17beta-diol glucuronide as a steroid correlate of visceral obesity in men. J Clin Endocrinol Metab. 1997;82(5):1528-34. Epub 1997/05/01. doi: 10.1210/jcem.82.5.3924. PubMed PMID: 9141545.
143. Pritchard J, Despres JP, Gagnon J, Tchernof A, Nadeau A, Tremblay A, Bouchard C. Plasma adrenal, gonadal, and conjugated steroids before and after long-term overfeeding in

identical twins. J Clin Endocrinol Metab. 1998;83(9):3277-84. Epub 1998/09/24. doi: 10.1210/jcem.83.9.5136. PubMed PMID: 9745441.
144. Ballesteros JA, Jensen AD, Liapakis G, Rasmussen SG, Shi L, Gether U, Javitch JA. Activation of the beta 2-adrenergic receptor involves disruption of an ionic lock between the cytoplasmic ends of transmembrane segments 3 and 6. J Biol Chem. 2001;276(31):29171-7. Epub 2001/05/29. doi: 10.1074/jbc.M103747200. PubMed PMID: 11375997.
145. Marrari Y, Crouthamel M, Irannejad R, Wedegaertner PB. Assembly and trafficking of heterotrimeric G proteins. Biochemistry. 2007;46(26):7665-77. Epub 2007/06/15. doi: 10.1021/bi700338m. PubMed PMID: 17559193; PMCID: PMC2527407.
146. Syrovatkina V, Alegre KO, Dey R, Huang XY. Regulation, Signaling, and Physiological Functions of G-Proteins. J Mol Biol. 2016;428(19):3850-68. Epub 2016/08/16. doi: 10.1016/j.jmb.2016.08.002. PubMed PMID: 27515397; PMCID: PMC5023507.
147. Neves SR, Ram PT, Iyengar R. G protein pathways. Science. 2002;296(5573):1636-9. Epub 2002/06/01. doi: 10.1126/science.1071550. PubMed PMID: 12040175.
148. New DC, Wong YH. Molecular mechanisms mediating the G protein-coupled receptor regulation of cell cycle progression. J Mol Signal. 2007;2:2. Epub 2007/02/27. doi: 10.1186/1750-2187-2-2. PubMed PMID: 17319972; PMCID: PMC1808056.
149. Kamato D, Thach L, Bernard R, Chan V, Zheng W, Kaur H, Brimble M, Osman N, Little PJ. Structure, Function, Pharmacology, and Therapeutic Potential of the G Protein, Galpha/q,11. Front Cardiovasc Med. 2015;2:14. Epub 2015/12/15. doi: 10.3389/fcvm.2015.00014. PubMed PMID: 26664886; PMCID: PMC4671355.
150. McCudden CR, Hains MD, Kimple RJ, Siderovski DP, Willard FS. G-protein signaling: back to the future. Cell Mol Life Sci. 2005;62(5):551-77. Epub 2005/03/05. doi: 10.1007/s00018-004-4462-3. PubMed PMID: 15747061; PMCID: PMC2794341.
151. Teicher BA, Fricker SP. CXCL12 (SDF-1)/CXCR4 pathway in cancer. Clin Cancer Res. 2010;16(11):2927-31. Epub 2010/05/21. doi: 10.1158/1078-0432.CCR-09-2329. PubMed PMID: 20484021.
152. Shan D, Chen L, Wang D, Tan YC, Gu JL, Huang XY. The G protein G alpha(13) is required for growth factor-induced cell migration. Dev Cell. 2006;10(6):707-18. Epub 2006/06/03. doi: 10.1016/j.devcel.2006.03.014. PubMed PMID: 16740474.
153. Busillo JM, Benovic JL. Regulation of CXCR4 signaling. Biochim Biophys Acta. 2007;1768(4):952-63. Epub 2006/12/16. doi: 10.1016/j.bbamem.2006.11.002. PubMed PMID: 17169327; PMCID: PMC1952230.
154. Federsppiel B, Melhado IG, Duncan AM, Delaney A, Schappert K, Clark-Lewis I, Jirik FR. Molecular cloning of the cDNA and chromosomal localization of the gene for a putative seven-transmembrane segment (7-TMS) receptor isolated from human spleen. Genomics. 1993;16(3):707-12. Epub 1993/06/01. doi: 10.1006/geno.1993.1251. PubMed PMID: 8325644.
155. Loetscher M, Geiser T, O'Reilly T, Zwahlen R, Baggiolini M, Moser B. Cloning of a human seven-transmembrane domain receptor, LESTR, that is highly expressed in leukocytes. J Biol Chem. 1994;269(1):232-7. Epub 1994/01/07. PubMed PMID: 8276799.
156. Kufareva I, Salanga CL, Handel TM. Chemokine and chemokine receptor structure and interactions: implications for therapeutic strategies. Immunol Cell Biol. 2015;93(4):372-83. Epub 2015/02/25. doi: 10.1038/icb.2015.15. PubMed PMID: 25708536; PMCID: PMC4406842.

157. Tan W, Martin D, Gutkind JS. The Galpha13-Rho signaling axis is required for SDF-1-induced migration through CXCR4. J Biol Chem. 2006;281(51):39542-9. Epub 2006/10/24. doi: 10.1074/jbc.M609062200. PubMed PMID: 17056591.
158. Kumar A, Kremer KN, Dominguez D, Tadi M, Hedin KE. Galpha13 and Rho mediate endosomal trafficking of CXCR4 into Rab11+ vesicles upon stromal cell-derived factor-1 stimulation. J Immunol. 2011;186(2):951-8. Epub 2010/12/15. doi: 10.4049/jimmunol.1002019. PubMed PMID: 21148034; PMCID: PMC3057048.
159. Soede RD, Zeelenberg IS, Wijnands YM, Kamp M, Roos E. Stromal cell-derived factor-1-induced LFA-1 activation during in vivo migration of T cell hybridoma cells requires Gq/11, RhoA, and myosin, as well as Gi and Cdc42. J Immunol. 2001;166(7):4293-301. Epub 2001/03/20. doi: 10.4049/jimmunol.166.7.4293. PubMed PMID: 11254681.
160. Doring Y, Pawig L, Weber C, Noels H. The CXCL12/CXCR4 chemokine ligand/receptor axis in cardiovascular disease. Front Physiol. 2014;5:212. Epub 2014/06/27. doi: 10.3389/fphys.2014.00212. PubMed PMID: 24966838; PMCID: PMC4052746.
161. Ara T, Tokoyoda K, Okamoto R, Koni PA, Nagasawa T. The role of CXCL12 in the organ-specific process of artery formation. Blood. 2005;105(8):3155-61. Epub 2005/01/01. doi: 10.1182/blood-2004-07-2563. PubMed PMID: 15626744.
162. Ara T, Tokoyoda K, Sugiyama T, Egawa T, Kawabata K, Nagasawa T. Long-term hematopoietic stem cells require stromal cell-derived factor-1 for colonizing bone marrow during ontogeny. Immunity. 2003;19(2):257-67. Epub 2003/08/23. doi: 10.1016/s1074-7613(03)00201-2. PubMed PMID: 12932359.
163. De Clercq E. AMD3100/CXCR4 Inhibitor. Front Immunol. 2015;6:276. Epub 2015/06/25. doi: 10.3389/fimmu.2015.00276. PubMed PMID: 26106388; PMCID: PMC4459229.
164. Liles WC, Broxmeyer HE, Rodger E, Wood B, Hubel K, Cooper S, Hangoc G, Bridger GJ, Henson GW, Calandra G, Dale DC. Mobilization of hematopoietic progenitor cells in healthy volunteers by AMD3100, a CXCR4 antagonist. Blood. 2003;102(8):2728-30. Epub 2003/07/12. doi: 10.1182/blood-2003-02-0663. PubMed PMID: 12855591.
165. Peled A, Klein S, Beider K, Burger JA, Abraham M. Role of CXCL12 and CXCR4 in the pathogenesis of hematological malignancies. Cytokine. 2018;109:11-6. Epub 2018/06/16. doi: 10.1016/j.cyto.2018.02.020. PubMed PMID: 29903571.
166. Liu JM, Zhao K, Du LX, Zhou Y, Long XH, Chen XY, Liu ZL. AMD3100 inhibits the migration and differentiation of neural stem cells after spinal cord injury. Sci Rep. 2017;7(1):64. Epub 2017/03/02. doi: 10.1038/s41598-017-00141-8. PubMed PMID: 28246405; PMCID: PMC5427924.
167. Nagasawa T, Kikutani H, Kishimoto T. Molecular cloning and structure of a pre-B-cell growth-stimulating factor. Proc Natl Acad Sci U S A. 1994;91(6):2305-9. Epub 1994/03/15. doi: 10.1073/pnas.91.6.2305. PubMed PMID: 8134392; PMCID: PMC43359.
168. Oberlin E, Amara A, Bachelerie F, Bessia C, Virelizier JL, Arenzana-Seisdedos F, Schwartz O, Heard JM, Clark-Lewis I, Legler DF, Loetscher M, Baggiolini M, Moser B. The CXC chemokine SDF-1 is the ligand for LESTR/fusin and prevents infection by T-cell-line-adapted HIV-1. Nature. 1996;382(6594):833-5. Epub 1996/08/29. doi: 10.1038/382833a0. PubMed PMID: 8752281.
169. Bleul CC, Farzan M, Choe H, Parolin C, Clark-Lewis I, Sodroski J, Springer TA. The lymphocyte chemoattractant SDF-1 is a ligand for LESTR/fusin and blocks HIV-1 entry. Nature. 1996;382(6594):829-33. Epub 1996/08/29. doi: 10.1038/382829a0. PubMed PMID: 8752280.

170. Guo JC, Li J, Zhou L, Yang JY, Zhang ZG, Liang ZY, Zhou WX, You L, Zhang TP, Zhao YP. CXCL12-CXCR7 axis contributes to the invasive phenotype of pancreatic cancer. Oncotarget. 2016;7(38):62006-18. Epub 2016/08/20. doi: 10.18632/oncotarget.11330. PubMed PMID: 27542220; PMCID: PMC5308707.
171. Sorrentino C, Miele L, Porta A, Pinto A, Morello S. Activation of the A2B adenosine receptor in B16 melanomas induces CXCL12 expression in FAP-positive tumor stromal cells, enhancing tumor progression. Oncotarget. 2016;7(39):64274-88. Epub 2016/09/04. doi: 10.18632/oncotarget.11729. PubMed PMID: 27590504; PMCID: PMC5325441.
172. Yu Y, Xiao CH, Tan LD, Wang QS, Li XQ, Feng YM. Cancer-associated fibroblasts induce epithelial-mesenchymal transition of breast cancer cells through paracrine TGF-beta signalling. Br J Cancer. 2014;110(3):724-32. Epub 2013/12/18. doi: 10.1038/bjc.2013.768. PubMed PMID: 24335925; PMCID: PMC3915130.
173. Broxmeyer HE, Orschell CM, Clapp DW, Hangoc G, Cooper S, Plett PA, Liles WC, Li X, Graham-Evans B, Campbell TB, Calandra G, Bridger G, Dale DC, Srour EF. Rapid mobilization of murine and human hematopoietic stem and progenitor cells with AMD3100, a CXCR4 antagonist. J Exp Med. 2005;201(8):1307-18. Epub 2005/04/20. doi: 10.1084/jem.20041385. PubMed PMID: 15837815; PMCID: PMC2213145.
174. De Clercq E. Mozobil(R) (Plerixafor, AMD3100), 10 years after its approval by the US Food and Drug Administration. Antivir Chem Chemother. 2019;27:2040206619829382. Epub 2019/02/20. doi: 10.1177/2040206619829382. PubMed PMID: 30776910; PMCID: PMC6379795.
175. Sugiyama T, Kohara H, Noda M, Nagasawa T. Maintenance of the hematopoietic stem cell pool by CXCL12-CXCR4 chemokine signaling in bone marrow stromal cell niches. Immunity. 2006;25(6):977-88. Epub 2006/12/19. doi: 10.1016/j.immuni.2006.10.016. PubMed PMID: 17174120.
176. Yao L, Heuser-Baker J, Herlea-Pana O, Zhang N, Szweda LI, Griffin TM, Barlic-Dicen J. Deficiency in adipocyte chemokine receptor CXCR4 exacerbates obesity and compromises thermoregulatory responses of brown adipose tissue in a mouse model of diet-induced obesity. FASEB J. 2014;28(10):4534-50. Epub 2014/07/13. doi: 10.1096/fj.14-249797. PubMed PMID: 25016030; PMCID: PMC4202106.
177. Gil-Ortega M, Garidou L, Barreau C, Maumus M, Breasson L, Tavernier G, Garcia-Prieto CF, Bouloumie A, Casteilla L, Sengenes C. Native adipose stromal cells egress from adipose tissue in vivo: evidence during lymph node activation. Stem Cells. 2013;31(7):1309-20. Epub 2013/03/28. doi: 10.1002/stem.1375. PubMed PMID: 23533182.
178. Girousse A, Gil-Ortega M, Bourlier V, Bergeaud C, Sastourne-Arrey Q, Moro C, Barreau C, Guissard C, Vion J, Arnaud E, Pradere JP, Juin N, Casteilla L, Sengenes C. The Release of Adipose Stromal Cells from Subcutaneous Adipose Tissue Regulates Ectopic Intramuscular Adipocyte Deposition. Cell Rep. 2019;27(2):323-33 e5. Epub 2019/04/11. doi: 10.1016/j.celrep.2019.03.038. PubMed PMID: 30970240.
179. Shin J, Fukuhara A, Onodera T, Kita S, Yokoyama C, Otsuki M, Shimomura I. SDF-1 Is an Autocrine Insulin-Desensitizing Factor in Adipocytes. Diabetes. 2018;67(6):1068-78. Epub 2018/03/28. doi: 10.2337/db17-0706. PubMed PMID: 29581126.
180. Kim D, Kim J, Yoon JH, Ghim J, Yea K, Song P, Park S, Lee A, Hong CP, Jang MS, Kwon Y, Park S, Jang MH, Berggren PO, Suh PG, Ryu SH. CXCL12 secreted from adipose tissue recruits

macrophages and induces insulin resistance in mice. Diabetologia. 2014;57(7):1456-65. Epub 2014/04/20. doi: 10.1007/s00125-014-3237-5. PubMed PMID: 24744121.
181. Wolf RM, Jaffe AE, Steele KE, Schweitzer MA, Magnuson TH, Wolfe A, Wong GW. Cytokine, Chemokine, and Cytokine Receptor Changes Are Associated With Metabolic Improvements After Bariatric Surgery. J Clin Endocrinol Metab. 2019;104(3):947-56. Epub 2018/12/14. doi: 10.1210/jc.2018-02245. PubMed PMID: 30544212; PMCID: PMC6364507.
182. Dos Santos EG, Dieudonne MN, Pecquery R, Le Moal V, Giudicelli Y, Lacasa D. Rapid nongenomic E2 effects on p42/p44 MAPK, activator protein-1, and cAMP response element binding protein in rat white adipocytes. Endocrinology. 2002;143(3):930-40. Epub 2002/02/28. doi: 10.1210/endo.143.3.8678. PubMed PMID: 11861515.
183. Sauve K, Lepage J, Sanchez M, Heveker N, Tremblay A. Positive feedback activation of estrogen receptors by the CXCL12-CXCR4 pathway. Cancer Res. 2009;69(14):5793-800. Epub 2009/07/09. doi: 10.1158/0008-5472.CAN-08-4924. PubMed PMID: 19584281.
184. Rodriguez-Lara V, Ignacio GS, Cerbon Cervantes MA. Estrogen induces CXCR4 overexpression and CXCR4/CXL12 pathway activation in lung adenocarcinoma cells in vitro. Endocr Res. 2017;42(3):219-31. Epub 2017/03/21. doi: 10.1080/07435800.2017.1292526. PubMed PMID: 28318328.
185. Pallottini V, Bulzomi P, Galluzzo P, Martini C, Marino M. Estrogen regulation of adipose tissue functions: involvement of estrogen receptor isoforms. Infect Disord Drug Targets. 2008;8(1):52-60. Epub 2008/05/14. doi: 10.2174/187152608784139631. PubMed PMID: 18473908.
186. Azariadis K, Kiagiadaki F, Pelekanou V, Bempi V, Alexakis K, Kampa M, Tsapis A, Castanas E, Notas G. Androgen Triggers the Pro-Migratory CXCL12/CXCR4 Axis in AR-Positive Breast Cancer Cell Lines: Underlying Mechanism and Possible Implications for the Use of Aromatase Inhibitors in Breast Cancer. Cell Physiol Biochem. 2017;44(1):66-84. Epub 2017/11/14. doi: 10.1159/000484584. PubMed PMID: 29131020.
187. Lam YT, Lecce L, Tan JT, Bursill CA, Handelsman DJ, Ng MK. Androgen Receptor-Mediated Genomic Androgen Action Augments Ischemia-Induced Neovascularization. Endocrinology. 2016;157(12):4853-64. Epub 2016/10/19. doi: 10.1210/en.2016-1301. PubMed PMID: 27754785.
188. Tumbar T, Guasch G, Greco V, Blanpain C, Lowry WE, Rendl M, Fuchs E. Defining the epithelial stem cell niche in skin. Science. 2004;303(5656):359-63. Epub 2003/12/13. doi: 10.1126/science.1092436. PubMed PMID: 14671312; PMCID: PMC2405920.
189. Ahler E, Sullivan WJ, Cass A, Braas D, York AG, Bensinger SJ, Graeber TG, Christofk HR. Doxycycline alters metabolism and proliferation of human cell lines. PLoS One. 2013;8(5):e64561. Epub 2013/06/07. doi: 10.1371/journal.pone.0064561. PubMed PMID: 23741339; PMCID: PMC3669316.
190. Feil R, Wagner J, Metzger D, Chambon P. Regulation of Cre recombinase activity by mutated estrogen receptor ligand-binding domains. Biochem Biophys Res Commun. 1997;237(3):752-7. Epub 1997/08/28. doi: 10.1006/bbrc.1997.7124. PubMed PMID: 9299439.
191. Cai X, Lin Y, Hauschka PV, Grottkau BE. Adipose stem cells originate from perivascular cells. Biol Cell. 2011;103(9):435-47. Epub 2011/06/18. doi: 10.1042/BC20110033. PubMed PMID: 21679159.

192. Armulik A, Genove G, Betsholtz C. Pericytes: developmental, physiological, and pathological perspectives, problems, and promises. Dev Cell. 2011;21(2):193-215. Epub 2011/08/16. doi: 10.1016/j.devcel.2011.07.001. PubMed PMID: 21839917.
193. Traktuev DO, Merfeld-Clauss S, Li J, Kolonin M, Arap W, Pasqualini R, Johnstone BH, March KL. A population of multipotent CD34-positive adipose stromal cells share pericyte and mesenchymal surface markers, reside in a periendothelial location, and stabilize endothelial networks. Circ Res. 2008;102(1):77-85. Epub 2007/10/31. doi: 10.1161/CIRCRESAHA.107.159475. PubMed PMID: 17967785.
194. Cohen P, Spiegelman BM. Brown and Beige Fat: Molecular Parts of a Thermogenic Machine. Diabetes. 2015;64(7):2346-51. Epub 2015/06/09. doi: 10.2337/db15-0318. PubMed PMID: 26050670; PMCID: PMC4477363.
195. Enerback S, Jacobsson A, Simpson EM, Guerra C, Yamashita H, Harper ME, Kozak LP. Mice lacking mitochondrial uncoupling protein are cold-sensitive but not obese. Nature. 1997;387(6628):90-4. Epub 1997/05/01. doi: 10.1038/387090a0. PubMed PMID: 9139827.
196. Bartelt A, Heeren J. Adipose tissue browning and metabolic health. Nat Rev Endocrinol. 2014;10(1):24-36. doi: 10.1038/nrendo.2013.204. PubMed PMID: 24146030.
197. Nedergaard J, Cannon B. The browning of white adipose tissue: some burning issues. Cell Metab. 2014;20(3):396-407. doi: 10.1016/j.cmet.2014.07.005. PubMed PMID: 25127354.
198. Sidossis L, Kajimura S. Brown and beige fat in humans: thermogenic adipocytes that control energy and glucose homeostasis. J Clin Invest. 2015;125(2):478-86. doi: 10.1172/JCI78362. PubMed PMID: 25642708; PMCID: PMC4319444.
199. Wang W, Seale P. Control of brown and beige fat development. Nat Rev Mol Cell Biol. 2016;17(11):691-702. Epub 2016/10/21. doi: 10.1038/nrm.2016.96. PubMed PMID: 27552974; PMCID: PMC5627770.
200. Graja A, Schulz TJ. Mechanisms of aging-related impairment of brown adipocyte development and function. Gerontology. 2015;61(3):211-7. Epub 2014/12/23. doi: 10.1159/000366557. PubMed PMID: 25531079.
201. Bartness TJ, Shrestha YB, Vaughan CH, Schwartz GJ, Song CK. Sensory and sympathetic nervous system control of white adipose tissue lipolysis. Mol Cell Endocrinol. 2010;318(1-2):34-43. Epub 2009/09/15. doi: 10.1016/j.mce.2009.08.031. PubMed PMID: 19747957; PMCID: PMC2826518.
202. Zeng W, Pirzgalska RM, Pereira MM, Kubasova N, Barateiro A, Seixas E, Lu YH, Kozlova A, Voss H, Martins GG, Friedman JM, Domingos AI. Sympathetic neuro-adipose connections mediate leptin-driven lipolysis. Cell. 2015;163(1):84-94. Epub 2015/09/26. doi: 10.1016/j.cell.2015.08.055. PubMed PMID: 26406372.
203. Bartness TJ, Vaughan CH, Song CK. Sympathetic and sensory innervation of brown adipose tissue. Int J Obes (Lond). 2010;34 Suppl 1:S36-42. Epub 2010/10/12. doi: 10.1038/ijo.2010.182. PubMed PMID: 20935665; PMCID: PMC3999344.
204. Zeng X, Ye M, Resch JM, Jedrychowski MP, Hu B, Lowell BB, Ginty DD, Spiegelman BM. Innervation of thermogenic adipose tissue via a calsyntenin 3beta-S100b axis. Nature. 2019;569(7755):229-35. Epub 2019/05/03. doi: 10.1038/s41586-019-1156-9. PubMed PMID: 31043739; PMCID: PMC6589139.
205. Chi J, Wu Z, Choi CHJ, Nguyen L, Tegegne S, Ackerman SE, Crane A, Marchildon F, Tessier-Lavigne M, Cohen P. Three-Dimensional Adipose Tissue Imaging Reveals Regional

Variation in Beige Fat Biogenesis and PRDM16-Dependent Sympathetic Neurite Density. Cell Metab. 2018;27(1):226-36 e3. Epub 2018/01/11. doi: 10.1016/j.cmet.2017.12.011. PubMed PMID: 29320703.
206. Villarroya F, Cereijo R, Villarroya J, Giralt M. Brown adipose tissue as a secretory organ. Nat Rev Endocrinol. 2017;13(1):26-35. Epub 2016/11/04. doi: 10.1038/nrendo.2016.136. PubMed PMID: 27616452.
207. Kenney MJ, Ganta CK. Autonomic nervous system and immune system interactions. Compr Physiol. 2014;4(3):1177-200. Epub 2014/06/20. doi: 10.1002/cphy.c130051. PubMed PMID: 24944034; PMCID: PMC4374437.
208. Morrison SF. Central neural control of thermoregulation and brown adipose tissue. Auton Neurosci. 2016;196:14-24. Epub 2016/03/01. doi: 10.1016/j.autneu.2016.02.010. PubMed PMID: 26924538; PMCID: PMC4846468.
209. Hu B, Jin C, Zeng X, Resch JM, Jedrychowski MP, Yang Z, Desai BN, Banks AS, Lowell BB, Mathis D, Spiegelman BM. gammadelta T cells and adipocyte IL-17RC control fat innervation and thermogenesis. Nature. 2020;578(7796):610-4. Epub 2020/02/23. doi: 10.1038/s41586-020-2028-z. PubMed PMID: 32076265; PMCID: PMC7055484.
210. Nguyen KD, Qiu Y, Cui X, Goh YP, Mwangi J, David T, Mukundan L, Brombacher F, Locksley RM, Chawla A. Alternatively activated macrophages produce catecholamines to sustain adaptive thermogenesis. Nature. 2011;480(7375):104-8. Epub 2011/11/22. doi: 10.1038/nature10653. PubMed PMID: 22101429; PMCID: PMC3371761.
211. Vargovic P, Manz G, Kvetnansky R. Continuous cold exposure induces an anti-inflammatory response in mesenteric adipose tissue associated with catecholamine production and thermogenin expression in rats. Endocr Regul. 2016;50(3):137-44. Epub 2016/08/26. doi: 10.1515/enr-2016-0015. PubMed PMID: 27560796.
212. Qiu Y, Nguyen KD, Odegaard JI, Cui X, Tian X, Locksley RM, Palmiter RD, Chawla A. Eosinophils and type 2 cytokine signaling in macrophages orchestrate development of functional beige fat. Cell. 2014;157(6):1292-308. Epub 2014/06/07. doi: 10.1016/j.cell.2014.03.066. PubMed PMID: 24906148; PMCID: PMC4129510.
213. Fischer K, Ruiz HH, Jhun K, Finan B, Oberlin DJ, van der Heide V, Kalinovich AV, Petrovic N, Wolf Y, Clemmensen C, Shin AC, Divanovic S, Brombacher F, Glasmacher E, Keipert S, Jastroch M, Nagler J, Schramm KW, Medrikova D, Collden G, Woods SC, Herzig S, Homann D, Jung S, Nedergaard J, Cannon B, Tschop MH, Muller TD, Buettner C. Alternatively activated macrophages do not synthesize catecholamines or contribute to adipose tissue adaptive thermogenesis. Nat Med. 2017;23(5):623-30. Epub 2017/04/18. doi: 10.1038/nm.4316. PubMed PMID: 28414329; PMCID: PMC5420449.
214. Fischer AW, de Jong JMA, Sass F, Schlein C, Heeren J, Petrovic N. Thermoneutrality-Induced Macrophage Accumulation in Brown Adipose Tissue Does Not Impair the Tissue's Competence for Cold-Induced Thermogenic Recruitment. Front Endocrinol (Lausanne). 2020;11:568682. Epub 2020/11/17. doi: 10.3389/fendo.2020.568682. PubMed PMID: 33193086; PMCID: PMC7662517.
215. Vidakovic M, Grdovic N, Dinic S, Mihailovic M, Uskokovic A, Arambasic Jovanovic J. The Importance of the CXCL12/CXCR4 Axis in Therapeutic Approaches to Diabetes Mellitus Attenuation. Front Immunol. 2015;6:403. Epub 2015/08/25. doi: 10.3389/fimmu.2015.00403. PubMed PMID: 26300887; PMCID: PMC4528295.

216. Kurita K, Ishikawa K, Takeda K, Fujimoto M, Ono H, Kumagai J, Inoue H, Yokoh H, Yokote K. CXCL12-CXCR4 pathway activates brown adipocytes and induces insulin resistance in CXCR4-deficient mice under high-fat diet. Sci Rep. 2019;9(1):6165. Epub 2019/04/18. doi: 10.1038/s41598-019-42127-8. PubMed PMID: 30992469; PMCID: PMC6467900.
217. Watanabe E, Wada T, Okekawa A, Kitamura F, Komatsu G, Onogi Y, Yamamoto S, Sasahara M, Kitada M, Koya D, Tsuneki H, Sasaoka T. Stromal cell-derived factor 1 (SDF1) attenuates platelet-derived growth factor-B (PDGF-B)-induced vascular remodeling for adipose tissue expansion in obesity. Angiogenesis. 2020;23(4):667-84. Epub 2020/07/24. doi: 10.1007/s10456-020-09738-6. PubMed PMID: 32699964.
218. Ding L, Morrison SJ. Haematopoietic stem cells and early lymphoid progenitors occupy distinct bone marrow niches. Nature. 2013;495(7440):231-5. Epub 2013/02/26. doi: 10.1038/nature11885. PubMed PMID: 23434755; PMCID: PMC3600153.
219. Nagasawa T. CXC chemokine ligand 12 (CXCL12) and its receptor CXCR4. J Mol Med (Berl). 2014;92(5):433-9. Epub 2014/04/12. doi: 10.1007/s00109-014-1123-8. PubMed PMID: 24722947.
220. Berry DC, Jiang Y, Arpke RW, Close EL, Uchida A, Reading D, Berglund ED, Kyba M, Graff JM. Cellular Aging Contributes to Failure of Cold-Induced Beige Adipocyte Formation in Old Mice and Humans. Cell Metab. 2017;25(1):166-81. doi: 10.1016/j.cmet.2016.10.023. PubMed PMID: 27889388; PMCID: PMC5226893.
221. Berry DC, Jiang Y, Graff JM. Emerging Roles of Adipose Progenitor Cells in Tissue Development, Homeostasis, Expansion and Thermogenesis. Trends Endocrinol Metab. 2016;27(8):574-85. doi: 10.1016/j.tem.2016.05.001. PubMed PMID: 27262681.
222. Berry DC, Jiang Y, Graff JM. Mouse strains to study cold-inducible beige progenitors and beige adipocyte formation and function. Nat Commun. 2016;7:10184. Epub 2016/01/06. doi: 10.1038/ncomms10184. PubMed PMID: 26729601; PMCID: PMC4728429.
223. Berry DC, Stenesen D, Zeve D, Graff JM. The developmental origins of adipose tissue. Development. 2013;140(19):3939-49. doi: 10.1242/dev.080549. PubMed PMID: 24046315; PMCID: 3775412.
224. Jiang Y, Berry DC, Graff JM. Distinct cellular and molecular mechanisms for beta3 adrenergic receptor-induced beige adipocyte formation. Elife. 2017;6. Epub 2017/10/12. doi: 10.7554/eLife.30329. PubMed PMID: 29019320; PMCID: PMC5667933.
225. Park J, Shin S, Liu L, Jahan I, Ong SG, Xu P, Berry DC, Jiang Y. Progenitor-like characteristics in a subgroup of UCP1+ cells within white adipose tissue. Dev Cell. 2021. Epub 2021/03/13. doi: 10.1016/j.devcel.2021.02.018. PubMed PMID: 33711247.
226. Wendling O, Bornert JM, Chambon P, Metzger D. Efficient temporally-controlled targeted mutagenesis in smooth muscle cells of the adult mouse. Genesis. 2009;47(1):14-8. doi: 10.1002/dvg.20448. PubMed PMID: 18942088.
227. Tschop MH, Speakman JR, Arch JR, Auwerx J, Bruning JC, Chan L, Eckel RH, Farese RV, Jr., Galgani JE, Hambly C, Herman MA, Horvath TL, Kahn BB, Kozma SC, Maratos-Flier E, Muller TD, Munzberg H, Pfluger PT, Plum L, Reitman ML, Rahmouni K, Shulman GI, Thomas G, Kahn CR, Ravussin E. A guide to analysis of mouse energy metabolism. Nat Methods. 2011;9(1):57-63. Epub 2011/12/30. doi: 10.1038/nmeth.1806. PubMed PMID: 22205519; PMCID: PMC3654855.
228. Guilherme A, Yenilmez B, Bedard AH, Henriques F, Liu D, Lee A, Goldstein L, Kelly M, Nicoloro SM, Chen M, Weinstein L, Collins S, Czech MP. Control of Adipocyte Thermogenesis

and Lipogenesis through beta3-Adrenergic and Thyroid Hormone Signal Integration. Cell Rep. 2020;31(5):107598. Epub 2020/05/07. doi: 10.1016/j.celrep.2020.107598. PubMed PMID: 32375048; PMCID: PMC7676427.
229. Lidell ME, Betz MJ, Enerback S. Brown adipose tissue and its therapeutic potential. J Intern Med. 2014. doi: 10.1111/joim.12255. PubMed PMID: 24717051.
230. Shi Y, Riese DJ, 2nd, Shen J. The Role of the CXCL12/CXCR4/CXCR7 Chemokine Axis in Cancer. Front Pharmacol. 2020;11:574667. Epub 2020/12/29. doi: 10.3389/fphar.2020.574667. PubMed PMID: 33363463; PMCID: PMC7753359.
231. Cashen AF, Nervi B, DiPersio J. AMD3100: CXCR4 antagonist and rapid stem cell-mobilizing agent. Future Oncol. 2007;3(1):19-27. Epub 2007/02/07. doi: 10.2217/14796694.3.1.19. PubMed PMID: 17280498.
232. Ganeshan K, Chawla A. Warming the mouse to model human diseases. Nat Rev Endocrinol. 2017;13(8):458-65. Epub 2017/05/13. doi: 10.1038/nrendo.2017.48. PubMed PMID: 28497813; PMCID: PMC5777302.
233. Tian XY, Ganeshan K, Hong C, Nguyen KD, Qiu Y, Kim J, Tangirala RK, Tontonoz P, Chawla A. Thermoneutral Housing Accelerates Metabolic Inflammation to Potentiate Atherosclerosis but Not Insulin Resistance. Cell Metab. 2016;23(1):165-78. Epub 2015/11/10. doi: 10.1016/j.cmet.2015.10.003. PubMed PMID: 26549485; PMCID: PMC4715491.
234. Chouchani ET, Kazak L, Spiegelman BM. New Advances in Adaptive Thermogenesis: UCP1 and Beyond. Cell Metab. 2019;29(1):27-37. Epub 2018/12/07. doi: 10.1016/j.cmet.2018.11.002. PubMed PMID: 30503034.
235. Liekens S, Schols D, Hatse S. CXCL12-CXCR4 axis in angiogenesis, metastasis and stem cell mobilization. Curr Pharm Des. 2010;16(35):3903-20. Epub 2010/12/17. doi: 10.2174/138161210794455003. PubMed PMID: 21158728.
236. Wang GX, Zhao XY, Meng ZX, Kern M, Dietrich A, Chen Z, Cozacov Z, Zhou D, Okunade AL, Su X, Li S, Bluher M, Lin JD. The brown fat-enriched secreted factor Nrg4 preserves metabolic homeostasis through attenuation of hepatic lipogenesis. Nat Med. 2014;20(12):1436-43. Epub 2014/11/18. doi: 10.1038/nm.3713. PubMed PMID: 25401691; PMCID: PMC4257907.
237. Hondares E, Iglesias R, Giralt A, Gonzalez FJ, Giralt M, Mampel T, Villarroya F. Thermogenic activation induces FGF21 expression and release in brown adipose tissue. J Biol Chem. 2011;286(15):12983-90. Epub 2011/02/15. doi: 10.1074/jbc.M110.215889. PubMed PMID: 21317437; PMCID: PMC3075644.
238. Tseng YH, Kokkotou E, Schulz TJ, Huang TL, Winnay JN, Taniguchi CM, Tran TT, Suzuki R, Espinoza DO, Yamamoto Y, Ahrens MJ, Dudley AT, Norris AW, Kulkarni RN, Kahn CR. New role of bone morphogenetic protein 7 in brown adipogenesis and energy expenditure. Nature. 2008;454(7207):1000-4. Epub 2008/08/23. doi: 10.1038/nature07221. PubMed PMID: 18719589; PMCID: PMC2745972.
239. Soriano P. Generalized lacZ expression with the ROSA26 Cre reporter strain. Nat Genet. 1999;21(1):70-1. doi: 10.1038/5007. PubMed PMID: 9916792.
240. Alcala M, Calderon-Dominguez M, Serra D, Herrero L, Viana M. Mechanisms of Impaired Brown Adipose Tissue Recruitment in Obesity. Front Physiol. 2019;10:94. Epub 2019/03/01. doi: 10.3389/fphys.2019.00094. PubMed PMID: 30814954; PMCID: PMC6381290.
241. Wolf Y, Boura-Halfon S, Cortese N, Haimon Z, Sar Shalom H, Kuperman Y, Kalchenko V, Brandis A, David E, Segal-Hayoun Y, Chappell-Maor L, Yaron A, Jung S. Brown-adipose-tissue

macrophages control tissue innervation and homeostatic energy expenditure. Nat Immunol. 2017;18(6):665-74. Epub 2017/05/02. doi: 10.1038/ni.3746. PubMed PMID: 28459435; PMCID: PMC5438596.
242. Chahrour M, Zoghbi HY. The story of Rett syndrome: from clinic to neurobiology. Neuron. 2007;56(3):422-37. Epub 2007/11/09. doi: 10.1016/j.neuron.2007.10.001. PubMed PMID: 17988628.
243. Yaron A, Huang PH, Cheng HJ, Tessier-Lavigne M. Differential requirement for Plexin-A3 and -A4 in mediating responses of sensory and sympathetic neurons to distinct class 3 Semaphorins. Neuron. 2005;45(4):513-23. Epub 2005/02/22. doi: 10.1016/j.neuron.2005.01.013. PubMed PMID: 15721238.
244. Suto F, Tsuboi M, Kamiya H, Mizuno H, Kiyama Y, Komai S, Shimizu M, Sanbo M, Yagi T, Hiromi Y, Chedotal A, Mitchell KJ, Manabe T, Fujisawa H. Interactions between plexin-A2, plexin-A4, and semaphorin 6A control lamina-restricted projection of hippocampal mossy fibers. Neuron. 2007;53(4):535-47. Epub 2007/02/14. doi: 10.1016/j.neuron.2007.01.028. PubMed PMID: 17296555.
245. Wang YN, Tang Y, He Z, Ma H, Wang L, Liu Y, Yang Q, Pan D, Zhu C, Qian S, Tang QQ. Slit3 secreted from M2-like macrophages increases sympathetic activity and thermogenesis in adipose tissue. Nat Metab. 2021;3(11):1536-51. Epub 2021/11/17. doi: 10.1038/s42255-021-00482-9. PubMed PMID: 34782792.
246. O'Neill LA, Kishton RJ, Rathmell J. A guide to immunometabolism for immunologists. Nat Rev Immunol. 2016;16(9):553-65. Epub 2016/07/12. doi: 10.1038/nri.2016.70. PubMed PMID: 27396447; PMCID: PMC5001910.
247. Crewe C, An YA, Scherer PE. The ominous triad of adipose tissue dysfunction: inflammation, fibrosis, and impaired angiogenesis. J Clin Invest. 2017;127(1):74-82. Epub 2017/01/04. doi: 10.1172/JCI88883. PubMed PMID: 28045400; PMCID: PMC5199684.
248. Brestoff JR, Kim BS, Saenz SA, Stine RR, Monticelli LA, Sonnenberg GF, Thome JJ, Farber DL, Lutfy K, Seale P, Artis D. Group 2 innate lymphoid cells promote beiging of white adipose tissue and limit obesity. Nature. 2015;519(7542):242-6. Epub 2014/12/24. doi: 10.1038/nature14115. PubMed PMID: 25533952; PMCID: PMC4447235.
249. Camell CD, Gunther P, Lee A, Goldberg EL, Spadaro O, Youm YH, Bartke A, Hubbard GB, Ikeno Y, Ruddle NH, Schultze J, Dixit VD. Aging Induces an Nlrp3 Inflammasome-Dependent Expansion of Adipose B Cells That Impairs Metabolic Homeostasis. Cell Metab. 2019;30(6):1024-39 e6. Epub 2019/11/19. doi: 10.1016/j.cmet.2019.10.006. PubMed PMID: 31735593; PMCID: PMC6944439.
250. Camell CD, Sander J, Spadaro O, Lee A, Nguyen KY, Wing A, Goldberg EL, Youm YH, Brown CW, Elsworth J, Rodeheffer MS, Schultze JL, Dixit VD. Inflammasome-driven catecholamine catabolism in macrophages blunts lipolysis during ageing. Nature. 2017;550(7674):119-23. Epub 2017/09/28. doi: 10.1038/nature24022. PubMed PMID: 28953873; PMCID: PMC5718149.
251. Chen S, Chen B, Wen Z, Huang Z, Ye L. IL-33/ST2-mediated inflammation in macrophages is directly abrogated by IL-10 during rheumatoid arthritis. Oncotarget. 2017;8(20):32407-18. Epub 2017/04/19. doi: 10.18632/oncotarget.16299. PubMed PMID: 28415811; PMCID: PMC5464798.

252. Nussbaum JC, Van Dyken SJ, von Moltke J, Cheng LE, Mohapatra A, Molofsky AB, Thornton EE, Krummel MF, Chawla A, Liang HE, Locksley RM. Type 2 innate lymphoid cells control eosinophil homeostasis. Nature. 2013;502(7470):245-8. Epub 2013/09/17. doi: 10.1038/nature12526. PubMed PMID: 24037376; PMCID: PMC3795960.
253. Zhao XY, Zhou L, Chen Z, Ji Y, Peng X, Qi L, Li S, Lin JD. The obesity-induced adipokine sST2 exacerbates adipose Treg and ILC2 depletion and promotes insulin resistance. Sci Adv. 2020;6(20):eaay6191. Epub 2020/05/20. doi: 10.1126/sciadv.aay6191. PubMed PMID: 32426492; PMCID: PMC7220368.
254. Samuelson I, Vidal-Puig A. Studying Brown Adipose Tissue in a Human in vitro Context. Front Endocrinol (Lausanne). 2020;11:629. Epub 2020/10/13. doi: 10.3389/fendo.2020.00629. PubMed PMID: 33042008; PMCID: PMC7523498.
255. Cereijo R, Gavalda-Navarro A, Cairo M, Quesada-Lopez T, Villarroya J, Moron-Ros S, Sanchez-Infantes D, Peyrou M, Iglesias R, Mampel T, Turatsinze JV, Eizirik DL, Giralt M, Villarroya F. CXCL14, a Brown Adipokine that Mediates Brown-Fat-to-Macrophage Communication in Thermogenic Adaptation. Cell Metab. 2018;28(5):750-63 e6. Epub 2018/08/21. doi: 10.1016/j.cmet.2018.07.015. PubMed PMID: 30122557.
256. Mina AI, LeClair RA, LeClair KB, Cohen DE, Lantier L, Banks AS. CalR: A Web-Based Analysis Tool for Indirect Calorimetry Experiments. Cell Metab. 2018;28(4):656-66 e1. Epub 2018/07/19. doi: 10.1016/j.cmet.2018.06.019. PubMed PMID: 30017358; PMCID: PMC6170709.
257. Hausman DB, Park HJ, Hausman GJ. Isolation and culture of preadipocytes from rodent white adipose tissue. Methods Mol Biol. 2008;456:201-19. Epub 2008/06/03. doi: 10.1007/978-1-59745-245-8_15. PubMed PMID: 18516563.
258. Kyrou I, Randeva HS, Tsigos C, Kaltsas G, Weickert MO. Clinical Problems Caused by Obesity. In: Feingold KR, Anawalt B, Boyce A, Chrousos G, de Herder WW, Dungan K, Grossman A, Hershman JM, Hofland HJ, Kaltsas G, Koch C, Kopp P, Korbonits M, McLachlan R, Morley JE, New M, Purnell J, Singer F, Stratakis CA, Trence DL, Wilson DP, editors. Endotext. South Dartmouth (MA)2000.
259. Muir LA, Neeley CK, Meyer KA, Baker NA, Brosius AM, Washabaugh AR, Varban OA, Finks JF, Zamarron BF, Flesher CG, Chang JS, DelProposto JB, Geletka L, Martinez-Santibanez G, Kaciroti N, Lumeng CN, O'Rourke RW. Adipose tissue fibrosis, hypertrophy, and hyperplasia: Correlations with diabetes in human obesity. Obesity (Silver Spring). 2016;24(3):597-605. Epub 2016/02/27. doi: 10.1002/oby.21377. PubMed PMID: 26916240; PMCID: PMC4920141.
260. Lee YS, Kim JW, Osborne O, Oh DY, Sasik R, Schenk S, Chen A, Chung H, Murphy A, Watkins SM, Quehenberger O, Johnson RS, Olefsky JM. Increased adipocyte O2 consumption triggers HIF-1alpha, causing inflammation and insulin resistance in obesity. Cell. 2014;157(6):1339-52. Epub 2014/06/07. doi: 10.1016/j.cell.2014.05.012. PubMed PMID: 24906151; PMCID: PMC4114226.
261. Kim JI, Huh JY, Sohn JH, Choe SS, Lee YS, Lim CY, Jo A, Park SB, Han W, Kim JB. Lipid-overloaded enlarged adipocytes provoke insulin resistance independent of inflammation. Mol Cell Biol. 2015;35(10):1686-99. Epub 2015/03/04. doi: 10.1128/MCB.01321-14. PubMed PMID: 25733684; PMCID: PMC4405637.

262. Salans LB, Knittle JL, Hirsch J. The role of adipose cell size and adipose tissue insulin sensitivity in the carbohydrate intolerance of human obesity. J Clin Invest. 1968;47(1):153-65. Epub 1968/01/01. doi: 10.1172/JCI105705. PubMed PMID: 16695937; PMCID: PMC297156.
263. Sims EA. Are there persons who are obese, but metabolically healthy? Metabolism. 2001;50(12):1499-504. Epub 2001/12/06. doi: 10.1053/meta.2001.27213. PubMed PMID: 11735101.
264. Primeau V, Coderre L, Karelis AD, Brochu M, Lavoie ME, Messier V, Sladek R, Rabasa-Lhoret R. Characterizing the profile of obese patients who are metabolically healthy. Int J Obes (Lond). 2011;35(7):971-81. Epub 2010/10/27. doi: 10.1038/ijo.2010.216. PubMed PMID: 20975726.
265. Banerjee A, Singh J. Remodeling adipose tissue inflammasome for type 2 diabetes mellitus treatment: Current perspective and translational strategies. Bioeng Transl Med. 2020;5(2):e10150. Epub 2020/05/23. doi: 10.1002/btm2.10150. PubMed PMID: 32440558; PMCID: PMC7237149.
266. Mathis D. Immunological goings-on in visceral adipose tissue. Cell Metab. 2013;17(6):851-9. Epub 2013/06/12. doi: 10.1016/j.cmet.2013.05.008. PubMed PMID: 23747244; PMCID: PMC4264591.
267. Ohlson LO, Larsson B, Svardsudd K, Welin L, Eriksson H, Wilhelmsen L, Bjorntorp P, Tibblin G. The influence of body fat distribution on the incidence of diabetes mellitus. 13.5 years of follow-up of the participants in the study of men born in 1913. Diabetes. 1985;34(10):1055-8. Epub 1985/10/01. doi: 10.2337/diab.34.10.1055. PubMed PMID: 4043554.
268. Appleton SL, Seaborn CJ, Visvanathan R, Hill CL, Gill TK, Taylor AW, Adams RJ, North West Adelaide Health Study T. Diabetes and cardiovascular disease outcomes in the metabolically healthy obese phenotype: a cohort study. Diabetes Care. 2013;36(8):2388-94. Epub 2013/03/16. doi: 10.2337/dc12-1971. PubMed PMID: 23491523; PMCID: PMC3714523.
269. Manolopoulos KN, Karpe F, Frayn KN. Gluteofemoral body fat as a determinant of metabolic health. Int J Obes (Lond). 2010;34(6):949-59. Epub 2010/01/13. doi: 10.1038/ijo.2009.286. PubMed PMID: 20065965.
270. Karastergiou K, Smith SR, Greenberg AS, Fried SK. Sex differences in human adipose tissues - the biology of pear shape. Biol Sex Differ. 2012;3(1):13. Epub 2012/06/02. doi: 10.1186/2042-6410-3-13. PubMed PMID: 22651247; PMCID: PMC3411490.
271. Shi H, Clegg DJ. Sex differences in the regulation of body weight. Physiol Behav. 2009;97(2):199-204. Epub 2009/03/03. doi: 10.1016/j.physbeh.2009.02.017. PubMed PMID: 19250944; PMCID: PMC4507503.
272. Poehlman ET, Tchernof A. Traversing the menopause: changes in energy expenditure and body composition. Coron Artery Dis. 1998;9(12):799-803. Epub 1999/01/23. PubMed PMID: 9894924.
273. Tchernof A, Calles-Escandon J, Sites CK, Poehlman ET. Menopause, central body fatness, and insulin resistance: effects of hormone-replacement therapy. Coron Artery Dis. 1998;9(8):503-11. Epub 1998/12/16. doi: 10.1097/00019501-199809080-00006. PubMed PMID: 9847982.
274. Tchernof A, Poehlman ET. Effects of the menopause transition on body fatness and body fat distribution. Obes Res. 1998;6(3):246-54. Epub 1998/06/09. doi: 10.1002/j.1550-8528.1998.tb00344.x. PubMed PMID: 9618130.

275. Schofield R. The relationship between the spleen colony-forming cell and the haemopoietic stem cell. Blood Cells. 1978;4(1-2):7-25. Epub 1978/01/01. PubMed PMID: 747780.
276. Jin DK, Shido K, Kopp HG, Petit I, Shmelkov SV, Young LM, Hooper AT, Amano H, Avecilla ST, Heissig B, Hattori K, Zhang F, Hicklin DJ, Wu Y, Zhu Z, Dunn A, Salari H, Werb Z, Hackett NR, Crystal RG, Lyden D, Rafii S. Cytokine-mediated deployment of SDF-1 induces revascularization through recruitment of CXCR4+ hemangiocytes. Nat Med. 2006;12(5):557-67. Epub 2006/05/02. doi: 10.1038/nm1400. PubMed PMID: 16648859; PMCID: PMC2754288.
277. Yu VW, Scadden DT. Hematopoietic Stem Cell and Its Bone Marrow Niche. Curr Top Dev Biol. 2016;118:21-44. Epub 2016/05/04. doi: 10.1016/bs.ctdb.2016.01.009. PubMed PMID: 27137653; PMCID: PMC6854531.
278. Moser B, Wolf M, Walz A, Loetscher P. Chemokines: multiple levels of leukocyte migration control. Trends Immunol. 2004;25(2):75-84. Epub 2004/04/23. doi: 10.1016/j.it.2003.12.005. PubMed PMID: 15102366.
279. Petit I, Jin D, Rafii S. The SDF-1-CXCR4 signaling pathway: a molecular hub modulating neo-angiogenesis. Trends Immunol. 2007;28(7):299-307. Epub 2007/06/15. doi: 10.1016/j.it.2007.05.007. PubMed PMID: 17560169; PMCID: PMC2952492.
280. Guo S, Scadden DT. A microRNA regulating adult hematopoietic stem cells. Cell Cycle. 2010;9(18):3637-8. Epub 2010/09/22. doi: 10.4161/cc.9.18.13174. PubMed PMID: 20855952.
281. Kiel MJ, Morrison SJ. Uncertainty in the niches that maintain haematopoietic stem cells. Nat Rev Immunol. 2008;8(4):290-301. Epub 2008/03/08. doi: 10.1038/nri2279. PubMed PMID: 18323850.
282. Pekovic V, Hutchison CJ. Adult stem cell maintenance and tissue regeneration in the ageing context: the role for A-type lamins as intrinsic modulators of ageing in adult stem cells and their niches. J Anat. 2008;213(1):5-25. Epub 2008/07/22. doi: 10.1111/j.1469-7580.2008.00928.x. PubMed PMID: 18638067; PMCID: PMC2475560.
283. Ng AP, Alexander WS. Haematopoietic stem cells: past, present and future. Cell Death Discov. 2017;3:17002. Epub 2017/02/10. doi: 10.1038/cddiscovery.2017.2. PubMed PMID: 28180000; PMCID: PMC5292770.
284. Morrison SJ, Spradling AC. Stem cells and niches: mechanisms that promote stem cell maintenance throughout life. Cell. 2008;132(4):598-611. Epub 2008/02/26. doi: 10.1016/j.cell.2008.01.038. PubMed PMID: 18295578; PMCID: PMC4505728.
285. Berry DC, Jiang Y, Graff JM. Emerging Roles of Adipose Progenitor Cells in Tissue Development, Homeostasis, Expansion and Thermogenesis. Trends Endocrinol Metab. 2016;27(8):574-85. Epub 2016/06/06. doi: 10.1016/j.tem.2016.05.001. PubMed PMID: 27262681.
286. Barak Y, Nelson MC, Ong ES, Jones YZ, Ruiz-Lozano P, Chien KR, Koder A, Evans RM. PPAR gamma is required for placental, cardiac, and adipose tissue development. Mol Cell. 1999;4(4):585-95. Epub 1999/11/05. doi: 10.1016/s1097-2765(00)80209-9. PubMed PMID: 10549290.
287. Vidal-Puig AJ, Considine RV, Jimenez-Linan M, Werman A, Pories WJ, Caro JF, Flier JS. Peroxisome proliferator-activated receptor gene expression in human tissues. Effects of obesity, weight loss, and regulation by insulin and glucocorticoids. J Clin Invest.

1997;99(10):2416-22. Epub 1997/05/15. doi: 10.1172/JCI119424. PubMed PMID: 9153284; PMCID: PMC508081.
288. Rogers NH, Perfield JW, 2nd, Strissel KJ, Obin MS, Greenberg AS. Reduced energy expenditure and increased inflammation are early events in the development of ovariectomy-induced obesity. Endocrinology. 2009;150(5):2161-8. Epub 2009/01/31. doi: 10.1210/en.2008-1405. PubMed PMID: 19179442; PMCID: PMC2671894.
289. Gentry RT, Wade GN. Androgenic control of food intake and body weight in male rats. J Comp Physiol Psychol. 1976;90(1):18-25. Epub 1976/01/01. doi: 10.1037/h0077264. PubMed PMID: 965512.
290. Tarttelin MF, Gorski RA. The effects of ovarian steroids on food and water intake and body weight in the female rat. Acta Endocrinol (Copenh). 1973;72(3):551-68. Epub 1973/03/01. doi: 10.1530/acta.0.0720551. PubMed PMID: 4739360.
291. Wade GN, Gray JM. Gonadal effects on food intake and adiposity: a metabolic hypothesis. Physiol Behav. 1979;22(3):583-93. Epub 1979/03/01. doi: 10.1016/0031-9384(79)90028-3. PubMed PMID: 379889.
292. American Diabetes A. 1. Improving Care and Promoting Health in Populations: Standards of Medical Care in Diabetes-2019. Diabetes Care. 2019;42(Suppl 1):S7-S12. Epub 2018/12/19. doi: 10.2337/dc19-S001. PubMed PMID: 30559227.
293. Carobbio S, Pellegrinelli V, Vidal-Puig A. Adipose Tissue Function and Expandability as Determinants of Lipotoxicity and the Metabolic Syndrome. Adv Exp Med Biol. 2017;960:161-96. Epub 2017/06/07. doi: 10.1007/978-3-319-48382-5_7. PubMed PMID: 28585199.
294. Rosen ED, Spiegelman BM. What we talk about when we talk about fat. Cell. 2014;156(1-2):20-44. Epub 2014/01/21. doi: 10.1016/j.cell.2013.12.012. PubMed PMID: 24439368; PMCID: PMC3934003.
295. Smith GI, Mittendorfer B, Klein S. Metabolically healthy obesity: facts and fantasies. J Clin Invest. 2019;129(10):3978-89. Epub 2019/09/17. doi: 10.1172/JCI129186. PubMed PMID: 31524630; PMCID: PMC6763224.
296. Spiegelman BM, Flier JS. Obesity and the regulation of energy balance. Cell. 2001;104(4):531-43. Epub 2001/03/10. doi: 10.1016/s0092-8674(01)00240-9. PubMed PMID: 11239410.
297. Nedungadi TP, Clegg DJ. Sexual dimorphism in body fat distribution and risk for cardiovascular diseases. J Cardiovasc Transl Res. 2009;2(3):321-7. Epub 2010/06/19. doi: 10.1007/s12265-009-9101-1. PubMed PMID: 20560019.
298. Menke A, Casagrande S, Geiss L, Cowie CC. Prevalence of and Trends in Diabetes Among Adults in the United States, 1988-2012. JAMA. 2015;314(10):1021-9. Epub 2015/09/09. doi: 10.1001/jama.2015.10029. PubMed PMID: 26348752.
299. Sengenes C, Miranville A, Maumus M, de Barros S, Busse R, Bouloumie A. Chemotaxis and differentiation of human adipose tissue CD34+/CD31- progenitor cells: role of stromal derived factor-1 released by adipose tissue capillary endothelial cells. Stem Cells. 2007;25(9):2269-76. Epub 2007/05/26. doi: 10.1634/stemcells.2007-0180. PubMed PMID: 17525234.
300. Law J, Bloor I, Budge H, Symonds ME. The influence of sex steroids on adipose tissue growth and function. Horm Mol Biol Clin Investig. 2014;19(1):13-24. Epub 2014/11/13. doi: 10.1515/hmbci-2014-0015. PubMed PMID: 25390013.

301. Orimo A, Weinberg RA. Stromal fibroblasts in cancer: a novel tumor-promoting cell type. Cell Cycle. 2006;5(15):1597-601. Epub 2006/08/02. doi: 10.4161/cc.5.15.3112. PubMed PMID: 16880743.
302. Margolis KL, Bonds DE, Rodabough RJ, Tinker L, Phillips LS, Allen C, Bassford T, Burke G, Torrens J, Howard BV, Women's Health Initiative I. Effect of oestrogen plus progestin on the incidence of diabetes in postmenopausal women: results from the Women's Health Initiative Hormone Trial. Diabetologia. 2004;47(7):1175-87. Epub 2004/07/15. doi: 10.1007/s00125-004-1448-x. PubMed PMID: 15252707.
303. Kanaya AM, Herrington D, Vittinghoff E, Lin F, Grady D, Bittner V, Cauley JA, Barrett-Connor E, Heart, Estrogen/progestin Replacement S. Glycemic effects of postmenopausal hormone therapy: the Heart and Estrogen/progestin Replacement Study. A randomized, double-blind, placebo-controlled trial. Ann Intern Med. 2003;138(1):1-9. Epub 2003/01/07. doi: 10.7326/0003-4819-138-1-200301070-00005. PubMed PMID: 12513038.
304. Chu MC, Cosper P, Nakhuda GS, Lobo RA. A comparison of oral and transdermal short-term estrogen therapy in postmenopausal women with metabolic syndrome. Fertil Steril. 2006;86(6):1669-75. Epub 2006/11/01. doi: 10.1016/j.fertnstert.2006.04.043. PubMed PMID: 17074346.
305. Mattiasson I, Rendell M, Tornquist C, Jeppsson S, Hulthen UL. Effects of estrogen replacement therapy on abdominal fat compartments as related to glucose and lipid metabolism in early postmenopausal women. Horm Metab Res. 2002;34(10):583-8. Epub 2002/11/20. doi: 10.1055/s-2002-35420. PubMed PMID: 12439787.